2010

Genetic studies of SH3PXD2B and its contributions to ocular diseases

Mao Mao
University of Iowa

GENETIC STUDIES OF SH3PXD2B AND ITS CONTRIBUTIONS TO OCULAR DISEASES

by

Mao Mao

An Abstract

Of a thesis submitted in partial fulfillment
of the requirements for the Doctor of
Philosophy degree in Molecular Physiology and Biophysics
in the Graduate College of
The University of Iowa

July 2010

Thesis Supervisor: Assistant Professor Michael G. Anderson

ABSTRACT

In cultured cells, the adaptor protein SH3PXD2B is capable of recruiting a variety of proteins involved in invadosome assembly and function. It is therefore considered as an essential organizer of invadosomes active in cellular responses that require extracellular matrix degradation. Despite increasing knowledge about its properties and functions at the molecular and cellular levels, its physiological role in whole animals has not previously been assessed. Here, we present that SH3PXD2B is essential for normal postnatal development and disrupting SH3PXD2B can lead to glaucoma.

Our work on SH3PXD2B is based on *nee*, a spontaneous mutation in mice which arose on an inbred background. Mice homozygous for the *nee* mutation were initially noted to exhibit runted growth, craniofacial abnormalities and ocular defects. Our additional physiological characterization has uncovered skeletal abnormalities, hearing impairment, infertility and a form of lipodystrophy. Using genetic mapping and DNA sequencing, the cause of *nee* phenotypes was identified as a 1-bp deletion within the *Sh3pxd2b* gene on mouse Chromosome 11. The *nee* mutation is predicted to cause a frameshift and a protein truncation altering a portion of the third SH3 domain and deleting the entire fourth SH3 domain. Molecular analysis showed that the fourth SH3 domain of SH3PXD2B can interact with a transmembrane member of a disintegrin and metalloproteinase family of proteins, ADAM15, and that GFP tagged SH3PXD2B protein truncation mislocalizes to the nucleus. Therefore, the mutant allele likely disrupts the normal function of SH3PXD2B and leads to *nee* phenotypes.

The initial ocular abnormalities of *nee* mutants suggested that they may develop glaucoma. To test this hypothesis, we performed detailed clinical and histological analyses. We find that *nee* mutants exhibit elevated intraocular pressure likely caused by a severe iridocorneal adhesion present early in development. During the same time that

intraocular pressure becomes elevated, retinal ganglion cells are damaged and optic nerve degeneration ensues. These results demonstrate that *nee* mutants develop an early onset form of closed angle glaucoma. To test the potential involvement of SH3PXD2B in human diseases, DNA sequencing analysis has been initiated in patients with developmental, primary open angle and syndromic glaucoma, and several missense variations have been identified. In conclusion, my results demonstrate a critical role of SH3PXD2B in normal development of multiple tissues and suggest that mutations in *SH3PXD2B* may also contribute to glaucoma.

Abstract Approved:_____
Thesis Supervisor

_____
Title and Department

_____
Date

GENETIC STUDIES OF SH3PXD2B AND ITS CONTRIBUTIONS TO OCULAR DISEASES

by

Mao Mao

A thesis submitted in partial fulfillment
of the requirements for the Doctor of
Philosophy degree in Molecular Physiology and Biophysics
in the Graduate College of
The University of Iowa

July 2010

Thesis Supervisor: Assistant Professor Michael G. Anderson

Graduate College
The University of Iowa
Iowa City, Iowa

CERTIFICATE OF APPROVAL

_____

PH.D. THESIS

_____

This is to certify that the Ph.D. thesis of

Mao Mao

has been approved by the Examining Committee
for the thesis requirement for the Doctor of Philosophy
degree in Molecular Physiology and Biophysics at the July 2010 graduation.

Thesis Committee: _____
Michael G. Anderson, Thesis Supervisor

_____
Michael Henry

_____
Wayne Johnson

_____
Andrew Russo

_____
Diane Slusarski

_____
Mark Stamnes

To my parents

Happy is he who gets to know the reasons for things.
Virgil

ACKNOWLEDGMENTS

I would like to express my deep thanks to my thesis advisor, Dr. Michael G. Anderson for his invaluable research guidance and friendly support during my graduate study. I greatly appreciate his inspiring input on my research and his scientific training on my thinking, presentation and writing. I also thank his patience, encouragement and sense of humor that helped me through all the difficulties and challenges. Joining his lab is the best decision I have made by far in my scientific career.

I would also like to thank my thesis committee members, Drs. Michael Henry, Wayne Johnson, Andrew Russo, Diane Slusarski, and Mark Stamnes. I highly appreciate their time, effort and support on my research project. Their suggestions and directions have helped me greatly to improve my research work.

I wish to thank my past and present colleagues from the Anderson laboratory, Greg Petersen, Dr. Colleen Trantow, Kaitlyn Peterson, Leslie Amonoo, Erin Alward, Katie Striegel, Dr. Bing Jiang, Dr. Geoffrey Lively, Dr. Demelza Koehn, Dr. Sachiyo Iwashita, Adam Hedberg-Buenz, and Tryphena Cuffy. I appreciate their technical and intellectual support on my research, and the warmth and fun they brought to the lab and my life. I have truly enjoyed working with them.

I like to thank members of the Eye Interest Group for many helpful discussions and collaborations over the years. I also like to thank our collaborators, Drs. Daniel Thedens, Bo Chang, Belina Harris, Qing Yin Zheng, Kenneth Johnson, Lea Rae Donahue, John Fingert, Robert Mullins, Peter Nagy, Arlene Drake and Ordan Lehmann for their contribution in the study. I thank Drs. Gloria Lee and Margaret Frame for generously providing reagents and Jianqiang Shao for his excellent technical assistance.

Finally, I would like to acknowledge the Department of Molecular Physiology and Biophysics, the Bioscience Program and the Neuroscience Program for giving the opportunity to be here and pursue my career in science.

I especially thank my Mom, Dad and friends for their love, support and encouragement. They are always the source of hope, courage and strength in the journey of my life.

ABSTRACT

In cultured cells, the adaptor protein SH3PXD2B is capable of recruiting a variety of proteins involved in invadosome assembly and function. It is therefore considered as an essential organizer of invadosomes active in cellular responses that require extracellular matrix degradation. Despite increasing knowledge about its properties and functions at the molecular and cellular levels, its physiological role in whole animals has not previously been assessed. Here, we present that SH3PXD2B is essential for normal postnatal development and disrupting SH3PXD2B can lead to glaucoma.

Our work on SH3PXD2B is based on *nee*, a spontaneous mutation in mice which arose on an inbred background. Mice homozygous for the *nee* mutation were initially noted to exhibit runted growth, craniofacial abnormalities and ocular defects. Our additional physiological characterization has uncovered skeletal abnormalities, hearing impairment, infertility and a form of lipodystrophy. Using genetic mapping and DNA sequencing, the cause of *nee* phenotypes was identified as a 1-bp deletion within the Sh3pxd2b gene on mouse Chromosome 11. The *nee* mutation is predicted to cause a frameshift and a protein truncation altering a portion of the third SH3 domain and deleting the entire fourth SH3 domain. Molecular analysis showed that the fourth SH3 domain of SH3PXD2B can interact with a transmembrane member of a disintegrin and metalloproteinase family of proteins, ADAM15, and that GFP tagged SH3PXD2B protein truncation mislocalizes to the nucleus. Therefore, the mutant allele likely disrupts the normal function of SH3PXD2B and leads to *nee* phenotypes.

The initial ocular abnormalities of *nee* mutants suggested that they may develop glaucoma. To test this hypothesis, we performed detailed clinical and histological analyses. We find that *nee* mutants exhibit elevated intraocular pressure likely caused by a severe iridocorneal adhesion present early in development. During the same time that

intraocular pressure becomes elevated, retinal ganglion cells are damaged and optic nerve degeneration ensues. These results demonstrate that *nee* mutants develop an early onset form of closed angle glaucoma. To test the potential involvement of SH3PXD2B in human diseases, DNA sequencing analysis has been initiated in patients with developmental, primary open angle and syndromic glaucoma, and several missense variations have been identified. In conclusion, my results demonstrate a critical role of SH3PXD2B in normal development of multiple tissues and suggest that mutations in SH3PXD2B may also contribute to glaucoma.

TABLE OF CONTENTS

LIST OF TABLES

LIST OF FIGURES

CHAPTER 1
INTRODUCTION

The glaucomas are a collection of ocular diseases which are characterized by retinal ganglion cell degeneration, optic nerve head excavation and progressive loss of vision (Ritch R 1996; Nickells RW 2002; Allingham RR 2004). Affecting approximately 70 million people worldwide, glaucoma is a leading cause of irreversible blindness. Thus, it represents an important health issue (Quigley 1996; Resnikoff, Pascolini et al. 2004; Quigley and Broman 2006).The etiology of glaucoma is complex. Despite much progress, most molecular mechanisms contributing to glaucoma remain unknown.

The overarching theme of this thesis is that studies with animal models such as mice can be a powerful tool to help dissect its molecular etiology. The experiments described in this thesis center around *nee*, a spontaneous mouse mutant strain with glaucomatous phenotypes. In subsequent chapters, I present the identification and characterization of its causative gene, *Sh3pxd2b* (SH3 and PX domains 2B), and characterize the molecular function of SH3PXD2B as an adaptor protein for invadosomes. Therefore, as a broad introduction to these topics, this chapter will introduce the following subjects: (1) glaucoma overview, (2) glaucoma pathophysiology, (3) glaucoma genetics, (4) mouse models of glaucoma, (5) ECM modulation and outflow resistance in glaucoma, (6) invadosomes and (7) the SH3 and PX domain containing family proteins.

Overview of glaucoma

Glaucoma is defined as a type of optic neuropathy (Foster, Buhrmann et al. 2002); however, historically glaucoma was considered as a group of diseases defined by

elevated intraocular pressure (IOP) because it associates with the majority of glaucoma cases. Thus, the two ocular structures that are important in understanding glaucoma are the iridocorneal angle structures in the anterior portion of the eye (which is the primary site for IOP regulation), and the retinal ganglion cells and the optic nerve head at the posterior portion (which are the cells giving rise to the neuropathy).

Iridocorneal structures (Figure 1) control IOP by regulating aqueous humor outflow resistance. These are the tissues located at the angle between the iris and cornea, mainly composed of the trabecular meshwork and Schlemm's canal. The retinal ganglion cells (Figure 2) are the type of neurons affected in glaucoma. The retinal ganglion cell layer is the innermost nuclear layer of the retina. These neurons send their axons posteriorly to the center of the retina, where they form bundles and exit the eye through pores of a sieve like connective tissue called the lamina cribrosa. The region in the eye where these axons exit is called the optic nerve head (Figure 2). In addition to neural and connective tissues at the optic nerve head, glial cells such as astrocytes and blood vessels are also present. Axons form the optic nerves send information to the brain relaying visual perception.

Glaucoma is a heterogeneous group of diseases. Clinically, glaucoma is typically divided into several categories: open angle glaucoma (the iridocorneal angle of the eye appears unobstructed) and angle closure glaucoma (the iridocorneal angle appears narrow or obstructed); developmental forms of glaucoma and adult onset glaucoma; primary glaucoma (the glaucoma is not associated with other observable ocular or systemic defects) and secondary glaucoma (the glaucoma is secondary to other ocular and systemic defects). The most common form of glaucoma in the United States is currently primary open angle glaucoma (POAG). The overall prevalence is 2% among people with ages of 40 or older (Friedman, Wolfs et al. 2004). The other common form of glaucoma is angle closure glaucoma, which is more common in Asian ethnic groups (Yip and Foster 2006). Other examples of less common forms of glaucoma includes congenital glaucoma or

glaucoma associated with anterior segment dysgenesis, secondary glaucoma such as pigmentary glaucoma or pseudoexfoliation glaucoma, and glaucoma associated with normal IOP. Although these subtypes are clinically different, they all share the same outcome, optic nerve damage.

Diagnosis of glaucoma usually includes measurement of IOP and examinations of the changes of the appearance of the optic nerve head and the visual field over time. Most glaucoma is slowly progressive and non-symptomatic, and the vision loss usually starts from the periphery. Therefore, by the time patients experience worsening vision and seek medical attention, the majority of axons have already been severely damaged. The damage to the neurons is irreversible. Therefore, improved diagnosis and identification of patients who are at high risk of developing glaucoma is one means of improving future outcomes.

The sole treatment for glaucoma is to decrease IOP by means of medication or surgery. Glaucoma neuroprotection (protecting axons regardless of IOP) is desirable, however clinical trials completed to date have thus far been unsuccessful, and extremely expensive to conduct (Danesh-Meyer and Levin 2009; Osborne 2009). Typical IOP lowering drugs include non-selective β-blockers, prostaglandin analogs, α-agonists and carbonic anhydrase inhibitors, which either reduce aqueous humor (see below) production or increase aqueous humor outflow. Surgical procedures include laser therapy or incisional surgery, which facilitates aqueous humor to exit the eye. These treatments are effective in many types of glaucoma. In the majority of cases, lowering IOP can only slow, but not completely stop, disease progression (Van Buskirk and Cioffi 1992; Leske, Heijl et al. 1999). Moreover, these treatments are not always successful in every patient (Zhou, Althin et al. 2004). Therefore, there is a medical need to improve glaucoma treatments by devising therapies aimed at treating the early-acting insults that cause IOP to become elevated, treating IOP through additional pathways, and seeking treatments for risk factors other than IOP.

Glaucoma pathophysiology

As mentioned above, glaucoma is defined as a type of optic neuropathy which usually associates with elevated IOP. Therefore, to improve diagnosis and treatment of glaucoma, there is a need to understand the pathophysiology of IOP elevation and glaucomatous neuropathy.

IOP is a function of aqueous humor dynamics. Aqueous humor is the fluid filling the space between the lens and the cornea and providing nutrients to the avascular structures of the anterior segment. Aqueous humor is produced by the ciliary body behind the iris. It flows through the pupil and enters the anterior chamber and finally drains out of the eye. There are two routes for aqueous humor to exit the eye (Figure 1b), the conventional or trabecular outflow pathway and the unconventional or uveoscleral outflow pathway (Johnson 2006). The conventional trabecular outflow pathway is composed of the trabecular meshwork, Schlemm's canal, the connecting channels and the aqueous veins (Tamm 2009). The unconventional or uveoscleral outflow pathway refers to a route that drains into the lymphatic drainage, mainly through the extracellular spaces in the ciliary muscle, the anterior choroid and suprachoroidal space, and the adjacent sclera (Weinreb 2000).

Although elevated IOP could theoretically be caused by impaired aqueous humor drainage or increased production of aqueous humor, in glaucoma it is always caused by changes to the drainage pathway. For instance, in developmental glaucoma, glaucoma usually associates with dysgenesis of the anterior segment structures involved in IOP regulation which blocks aqueous humor outflow (Gould and John 2002). In secondary forms of glaucoma such as pigmentary glaucoma or pseudoexfoliation glaucoma, visible materials such as pigment and cell debris accumulate in the iridocorneal angle (Ritch and

Schlotzer-Schrehardt 2001; Sowka 2004), and impede outflow. In POAG, there are no clinically detectable changes occurring in the eye, although an increased outflow resistance is thought to be present (Grant 1963; Gabelt and Kaufman 2005). Loss of trabecular meshwork cells, accumulation of ECM materials and altered stiffness of the cytoskeleton of trabecular meshwork cells are often found in glaucomatous eyes, therefore are thought to be the changes that lead to increased outflow resistance (Tan, Peters et al. 2006).

Elevated IOP is the major cause of optic neuropathy in many glaucoma cases. However, the exact mechanism translating elevated IOP in the anterior chamber to glaucomatous damage in the retina is not clearly defined. It is typically considered as a type of mechanical stress that is applied to the optic nerve head and the retina, leading to optic nerve head atrophy and retinal ganglion cell apoptosis. However, elevated IOP is not the only stress associated with neuronal damage in glaucoma. Some patients have glaucomatous damage but never develop high IOP, suggesting other non-IOP related factors may independently trigger glaucomatous optic neuropathy. Insufficient autoregulation of the blood flow in the optic nerve head, which can lead to optic nerve ischemia, is thought to be one of these factors (Flammer, Orgul et al. 2002).

The glaucomatous optic neuropathy includes damage of both the retinal ganglion cell soma and their axons. A clinical hallmark of glaucoma differentiating it from other optic neuropathies is the characteristic damage to the optic nerve head, which is called optic nerve head excavation or optic nerve head cupping (Foster, Buhrmann et al. 2002) (Figure 3). Morphologically, optic nerve head excavation involves loss of tissues at the optic nerve head, including not only the nerve fibers, but also the glial cells and the supporting blood vessels. As a consequence, a tissue remodeling process ensues, which leads to bowing or compression of the lamina cribrosa (Vrabec and Levin 2007). Mechanistically, despite extensive studies on this topic, the underlying pathophysiology initiating these changes is largely undefined.

There are multiple mechanisms proposed in glaucomatous neuropathy, and it is suggested that several mechanisms may simultaneously exist in individual glaucoma cases (Wax and Tezel 2002; Morrison, Johnson et al. 2005; Flammer and Mozaffarieh 2007; Agarwal, Gupta et al. 2009). One main mechanism involves disrupted axonal transportation induced by mechanical stress such as elevated IOP. Disturbed axonal anterograde and retrograde transportation can lead to deficiency of neurotrophic factors, triggering apoptosis of the retinal ganglion cells. In addition, abnormal activation of glial cells induced by mechanical or ischemia stress also contributes to optic neuropathy. Glial cells such as astrocytes were found to be able to response to these stresses by increasing proteolytic activity and migration activity, subsequently changing the mechanical properties of the optic nerve head, leading to the excavated morphology. Activated astrocytes may also release some noxious products such as nitric oxide, leading to axonal injury. Moreover, reduced ocular blood flow due to mechanical compression or atrophy of the blood vessels, or vascular dysregulation can result in ischemic injury to the neuronal tissue as well. Other mechanisms such as glutamate excitotoxicity, immune system misregulation and oxidative stress have also been proposed to be involved (Flammer and Mozaffarieh 2007; Agarwal, Gupta et al. 2009).

In sum, multiple biological processes are likely involved in glaucoma, suggesting a complex molecular etiology. A better understanding of these underlying processes is needed for future diagnosis and treatment of glaucoma.

Glaucoma genetics

Genetic approaches are one way to dissect the complex molecular basis of glaucoma. Investigations on the genetic basis of glaucoma would also help predict individuals who are at high risk of developing glaucoma. Eventually, glaucoma genetics

might be utilized to help direct a more effective treatment of glaucoma depending on the specific molecular pathways involved in different types or stages of glaucoma, or on the genetic profile of each individual.

Glaucoma has a strong hereditary basis. For many years there was a debate on whether glaucoma is inheritable, since most glaucoma cases appear sporadic. However, this debate has since resolved as the case for heritable contributions has grown. The first hint was provided by epidemiological studies showing that family history as a risk factor for glaucoma (Wilson MR 1996). In a population based study, subjects whose first degree relatives have glaucoma were found to have a 3-9 fold increase of risk of developing glaucoma (Friedman, Wolfs et al. 2004). Additional evidence were provided by twin studies which demonstrated a concordance in monozygotic twin pairs, suggesting a predominance of genetic factors (Gottfredsdottir, Sverrisson et al. 1999). Moreover, several family studies in the past two decades have successfully identified several disease causing mutations, definitively establishing a hereditary link.

Glaucoma can be inherited in Mendelian autosomal dominant or Mendelian autosomal recessive patterns; however the most common glaucoma is thought to be heterogeneous and multifactorial (Sarfarazi 1997). There are 8 genes and over 20 loci linked to glaucoma so far (Wiggs 2007) (Table 1). Most of the genes and loci were identified with genetic linkage analysis of families with Mendelian inheritance. The first locus for glaucoma was mapped to chromosome 1q21-q31 at the University of Iowa by using a single large family of juvenile onset open angle glaucoma (JOAG) (Sheffield, Stone et al. 1993). Later, linkage to the same locus was reported in several other families with different ethnic backgrounds (Meyer, Valtot et al. 1994; Richards, Lichter et al. 1994; Wiggs, Haines et al. 1994; Graff, Urbak et al. 1995). Using additional families, the locus was further narrowed (Sunden, Alward et al. 1996). In 1997, the first three gene mutations were identified in the myocilin gene (*MYOC)* (Stone, Fingert et al. 1997). Interestingly, the clinical features of the majority of the affected individuals associated

with *MYOC* are very similar. Most patients were diagnosed at an early age (average of 18 years). Their IOP measurements are usually between 40-50 mmHg, and patients are all refractory to glaucoma medicine (Sarfarazi 1997). Thus, the similar clinical presentation and early onset of glaucoma likely helped identify the genetic cause. In addition to JOAG, multiple genes and chromosome loci have also been associated with developmental forms of glaucoma, and a few familial cases of adult onset primary open angle glaucoma. Similarly, these loci were found when large size pedigrees with clear Mendelian inheritance exist.

For more common and complex forms of glaucoma, such as the majority of POAG cases, identification of the genetic causes remains difficult. Genome-wide association studies (GWAS), which uses high density single nucleotide polymorphism (SNP) array to determine a statistical association between genetic variations and disease, has gained some success in glaucoma. In a recent association study of exfoliation glaucoma (Thorleifsson, Magnusson et al. 2007), two high risk nonsynonymous SNPs in the lysyl oxidase-like 1 (*LOXL1*) gene were found to exhibit a strong association. GWAS is now being increasingly used to also study additional types of glaucoma. However, unlike the study of other forms of ocular diseases which were revolutionized by GWAS (Allingham, Wiggs et al. 2005; Edwards, Ritter et al. 2005; Klein, Zeiss et al. 2005), early reports suggest that GWAS will be less successful in studies of common forms of glaucoma.

The genes and loci identified so far only represent a small fraction of glaucoma cases, and the majority of disease causing genes are not known (Challa 2004; Wiggs 2007; Challa 2008). Human genetic approaches face several challenges in studies of glaucoma. As mentioned above, most genes or loci found to date were found in glaucoma cases when large pedigrees with obvious Mendelian inheritance were available. However, most glaucoma is late onset; therefore the pedigree size is usually small. Even for early onset glaucoma, sometimes patients in the same family have different disease

expressivity and incomplete penetrance, thus obscuring the inheritance pattern (Gould and John 2002). Moreover, family linkage studies usually result in chromosome loci with large sizes and many genes, thus making it difficult to unravel the causative gene.

GWAS is thought to be more effective in dissecting complex traits; however, there are also limitations associated with this kind of approach. There are some genetic variants that can not be identified easily with GWAS, including alleles with moderate effects, which can be masked in the background signals when sample size is not large enough, and rare alleles because markers included on the array are usually common SNPs. In addition, the heterogeneity of glaucoma can confound GWAS analysis. Mutations in different genes can result in similar symptoms. Combining patients with different molecular causes as a single cohort will lead to failure. Moreover, even if candidate disease causing alleles are suggested in GWAS analysis, it might be difficult to prove a functional relationship between the candidate alleles and the complex traits (Jacobs, Yeager et al. 2009). Therefore, GWAS will certainly be challenged by complex nature of glaucoma, perhaps insurmountably so.

Taken together, genetic studies starting with human samples face challenges. As this thesis illustrates, one way to move forward is to use animal models such as mice which can serve as a complementary approach to identify disease causing mutations.

Mouse models of glaucoma

Mice have been widely used as a model organism in many diseases, including glaucoma (Paigen 1995). Mice have a relatively similar ocular anatomy and physiology to humans. The anterior angle structures of mice contain a trabecular meshwork made up of ECM beams covered by endothelial cells as well as a true canal cavity representing the Schlemm's canal. The aqueous humor production and outflow rate are similar to humans,

and both conventional and uveoscleral outflow facilities exist (Aihara, Lindsey et al. 2003). The architecture of the mouse retina is also similar to humans and the vasculature support to the retina and optic nerve head is analogous. However, there are slight morphological changes between the mouse optic nerve head morphology and humans. Mice do not have a lamina cribrosa made up of connective tissues. Instead, the mouse optic nerve head has a cellular "lamina cribrosa" composed of elongated astrocytes traversing the optic nerve head (Klein, Zeiss et al. 2005; Morrison, Johnson et al. 2005). However, elevated IOP in mice does cause retina ganglion cell apoptosis in mice, suggesting mechanisms other than tissue modeling of the lamina cribrosa contribute to the glaucoma pathology. Therefore, despite the subtle dissimilarity of the optic nerve head, the ocular anatomy of mice has enough similarity to humans to empower many studies.

Resources for manipulating and studying the mouse genome are nearly, if not completely, unequalled among vertebrate systems and therefore ideal for studying many complex diseases (John, Anderson et al. 1999). Genetic studies with mice have advantages of controlled environmental factors, constant genetic backgrounds and short breeding time. Manipulation of the mouse genome can help characterize the function of candidate genes initially identified in human studies and help isolate causative genes from large candidate loci. Large scale mutagenesis in mice can lead to the discovery of unexpected genes or molecular pathways. Many tools to assess glaucoma related phenotypes in mice have been developed to assist assessment of glaucoma related phenotypes (Pang and Clark 2007). With these tools, accurate measurement of IOP and outflow facility and noninvasive assessment of the axonal damage are now possible. Thus, mouse genetics are powerful tools to expand our knowledge of glaucoma mechanisms.

There are both inducible and naturally occurring mouse models of glaucoma (Table 2), each has advantages and limitations. Ocular hypertension can be induced by

blockage of the episcleral veins either with a laser or a hand hold cautery, or by sclerosis of the episcleral veins with hypertonic saline injection (McKinnon, Schlamp et al. 2009). These approaches ablate outflow through the trabecular meshwork pathway and therefore lead to aqueous humor accumulation in the anterior chamber. In addition to these pressure models, there are other inducible models without high IOP, which can be used to study the non-pressure related mechanisms of optic neuropathy. For instance, there are models with intravitreally injected glutamate to mimic the excitotoxicity effect, models with transected optic nerves to mimic the loss of neurotrophic effect, and models with occluded central optic nerve artery to mimic the ischemic effect (Pang and Clark 2007). These models are usually less costly, as diseases can develop within a relatively short time. However, because of the small size of the mouse eye, inducible models all suffer from a requirement for substantial surgical skills. In addition, diseases in induced mouse models are moderate. They often result in a mild level of IOP elevation and limited retinal ganglion cell loss. Moreover, the level of IOP elevation and axon damage often varies, thus confounding the interpretation of results.

Mice can also develop glaucoma spontaneously. The most widely utilized spontaneous mouse model is DBA/2J (John, Smith et al. 1998; Chang, Smith et al. 1999; Anderson, Smith et al. 2002). DBA/2J mice are an inbred strain that develop a form of pigmentary glaucoma as consequence of mutations in two genes, *Gpnmb* and *Tyrp1*. These genes both encode melanosomal proteins and the mutant alleles lead to iris disease characterized by iris atrophy and pigment dispersion. The liberated pigment from the diseased iris results in blockage of the trabecular meshwork pathway, IOP elevation and optic nerve damage. In addition to DBA/2J mice, a few other spontaneous mouse models have been reported; however, these models are less characterized and in some cases have not been replicated (Aihara, Lindsey et al. 2003; Mabuchi, Lindsey et al. 2004). Compared to induced models, all current spontaneous models require extensive aging before glaucoma develops, making them relatively expensive. However, glaucoma in

spontaneous models tends to be severe and is less variable, thus simplifying data interpretation.

Advent of mouse models of glaucoma has begun to open many new opportunities. In addition to gains in basic biology, because of relative ease of handling and low cost of maintenance compared to other models such as primates, mouse models have begun to be used to test the effectiveness of potential glaucoma treatment in the pharmaceutical industry (Clark and Yorio 2003). Thus, studies with mice can be beneficial to glaucoma research in many aspects.

ECM modulation in outflow resistance and glaucoma

As mentioned in previous sections, increased outflow resistance is thought to be the main cause for IOP elevation in primary open angle glaucoma. The main anatomical site controlling outflow resistance lies in the conventional pathway, especially in the juxtacanalicular region of the trabecular meshwork (Overby, Stamer et al. 2009). The unconventional outflow pathway accounts for a small portion of drainage (Nilsson 1997) and it is not thought to contribute to the outflow resistance in glaucoma (Overby, Stamer et al. 2009).

The trabecular meshwork is an ECM-rich tissue. Anatomically it contains three regions: the uveal trabecular, the corneoscleral trabecular and the juxtacanalicular region. The uveal and corneoscleral regions of the trabecular meshwork (the regions facing the anterior chamber) are composed of lamellae or beams of ECM. The core of the lamella is made of elastins, collagen fibers and glycosaminoglycans. The ECM core is covered by a basement membrane, on which lies the trabecular meshwork cells (Acott and Kelley 2008). Aqueous humor flows through pores between the ECM beams. These pores are of considerable size, therefore it is not considered as a major contributor to outflow

resistance. The juxtacanalicular region (the region next to the Schlemm's canal) of the trabecular meshwork does not have the lamellae arrangement. Instead, it contains a loose ECM within which the trabecular meshwork cells are irregularly dispersed. Aqueous humor passes through the extracellular space between the trabecular meshwork cells and the surrounding fibrillar ECM (Overby, Stamer et al. 2009; Tamm 2009). The small size of the open space in the juxtacanalicular region is likely the source of outflow resistance (Gong, Ruberti et al. 2002). The trabecular meshwork endothelial cells are the only cell type normally found in the trabecular meshwork. These cells morphologically resemble endothelial cells, but functionally they resemble a variety of other cell types. They are capable of synthesizing and secreting a variety of structural components of the ECM and their modifying enzymes (Aga, Bradley et al. 2008). They can phagocytose cellular debris or pigment granules coming from the aqueous humor (Rohen and Witmer 1972; Stone, Fingert et al. 1997), and have some contractility (Barany 1962; Coroneo, Korbmacher et al. 1991).

Both trabecular meshwork cells and their ECM contribute to outflow resistance. Several electron microscopic and immunolabeling studies of eyes from glaucoma patients found a deposit of plaque-like materials in the trabecular meshwork (Rohen and Witmer 1972; Alvarado, Murphy et al. 1984; Clark, Miggans et al. 1995). Although the exact composition of the material is not clear, one component was thought to derived from the sheath of elastic like fibers (Lutjen-Drecoll, Shimizu et al. 1986). Therefore, changes of the quality and quantity of ECM are suspected to be a major contributor to increased outflow resistance (Tan, Peters et al. 2006).

The exact molecular mechanisms leading to these changes in ECM are not clear. Proteinases such as MMPs (matrix metalloproteinases) and ADAMs (a disintegrin and metalloproteinases) are thought to have an important role in regulating outflow resistance (Clark 1998; La Rosa and Lee 2000; Aga, Bradley et al. 2008). Many MMPs are capable of degrading a variety of ECM components. Moreover, some MMPs or ADAMs have a

sheddase activity, which can convert latent non-ECM proteins to their active form and facilitate signal transduction, influencing cell activities (Page-McCaw, Ewald et al. 2007). Thus, MMPs are one type of candidate molecule that may regulate outflow resistance.

There are lines of evidence supporting the involvement of MMPs in outflow resistance regulation. Expression of basal levels of many matrix metalloproteinases and their inhibitors in trabecular meshwork cells have been observed (Bradley, Vranka et al. 1998; Kim, Huang et al. 2007). Elevated levels of these proteins can be induced in response to various glaucomatous stimuli such as increased IOP, mechanical stretch, growth factors (e.g. transforming growth factor β, TGFβ) and cytokines (e.g. interlukin 1-α, IL1 1α) in cultured trabecular meshwork cells or perfused anterior segment organ culture models (Borras 2003). Gene expression analysis comparing normal and glaucomatous eyes found changes in MMPs and their inhibitors (Ronkko, Rekonen et al. 2007; Acott and Kelley 2008). In addition, modulating the activity of MMPs by injecting purified MMPs or inhibiting the endogenous MMPs with synthetic inhibitors can change the outflow resistance (Bradley, Vranka et al. 1998). Interestingly, therapies such as argon laser trabeculoplastry, which lowers IOP, can modulate levels of MMPs at the juxtacanicular trabecular meshwork (Parshley, Bradley et al. 1995; Parshley, Bradley et al. 1996). Together, these findings support a critical role of MMPs in outflow resistance regulation.

There are many different substrates for MMPs. To ensure precise ECM modulation and IOP regulation, trabecular meshwork cells may need a way to ensure precise modulation of certain ECM substrates in the pericellular environment. Consequently, a controlled ECM activity in certain compartments of the cell surface is required (Poincloux, Lizarraga et al. 2009). Some MMPs such as MMP2 or MMP14 are only active at the cell surface (Ra and Parks 2007). These MMPs are found to be enriched in invadosomes which are sites of cell-ECM adhesions (see below). Therefore, it is

possible that trabecular meshwork cells regulate ECM modulation and IOP through invadosomes.

Overview of invadosomes: identification, biological roles and assembling machinery

Invadosomes represent one type of subcellular structure that is involved in focal ECM degradation (Linder 2009). Invadosomes are adhesion sites which typically contain dot-like F-actin accumulations along with actin regulatory proteins forming at the cell-ECM contacting surface (Gimona and Buccione 2006; Linder 2009). Proteinases such as matrix metalloproteinases and serine proteinases have been found to be enriched in invadosomes thus allowing the ECM degradation activity (Chen 1996; Linder 2009). Therefore, invadosomes are sites of cell-ECM adhesions with ECM degradation activity.

Invadosomes can form spontaneously or under stimulated conditions in a variety of cell types that require ECM degradation and motility as their normal function, such as *SRC* transformed fibroblasts, monocytes, dendritic cells, vascular endothelial cells, smooth muscle cells, epithelial cells and cancer cells (Thompson, Kleino et al. 2008). Traditionally, invadosomes in cancer cells are usually called invadopodia, and in other normal cells they are called podosomes. Both of them are finger-like membrane protrusions that degrade ECM, and both share many common molecular markers. Despite these similar features, there are differences between podosomes and invadopodia. For instance, podosomes are more dynamic (with a half life of 2-12 minutes) than invadosomes (with a half life of more than 1 hour). The ECM degradation of podosomes is usually more shallow and widespread, while the invadopodia was thought to protrude deep in ECM. Podosomes and invadopodia also vary in size (1 μm X 0.4 μm vs. 8 μm X 5 μm) and numbers typically present in each cell (~100 vs. ~10). In addition, although podosomes and invadopodia have similar protein compositions, their organization is

slightly different. Podosomes have a core of F-actin, and a ring of actin associated proteins. In contrast, invadopodia do not have the ring of associated proteins; most of them colocalize with F-actin. Because of these similarities and differences, podosomes and invadopodia are considered as two ends of a spectrum for invadosomes (Figure 4).

Invadosomes from different cell types have slightly different morphology and molecular composition. Current convention to identify invadosomes is by molecular markers such as ARP2/3 complex, cortactin, and phosphotyrosine. Additionally, colocalization of these structures to areas of ECM degradation is another criterion. If the core F-actin is surrounded by a ring of talin or vinculin, it is considered as a podosome, otherwise it is more likely a invadopodia (Linder 2009).

Invadosomes have been implicated in multiple biological processes that involve ECM degradation, cell migration and invasion. For instance, bone absorbing osteoclasts need a belt of podosome array called sealing zone to ensure tight adhesion to bone (Basbaum and Werb 1996). The tight adhesion restricts secreted protons and proteinases to a localized region, thus promoting efficient bone resorption (Teti, Colucci et al. 1992; Destaing, Saltel et al. 2005; Chabadel, Banon-Rodriguez et al. 2007; Luxenburg, Geblinger et al. 2007). Macrophages are another example of a cell with well characterized dependence on podosomes. In rare diseases of macrophage deficiency such as Wiskott-Aldrich syndrome (WAS), patients lack WASP protein, a key regulator of podosomes (see below). Macrophages isolated from these patients failed to form podosomes, suggesting a role of podosomes in macrophage function (Moulding, Blundell et al. 2007; Linder 2009). Invadopodia are also well characterized in cancer invasion and tumor metastasis. Cancer cells require polarized ECM degradation to facilitate directional migration and invasion, and invadopodia are sites allowing enrichment of protease activity at the cell surface promoting these activities (Basbaum and Werb 1996; Weaver 2006; Caldieri and Buccione 2010).

In addition to these well studied cell types, invadosomes have also been identified in a variety of other cells, and the list of cell types is growing (Thompson, Kleino et al. 2008; Onel and Renkawitz-Pohl 2009; Proszynski, Gingras et al. 2009). Additional invadosome-like structures have been described, though their exact relationship to invadosome is not clear. One example is the "invadosome-like protrusions" of leukocytes, which were thought to be a structure probing vascular endothelial cells to facilitate transcellular diapedesis (Carman, Sage et al. 2007; Carman 2009). Recently, invadosome-like structures have also been found in both porcine and human trabecular meshwork cells cultured under mechanical pressure and in perfused anterior segment organ culture (Hishida, Eguchi et al. 2008), suggesting that invadosomes might contribute to outflow resistance regulation. Notably, however, most of the biological functions of invadosomes were inferred by in vitro cell biology studies. The exact appearance and function of invadosomes in vivo remains a hot topic.

Assembly of the invadosome machinery requires multiple molecular events. The key events include actin nucleation and elongation, membrane deformation and SRC signaling (Thompson, Kleino et al. 2008; Albiges-Rizo, Destaing et al. 2009; Linder 2009). Actin nucleation was a prerequisite for invadosome assembly. Actin nucleation factor ARP2/3 complex and its activators WASP (Wiskott-Aldrich syndrome protein) or N-WASP (neuronal WASP) are enriched in podosomes and lack of these proteins disrupts invadosome formation (Hurst, Zuo et al. 2004; Yamaguchi, Lorenz et al. 2005; Olivier, Jeanson-Leh et al. 2006). WASP and N-WASP are activated by WIP (WASP interacting protein) and cortactin, which facilitates their interaction with ARP2/3. These proteins compose the key machinery that is indispensable for invadosome assembly. Actin elongation factors such as ENA/VASP family proteins were through to determine the rate of actin polymerization, thus contributing to invadosome dynamics (Albiges-Rizo, Destaing et al. 2009). As invadosomes are protrusive structures, factors such as BAR and F-BAR family proteins that mediate membrane curvature are likely also

important. These proteins form a local interaction with actin nucleation machinery therefore coordinating membrane deformation with actin assembly (Thomas, Sekhar et al. 2004). Non-receptor tyrosine kinase SRC is a master regulator of invadosome assembly and dynamics (Tarone, Cirillo et al. 1985; Soriano, Montgomery et al. 1991), as many of the key invadosome proteins can be phosphorylated by SRC. SRC phosphorylation not only directly regulates actin nucleation factors, but also regulates multidomain adaptor proteins which serve as a platform for invadosome assembly. One of the key adaptor proteins is the SH3 and PX domain containing family proteins.

The SH3 and PX domain containing family proteins

As a key structure regulating ECM, a function of invadosomes is to regulate the localization of MMPs. While MMPs could simply be secreted, as in some tissues they are, but other tissues require a more specific localization. The SH3 and PX domain containing family proteins play this role.

The SH3 and PX domain containing family proteins (also known as tyrosine kinase substrate family scaffold proteins) are a type of adaptor protein that has only recently been characterized. Currently there are two known molecules in this family, SH3PXD2A (also referred as FISH or TKS5) and SH3PXD2B (also referred as FAD49 or TKS4). As implied by their names, these proteins contain a Phox homolog (PX) domain at the N terminus followed by multiple SRC homology 3 (SH3) domains (five in SH3PXD2A and four in SH3PXD2B) at the C terminus. PX domains have phosphoinositide binding ability which facilitates protein docking to the membrane (Sato, Overduin et al. 2001; Wientjes and Segal 2003). SH3 domains are protein-protein interaction module recognizing mainly PXXP motifs as well as others (Kaneko, Li et al. 2008). In addition, the SH3 and PX domain family proteins contain several polyproline

motifs and SRC phosphorylation sites. The domain structures suggest that proteins in this family probably function as a dock recruiting other proteins to modulate signaling in localized subcellular domains.

SH3PXD2A is the first characterized protein in this family. It was initially identified in an antibody based cDNA library screen for Src tyrosine kinase substrates (Lock, Abram et al. 1998). When expressed in Src transformed cells, SH3PXD2A was shown to localize at punctuate structures which were found to be podosomes (Abram, Seals et al. 2003). The first binding partners for SH3PXD2A identified were metalloproteinases. With a phage display screen, SH3PXD2A was found to interact with several members of the a disintegrin and metalloproteinase (ADAMs) family. SH3PXD2A and ADAMs colocalize in podosomes. Knocking down endogenous SH3PXD2A levels disrupts podosomes (Seals, Azucena et al. 2005), suggesting a molecular requirement for SH3PXD2A in podosomes. SH3PXD2B remains less characterized. Similar to SH3PXD2A, SH3PXD2B is considered as a key podosomal adaptor protein (Buschman, Bromann et al. 2009). In cells lacking *Sh3pxd2b*, podosome formation is incomplete, and cells no longer degrade ECM. This phenotype can be restored by reintroducing *Sh3pxd2b*, but not *Sh3pxd2a*, suggesting the two molecules may have similar but not identical molecular functions.

Several studies have established the SH3 and PX domain containing proteins as essential organizers for invadosomes (Symons 2008; Oikawa and Takenawa 2009; Weaver 2009). In addition to metalloproteinases and SRC, these proteins can interact with multiple actin regulators required for invadosome formation. The known proteins include adaptor protein AFAP-110; RhoA regulator, p190RhoGAP; the SH3/SH2 adaptor, Grb2; the actin nucleation promoting factor N-WASP and cortactin (Oikawa, Itoh et al. 2008; Stylli, Stacey et al. 2009). Induced mislocalization of SH3PXD2A to mitochondria disrupts the distribution of some of these proteins (Crimaldi, Courtneidge et al. 2009), suggesting that SH3PXD2A is a main scaffold protein recruiting other key

proteins to sites of invadosome assembly. Interestingly, recent studies have demonstrated that reactive oxygen species produced by Nox (the reduced form of nicotinamide adenine dinucleotide phosphate oxidase) proteins are required for invadosome formation, and that the SH3 and PX domain containing proteins were the Nox organizers recruiting the Nox complex to sites of nascent invadosomes (Diaz, Shani et al. 2009; Gianni, Diaz et al. 2009; Weaver 2009). Therefore, the SH3 and PX domain containing family proteins link tyrosine kinase signaling, actin assembly machinery and reactive oxygen species together to promote cell migration, ECM degradation and invasion.

The SH3 and PX domain containing proteins have been implicated in several pathological conditions. Human cancer cell lines with reduced expression of SH3PXD2A and SH3PXD2B showed reduced gelatin degradation and invasion in vitro (Seals, Azucena et al. 2005; Buschman, Bromann et al. 2009). Similarly, delayed tumor growth and smaller sized lung metastases were observed when *Src* transformed NIH3T3 fibroblasts with reduced SH3PXD2A expression were either subcutaneously implanted or tail vein injected into immunocompromised mice (Blouw, Seals et al. 2008). The ability of cancer cells to invade correlates with their ability to form invadosomes. Thus, the SH3 and PX domain containing proteins likely contributes to tumor progression.

In addition to their role in invadosomes and cancer biology, SH3PXD2A and SH3PXD2B have been implicated in other diseases. It was found that the interaction between SH3PXD2A and its binding partner ADAM12 mediates Aβ induced neurotoxicity in primary cortical neuronal culture (Malinin, Wright et al. 2005). Both SH3PXD2A and ADAM12 are on human chromosome 10, near a locus previously linked to a form of late onset Alzheimer's diseases (Bertram, Blacker et al. 2000). Interaction between these two genes was indicated in an association study as contributing to the susceptibility to Alzheimer's disease (Harold, Jehu et al. 2007); although another large scale study failed to replicate the result (Laumet, Petitprez et al.). SH3PXD2B has also been implicated in obesity. In an in vitro model of preadipocyte differentiation, *Sh3pxd2b*

expression was found to be indispensable in the early stage of differentiation (Hishida, Eguchi et al. 2008; Hishida, Nishizuka et al. 2009). A few genome-wide association studies have reported an association between SNPs from *SH3PXD2B* and increased body mass index (Zhao, Pearson et al. 2003; Liu, Wang et al. 2008); however in another independent study, the association was not confirmed (Vogel, Greene et al. 2009). Both Alzheimer's diseases and obesity are complex traits. Thus, the conflicting results of various studies may just reflect challenges intrinsic to this kind of analysis. Further investigations are obviously required, and mouse models with mutations in the SH3 and PX domain family proteins may be required to more stringently test the potential disease pathogenecity of these variations.

The overall goal for my thesis work has been to utilize mouse genetics to expand the glaucoma genetic pathway. The findings of this thesis are organized as follows. In chapter 2, I will describe the initial identification and characterization of the *nee* strain and the disease causing mutation, *Sh3pxd2b*, and the characterization of the molecular function of SH3PXD2B. This part of the thesis work has been published (Mammalian Genome. 2009 Aug; 20(8):462-75) where it was also featured on the cover. Because the initial ocular phenotypes of *nee* are suggestive of glaucoma, in chapter 3, I will specifically examine glaucoma related aspects of the *nee* phenotype. In Chapter 4, I will present the relevance of *SH3PXD2B* in human diseases. Finally, in Chapter 5, I summarize the overall conclusions of my work and offer suggestions for potential new avenues of research that may stem from these findings.

Figure 1. Iridocorneal angle.

(**a**) The major structures in the anterior segment of the eye are shown. The anterior segment refers to the structures in front of the vitreous humor, including the cornea, iris, ciliary body and lens. The anterior chamber refers to the space between the posterior cornea and the iris. Iridocorneal angle structures refer to the trabecular meshwork and the Schlemm's canal located at the angle between the iris and cornea. (**b**) Aqueous humor flow in the anterior chamber. Aqueous humor is produced by the ciliary body process. It then flows through the pupil into the anterior chamber and exits the eye mainly through the trabecular outflow pathway (through the trabecular meshwork, the Schlemm's canal and the connecting tubes in the sclera). The black arrows indicate the major flow route. Additionally, a small portion of the aqueous humor flows through the uveoscleral outflow pathway (through the extracellular spaces in the ciliary muscle, the anterior choroid and suprachoroidal space, and the adjacent sclera). The dashed arrows indicate the uveoscleral outflow route. Images courtesy of National Eye Institute.

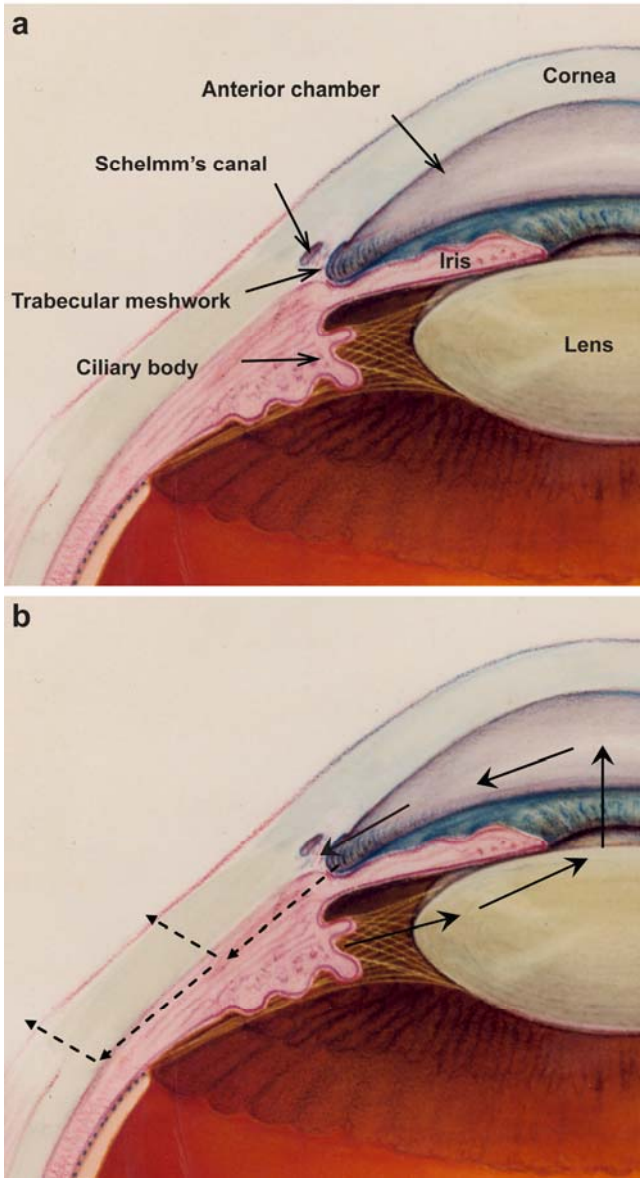
a
Anterior chamber
Cornea
Schelmm's canal
Iris
Trabecular meshwork
Lens
Ciliary body
b

Figure 2. The anatomy of the retina and optic nerve head.

(**a**) The main structures in the posterior eye. (**b**) Layers of neurons in the retina. The light is received by rods and cones (photoreceptor cells), which synapse directly onto bipolar cells. Bipolar cells synapse with retinal ganglion cells which conduct action potentials to the brain. Horizontal and amacrine cells transmit laterally information (modify signals from neurons in the same layer). Ganglion cells and their axons are the cells influenced by glaucoma. Images courtesy of National Eye Institute.

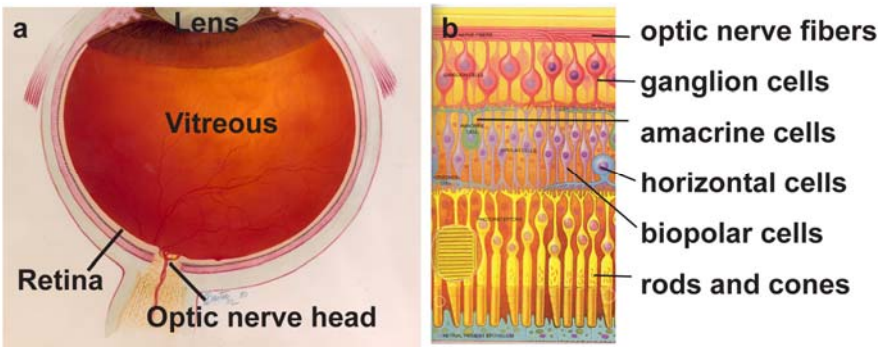
a
Lens
Vitreous
Retina
Optic nerve head
b
optic nerve fibers
ganglion cells
amacrine cells
horizontal cells
biopolar cells
rods and cones

Figure 3. Optic nerve head excavation.

(**a**) The normal healthy optic nerve head, also referred as the optic disc, is the circular area in the back of the inside of the eye where the optic nerve connects to the retina. There is a central depression in the optic nerve head, which is called the optic cup. The ratio of the size of the optic cup to the optic disc is used to measure glaucoma. (**b**) In the advanced glaucomatous state, while the optic disc stays the same, the optic cup is broader and deeper than a physiological cup in a normal eye. Images courtesy of National Eye Institute.

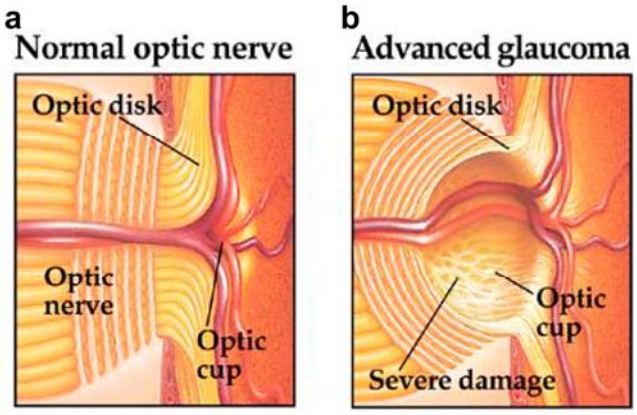
a
Normal optic nerve
Optic disk
Optic nerve
Optic cup
b
Advanced glaucoma
Optic disk
Optic cup
Severe damage

Figure 4. Invadosomes.

(**a**) Podosomes in primary macrophages. The podosomes have a core structure (stained for F-actin, blue) and a surrounding ring structure (stained for vinculin, red). (**b**) Invadopodia in melanoma cells. The invadopodia mostly comprise core structures (stained for F-actin, blue and cortactin, red). This figure was reproduced with permission from Linder, S (2009) Invadosome at a glance. J Cell Sci 122(Pt17): 3009-13.

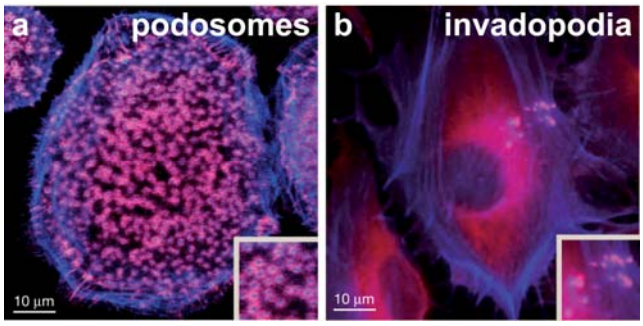
a
podosomes
10 µm
b
invadopodia
10 µm

Table 1. Genes and loci associated with glaucoma

Chromosal Location	Phenotype	Locus	Gene
1q21-31	Early and adult onset POAG	GLC1A (JOAG1)	*MYOC*
2cen-q31	Adult onset POAG	GLC1B	
3q21-24	Adult onset POAG	GLC1C	
8p23	Adult onset POAG	GLC1D	
10p15-14	Adult onset POAG, low tension glaucoma	GLC1E	*OPTN*
7q35-q36	Adult onset POAG	GLC1F	
5q22.1	Adult onset POAG	GLC1G	*WDR36*
14q11-q13	Adult onset POAG	GLC1H	
15q11-13	Adult onset POAG	GLC1I	
9q22	Early and adult onset POAG	GLC1J (JOAG2)	
20p12	Early and adult onset POAG	GLC1K (JOAG3)	
3p21-22	Early and adult onset POAG	GLC1L (JOAG4)	
5q22.1-q32	Early and adult onset POAG	GLC1M (JOAG5)	
15q22-q24	Early and adult onset POAG	GLC1N (JOAG6)	
19q12	Adult onset POAG		
17q25.1-25.3	Adult onset POAG		
14q11.1-11.2	Adult onset POAG		
14q21.1-q21.3	Adult onset POAG		
17p13	Adult onset POAG		
10p12.33-p12.1	Adult onset POAG		
2q33.1-q33.3	Adult onset POAG		
2p14	Adult onset POAG		
2p15-16	Adult onset POAG		
1p32	Adult onset POAG		
10q22	Adult onset POAG		
2p21	Congenital glaucoma, Peter's anomaly	GLC3A	*CYP1B1*
1p36	Congenital glaucoma	GLC3B	
14q24.3	Congenital glaucoma	GLC3C	
6p25	Axenfeld-Reiger, congenital glaucoma	IRD1	*FOXC1*
4q25-27	Axenfeld-Reiger, iridogoniodysgenesis	RIEG (IRD2)	*PITX2*
13q14	Axenfeld-Reiger	RIEG2	
11p13	Aniridia, Peters anaomaly, Axenfield-Reiger	AN2	*PAX6*
7q35-q36	Pigment dyspersion syndrome	GPDS1	
15q24.1	Exfoliation glaucoma		*LOXL1*
11p	Nanophthalmos	NNO1	
11q12	Nanophthalmos	VMD2	
11q23	Nanophthalmos	MFRP	

Abbreviations: POAG, primary open angle glaucoma; JOAG, juvenile open angle glaucoma; *MYOC*, myocilin; *OPTN*, optineurin; CY*P1B1*, cytochrome P450 1b1; *FOXC1*, forkhead box C1; *PITX2*, paired-like homeodomain 2; *PAX6*; paired box gene 6; *LOXL1,* lysyl oxidase-like 1.

Table 2. Mouse models of glaucoma

Model	Mechanisms	Onset of Elevated IOP	Onset of ON damage	Techanical Difficulty
Pressure models (spontaneous)				
DBA/2J	Gene prediposed to outflow blockage	8-12 month	11-15 month	N/A
DBA/2NNia	Gene prediposed to outflow blockage	6-9 month	15 month	N/A
AKXD-28/Ty	Gene prediposed to outflow blockage	15-18 month	17-22 month	N/A
Col1a1 $^{r/r}$	Gene prediposed to outflow blockage	4 month	12 month	N/A
MYOC Y437H transgenic	Gene prediposed to outflow blockage	18 month	18 month	N/A
Vav2 $^{-/-}$ *Vav3* $^{-/-}$	Gene prediposed to outflow blockage	1.5 month	3 month	N/A
Pressure models (induced)				
Episcleral hypertonic saline	Sclerosis of aqueous outflow pathway	2 weeks post injection	3 month post injection	High
Photocoagulation	Photo occlusion of outflow pathway	4 weeks post treatment	4 weeks post treatment	Medium
Extraocular vein cautery	Occlusion of outflow pathway	1 week post surgery	2 weeks post surgery	Low
Nonpressure models (induced)				
Intravitreal excitatory amino acid	NMDA receptor mediated RGC toxicity	N/A	6 day after injection	Low
Optic nerve injury	Optic nerve transection/crush induced damage	N/A	14-60 days after treatment	Medium
Retinal ischemia reperfusion	Transient ischemia induced damage	N/A	12 hours after reperfusion	Medium
Endothelin	Direct endothelin toxicity and vessel constriction	N/A	21-84 days of treatment	Medium/High

Table adapted from source: Pang, I. H. and A. F. Clark (2007). "Rodent models for glaucoma retinopathy and optic neuropathy." J Glaucoma **16**(5): 483-505.

CHAPTER 2
INDENTIFICATION AND CHARACTERIZATION OF NEE, A SPONTANEOUS SH3PXD2B MOUSE MUTANT

Introduction

Invadosomes (podosomes and invadopodia) are specialized adhesion structures involved in cell matrix adhesion and extracellular matrix (ECM) remodeling. Structurally, Invadosomes are characterized by an actin dense core surrounded by a ring of additional proteins that drive focal membrane protrusions into surrounding tissues. Functionally, adhesion molecules and matrix metalloproteinases are enriched in Invadosomes, allowing these finger-like protrusions to interact with and modify surrounding ECM. These features are thought to allow Invadosomes to play important physiologic roles in several cell types requiring motility or ECM degradation (Spinardi and Marchisio 2006; Weaver 2008; Linder 2009).

Many protein components of the podosome-type adhesion machinery have been identified. These include actin and actin modulating proteins that form the core structure, cell adhesion receptors linking cells to ECM, proteinases mediating ECM remodeling, protein kinase transducing signals, and membrane trafficking proteins facilitating protein recruitment (Thompson, Kleino et al. 2008; Linder 2009). Amongst these proteins, two key regulators are SRC and SH3PXD2A (commonly referred to as TKS5). The tyrosinase kinase SRC is a key molecule for inducing Invadosomes (Destaing, Sanjay et al. 2008; Thompson, Kleino et al. 2008). SH3PXD2A is a substrate of SRC (Lock, Abram et al. 1998) and has been described as a major organizer of Invadosomes by multiple groups (Seals, Azucena et al. 2005; Oikawa, Itoh et al. 2008; Symons 2008; Thompson, Kleino et al. 2008). Upon SRC activation SH3PXD2A is recruited to the plasma membrane through interactions with PtdIns(3,4)P_2, which is enriched in podosomes (Abram, Seals et

al. 2003; Oikawa, Itoh et al. 2008). Recruitment of SH3PXD2A subsequently recruits other molecules such as WAS and WASL (commonly referred to as WASp and N-WASp, respectively), which stimulate ARP 2/3 complex-mediated actin nucleation and podosome extension (Oikawa, Itoh et al. 2008). Recently, a homolog of SH3PXD2A, SH3PXD2B, has been identified and shown to also influence podosomes of cells in culture (Seals, Azucena et al. 2005; Buschman, Bromann et al. 2009). Although identification of SH3PXD2A and SH3PXD2B in cells in culture suggests that these adaptor proteins are likely to play determinative roles influencing behavior of Invadosomes, much remains unknown concerning the function of these proteins within the physiological context of the whole animal.

Here, we present identification and mutant phenotypes associated with a unique spontaneously arising allele of *Sh3pxd2b* in mice. Mice homozygous for the *nee* mutation exhibit runted growth and striking developmental abnormalities of several mesenchymal derived tissues, including craniofacial structures, the ocular irideocorneal angle, and white adipose tissue. Through genetic crosses designed to identify the basis of the *nee* mutation, we demonstrate a 1 bp deletion in the *Sh3pxd2b* gene. Based on sequence homology, the *Sh3pxd2b* gene is predicted to encode an adaptor protein with homology to SH3PXD2A, a key regulator of Invadosomes. Testing the hypothesis that the SH3PXD2B protein is indeed a podosomal-adaptor protein, we demonstrate here that SH3PXD2B also localizes to podosomes, and as expected for an adaptor protein, is capable of binding transmembrane metalloproteinases such as ADAM15. Combined, these data support a role for SH3PXD2B as a podosomal-adaptor protein and implicate podosomes as important biological regulators of mammalian postnatal growth and development.

Materials and methods

Animal husbandry

All mice were obtained from The Jackson Laboratory, Bar Harbor, Maine. Mice were subsequently housed and bred at the University of Iowa Research Animal Facility. The spontaneous *nee* mutation arose in strain B10.A-*H2*^{h4}/(4R)SgDvEg at generation F51 and subsequently was maintained by the Mouse Mutant Resource of The Jackson Laboratory (http://mousemutant.jax.org/index.html). Since both male and female homozygotes are infertile, the strain was maintained by progeny testing or ovarian transplantation. In the past, the mutation has also been referred to as *nm2702* (Chang, Hawes et al. 2005). With advice of The Mouse Genomic Nomenclature Committee, the mutation will here after be referred to as *nee* to indicate phenotypic defects associated with the mutation (nose, eye, ear). Upon molecular identification of the mutation, mice were genotyped by assaying the absence or presence of an *RsaI* restriction enzyme site abolished by the *nee* mutation and the stock maintained in heterozygote X heterozygote crosses. Mice were maintained on a 4% fat NIH 31 diet provided *ad libitum* and were housed in cages containing dry bedding (Cellu-dri; Shepherd Specialty Papers, Kalamazoo, MI). The environment was kept at 21°C with a 12-hour light: 12-hour dark cycle. All animals were treated in accordance with the Association for Research in Vision and Ophthalmology Statement for the Use of Animals in Ophthalmic and Vision Research. All experimental protocols were approved by the Animal Care and Use Committee of The University of Iowa or The Jackson Laboratory.

Craniofacial assessment

Craniofacial measurements were made for mutants and controls on skulls prepared by incomplete maceration in potassium hydroxide, stained with alizarin red, and

stored in undiluted glycerin (Green 1952). A set of 7 standard skull measurements were collected using digital hand calipers (Stoelting, Wood Dale, IL). Landmarks were adapted from those used by Dr. Joan Richtsmeier to characterize craniofacial morphology in mouse models of Down Syndrome (Richtsmeier, Baxter et al. 2000) and have been validated for accuracy and precision by the Craniofacial Resource at The Jackson Laboratory (http://craniofacial.jax.org/).

Slit-lamp examination

Anterior chamber phenotypes were assessed with a slit-lamp (SL-D7; Topcon, Tokyo, Japan) and photodocumented with a digital camera (D100; Nikon, Tokyo, Japan). Images were taken with identical camera settings and prepared with identical image software processing.

Magnetic resonance and X-ray imaging

Imaging of adipose tissue by magnetic resonance imaging (MRI) was performed on a 4.7 Tesla Varian Unity/INOVA small-bore MRI system (Varian Inc., Palo Alto, CA). After anesthesia with isoflurane, T1-weighted images were acquired in the coronal plane using a fast spin-echo pulse sequence with TR/TE = 600/12 ms, an echo train length of 2, and 4 averages. A matrix size of 512 x 128 covered a field of view of 60–90 mm x 30 mm with 15 slices of 1.1–1.5 mm thickness separated by a 0.2–0.5 mm gap depending on the size of the animal. Imaging of skeletal morphology by X-ray was performed with euthanized mice and a Faxitron MX20 Specimen X-ray system (Faxitron X-Ray LLC, Lincolnshire, IL) using 25 kV 1 min exposures on Kodak Portal Pack Oncology X-ray film.

Auditory-evoked brain stem response analysis and ear histology

Auditory-evoked brain stem response (ABR) threshold analysis was performed using previously described methods (Mao, Thedens et al. 2009). Briefly, mice anesthetized with tribromoethanol were presented with broad-band click and pure tone 8-, 16-, and 32-kHz stimuli at intensities varying between 10 and 100 dB SPL (decibels sound pressure level), and the evoked brain stem responses were recorded. Auditory thresholds were obtained for each stimulus by varying the SPL at 5-dB steps to identify the lowest level at which an ABR pattern can be recognized. Inner and middle ears were dissected from the skull following perfusion with Bouin's fixative. Tissues were decalcified in Bouin's fixative for 14 days and embedded in paraffin. Cross sections were cut at 7 μm, mounted on glass slides, and stained with hematoxylin/eosin.

Measurement of body composition and bone mineral density

Areal bone mineral density of the whole body and percent fat body mass were determined on mice anesthetized by intraperitoneal injection with Avertin (tribromoethanol stabilized in tertiary amyl hydrate), 1 mg per 2 g of body weight. Data were collected using a PIXImus small animal dual-energy X-ray absorptiometry (DEXA) densitometer (GE Healthcare, Waukesha, WI), reconfigured with lower X-ray energy than in human DEXA machines in order to achieve contrast in small specimens, and utilizing manufacturer supplied software (Lunar PIXImus version 1.46). Resolution of the PIXImus is 0.18 x 0.18 mm pixels with a usable scanning area of 80 x 65 mm. Calibration and daily quality assurance was achieved using a phantom with known values.

Gene mapping and sequencing

To determine the chromosomal location of the *nee* mutation, B10.A-*H2*^{h4}/(4R)SgDvEg-*nee* mice were mated with CAST/EiJ mice and the F1 mice, which exhibited no visible abnormalities, were intercrossed to produce F2 mice. Genomic DNA of 45 affected F2 progeny was prepared as previously described (Buffone and Darlington 1985) and genotyped by analyzing polymorphic microsatellite markers by agarose electrophoresis, utilizing standard conditions and protocols. The initial genome scan was carried out on pooled DNA samples. After detection of linkage on Chr 11, microsatellite markers *D11Mit295, D11Mit19, D11Mit152, D11Mit215* and *D11Mit186* were scored on individual DNA samples. Candidate genes localized to the critical region between markers *D11Mit19* and *D11Mit186* were identified by scanning the Ensembl genome database (Release 53). Following PCR amplification of exons of interest from genomic DNA isolated from either the mutant B10.A-*H2*^{h4}/(4R)SgDvEg-*nee* or wild-type parental B10.A-*H2*^{h4}/(4R)SgDvEg strain, products were purified (QIAquick PCR Purification Kit; Qiagen, Inc., Valencia, CA), sequenced by automated fluorescence tagged sequencing, and directly compared to each other. Confirmation of the *nee* mutation was performed by PCR amplification of a 713 bp DNA fragment flanking the deleted adenine residue (using primers: forward: 5' AGGCTCAGTTGCCCTGAATGTA 3'; reverse: 5' TTCTCAGCGGGAACTTGCTCTT 3') from various strains of mice and digestion of the amplicons with *Rsa*I. DNA containing the *nee* allele is predicted to be resistant to cleavage, while wild-type alleles are predicted to give rise to products of 546 bp and 167 bp. Numeration for the *Sh3pxd2b* mRNA is based on NCBI RefSeq NM_177364.3.

Preparation of anti-SH3PXD2B antiserum

Constructs generating GST-fused SH3PXD2B were generated by PCR-assisted cloning. To reduce the possibility for cross reaction with the closely related SH3PXD2A

protein, the antibody was raised against a region between the third and fourth SH3 domains of SH3PXD2B having low identity with SH3PXD2A. Using oligonucleotides specific to a portion of *Sh3pxd2b* exon 13 (encoding amino acids 440–751) and genomic DNA of C57BL/6J mice as template, the resulting amplification product was first cloned into a TA cloning vector (pCR2.1-TOPO vector; Invitrogen, Carlsbad, CA) and then subcloned into a GST gene fusion vector (pGEX6p-1; GE Healthcare, Piscataway, NJ). Correct fusion of this construct was confirmed by automated fluorescence tagged sequencing. Following transformation into the BL21 (DE3) strain of *Escherichia coli*, protein expression was induced and cell lysates collected. GST-fused protein was first purified using a glutathione-Sepharose 4B column followed by excision of GST from the protein (PreScission protease; GE Healthcare, Piscataway, NJ). SH3PXD2B-specific antiserum was generated in rabbits and affinity purified (Sigma-Genosys; The Woodlands, TX).

Construction of plasmids encoding GFP-SH3PXD2B

Plasmids encoding GFP-fused full-length SH3PXD2B (GFP-SH3PXD2B) were constructed by PCR-assisted cloning. DNA fragments containing wild-type *Sh3pxd2b* were amplified by RT-PCR from total RNA extracted from eyes of C57BL/6J mice. The resulting fragments were first cloned into an entry vector (pCR8/GW/TOPO; Invitrogen, Carlsbad, CA) and then subcloned by LR recombination into an expression vector containing an N-terminus GFP tag (pcDNA-DEST53; Invitrogen, Carlsbad, CA). Plasmids encoding GFP-fused mutant SH3PXD2B with the 1303A deletion (GFP-SH3PXD2B^{1303delA}) were constructed by PCR based site-directed mutagenesis using the wild-type construct as a template. Sequences of both plasmid inserts were confirmed by automated fluorescence tagged sequencing.

Cell culture and transfection

Cells were maintained at 37°C in a humidified atmosphere containing 5% CO_2. HEK 293T and mouse NIH3T3 cells were cultured in DMEM supplemented with 10% FBS, 100 units/ml penicillin, and 100 units/ml streptomycin. Formation of podosomes was induced by transient transfection of a previously described constitutively active *Src* (Y529F) construct (Hewitt, Sharma et al. 2008). Transfections utilized the Lipofectamine 2000 transfection reagent (Invitrogen, Carlsbad, CA) with additional use of the PLUS Reagent enhancing agent (Invitrogen, Carlsbad, CA) in NIH3T3 cells, following the manufacturer's recommended protocols.

Immunofluorescence and microscopy

Cells cultured on coverslips were fixed in 4% paraformaldehyde in PBS for 10 min and incubated in permeabilization buffer (0.1M glycine, 0.05% Triton X-100 in PBS) containing 3% BSA for 30 min. Following permeabilization, cells were blocked with permeabilization buffer containing 15% goat serum and 3% BSA for 15 min. Fixed cells were incubated with anti-SH3PXD2B antibody for 1 hr (1:200 dilution in permeabilization buffer with 1% BSA and 1% goat serum), washed with PBS, and incubated with a 1:200 dilution of secondary antibody and 1:100 dilution of phalloidin (Alexa633-conjugated goat anti-rabbit and Alexa546-phalloidin; Invitrogen, Carlsbad, CA). After mounting (ProlongGold; Invitrogen, Carlsbad, CA), cells were imaged with a confocal microscope (Zeiss LCM 510; Carl Zeiss MicroImaging, Inc., Thornwood, NY). Cells transfected with GFP-fusion plasmids were fixed with 4% paraformaldehyde in PBS for 10 min; following washes, cells were mounted and imaged as described above.

GST pull-down assay

GST and a GST-fusion containing the fourth SH3 domain spanning amino acids 842-908 of SH3PXD2B (GST-SH3#4) were expressed in BL21 (DE3) cells and purified using a glutathione-Sepharose 4B column (GE Healthcare, Piscataway, NJ). Cell lysates (50 µg) were incubated with glutathione-Sepharose 4B beads for 2 h at 4°C, washed, and then blocked in EB buffer (10 mM Tris-HCl pH 7.4, 50 mM NaCl, 1% Triton X-100, 50 mM NaF, 0.1% BSA, 2 mM Na_3VO_4) supplemented with an additional 5% BSA at 4°C overnight. HEK 293T cells expressing MYC-tagged full length ADAM15 were generated using PCR to amplify the *Adam15* cDNA followed by cloning with gateway technology into an expression vector (pcDNA-DEST53; Invitrogen, Carlsbad, CA). 293T cells transfected with *Adam15-myc* plasmid were lysed 48 h after transfection in EB buffer supplemented with 1 mM PMSF and a mix of additional protease inhibitors (Complete Mini Protease Inhibitor Cocktail; Roche Applied Science, Indianapolis, IN). Cell debris was removed by centrifuging at 12,000 rpm for 10 min. GST-fusion coated beads were washed 3 times with EB buffer and incubated with 1 mg total cell lysates for 2 hours at 4°C. Following 6 washes with EB buffer, beads were recovered by centrifugation and dissolved in Laemmli buffer. Bound protein was analyzed by 7.5% SDS-PAGE and immunoblotting. Blots were blocked with 10% BSA in TBST (Tris-buffered saline with 0.1% Tween-20) followed by antibody incubations and washes in TBST using 1:1000 dilution of anti-c-MYC rabbit polyclonal antibody (Novus Biologicals, Littleton, CO) and 1:4000 dilution of horseradish peroxidase conjugated goat anti-rabbit IgG (Invitrogen, Carlsbad, CA). Immunoreactivity was detected by enhanced chemiluminescence methodology (GE Healthcare, Piscataway, NJ).

Tissue expression analysis

Protein levels of SH3PXD2B in various tissues were analyzed with western blot. Tissues dissected from a mouse from the *nee* colony homozygous for wild-type *Sh3pxd2b* alleles were minced and homogenized with a rotor/stator tissue homogenizer in cell lysis buffer (50mM Tris-HCl pH 7.4, 150mM NaCl, 1mM EDTA, 0.1% Triton X-100, 0.1% SDS) supplemented with 1 mM PMSF and a mix of additional protease inhibitors (Halt Proteinase Inhibitor Cocktail; Thermo Scientific, Rockford, IL). Total tissue lysates were centrifuged at 14,000 rpm for 20 min at 4°C. Protein concentration in the resulting supernatant was determined using the BCA protein assay reagent (Sigma-Aldrich, St Louis, MO). Using 50 µg of lysate per lane, protein from each tissue was electrophoresed on 7.5% SDS-PAGE gels and transferred to membranes (Immobilon-FL membrane; Millipore, Bedford, MA). Membranes were blocked for 1 h at room temperature in Odyssey Blocking Buffer (LI-COR Biosciences, Lincoln, NE) diluted 1:1 in PBS. All antibody incubations were performed using a 1:1 solution of Odyssey Blocking Buffer and PBS supplemented with 0.2% Tween-20. Primary antibody was incubated with membranes at 4°C overnight using a 1:2000 dilution of anti-SH3PXD2B rabbit polyclonal antibody. As a control for protein transfer, membranes were similarly incubated with 1:1000 dilution of anti-β-actin rabbit polyclonal antibody (Sigma-Aldrich, St Louis, MO). After washes with PBS, membranes were incubated for 1 h at room temperature with secondary antibody diluted 1:2000 (IRDye680 goat anti-rabbit IgG; LI-COR Biosciences, Lincoln, NE) and visualized with an infrared scanner (Odyssey Infrared Imaging System; LI-COR Biosciences, Lincoln, NE).

Results

The spontaneous *nee* mutation causes growth, craniofacial, ocular, and ear defects

Following a phenotype-driven approach for identifying new mouse models of human disease, the *nee* mutation is a spontaneously arising mutation that was initially identified by the Mouse Mutant Resource of The Jackson Laboratory. Mice homozygous for the *nee* mutation were initially recognized because of their small body size, abnormal craniofacial morphology, and ocular defects (Figure 5).

The most obvious defect of *nee* homozygotes was their small body size (Figure 5a, b). At birth, *nee* homozygotes were visibly indistinguishable from wild-type mice. By 2 months of age, *nee* homozygotes were dramatically smaller in body weight (10.2 ± 1.5 g; mean ± SD; $n = 4$) compared to either heterozygote (18.8 ± 0.7 g; $n = 9$) or wild-type (18.0 ± 1.9 g; $n = 5$) littermates ($P < 0.004$ in both comparisons, Student's *t*-test). Subsequent to 2 months of age, while heterozygous and wild-type mice both continued to grow in body weight, mice homozygous for the *nee* mutation did not. As heterozygous and wild-type mice reached normal adult weights by 6–12 months of age (28.3 ± 5.1 g; $n = 11$ and 28.0 ± 7.9 g; $n = 5$; respectively), *nee* homozygotes remained runted at both the 3–5 month (10.9 ± 1.9 g; $n = 8$) and 6–12 month (11.7 ± 2.7 g; $n = 7$) age periods. As a consequence, the difference in body weight among adult mice was highly significant ($P < 0.0007$ comparing homozygotes to heterozygotes or wild-type littermates, 6–12 month old mice, Student's *t*-test).

Two additional externally visible phenotypes were initially appreciated in *nee* homozygotes. All *nee* homozygotes have craniofacial and ocular abnormalities. Compared to control mice, all *nee* homozygotes had shortened noses (nose length: skull length = 0.629; heterozygous littermates = 0.687) and domed skulls (skull length: skull width = 1.750; heterozygous littermates = 2.141; $n = 12$ mice per group; $P < 0.0001$;

Student's *t*-test) (Figure 5c, d). Also, eyes of all *nee* homozygotes had abnormalities (Figure 5e–h), typically appearing bulging with white corneal opacities. Examined by ophthalmic slit-lamp, corneal opacities of varying severity were confirmed in all eyes of *nee* homozygotes (n = 14 mice, 1–8 months in age), whereas corneal opacities were rare in eyes of age-matched controls (a single corneal opacity was observed from all mice examined; n = 12 heterozygous littermate controls, 11 wild-type littermate controls). Where unobstructed views of the anterior chamber were possible in *nee* homozygotes, peripheral anterior synechia were always observed and the anterior chamber depth was increased. Combined, these clinical observations indicated that *nee* homozygotes have a developmental anterior segment dysgenesis.

In addition to the externally visible phenotypes of *nee* homozygotes described above, several other phenotypes were also discovered. First, both male and female homozygotes were infertile. Fertility could be restored by ovarian transplants of ovaries from homozygotes to wild-type mice and mating to heterozygous males, indicating that the reason for female infertility did not reside in the ovary but elsewhere in the female reproductive tract. Second, *nee* homozygotes had multiple skeletal abnormalities (Figure 6). Examination of skeletal structures by radiographic analysis indicated that *nee* homozygotes have a proportionally smaller skeleton (Figure 6a) and abnormalities of the skull (Figure 6b, c). Radiography of the skull from *nee* homozygotes again indicated a reduced length along the anterior-posterior axis. Higher magnification images of the hind leg (Figure 6d, e) showed reduced dimensions, but otherwise normal gross anatomy. Both the skull and hind leg of *nee* homozygotes exhibited decreased radio-opacity, suggesting a potential decrease in bone density. To test this quantitatively, DEXA analyses were performed. In comparison to sex-matched heterozygous littermates, 12-week-old *nee* homozygotes exhibited reduced areal bone mineral density (aBMD). This difference was present in both males (*nee* homozygotes, 0.035 g/cm^2; heterozygous littermates, 0.048 g/cm^2) and females (*nee* homozygotes 0.031 g/cm^2; heterozygous littermates, 0.049

g/cm^2) and was statistically significant (n = 6 mice per sex per genotype; $P < 0.0001$; Student's t-test). Female homozygotes had significantly lower aBMD than male homozygotes ($P < 0.001$; Student's t-test); there was no sex difference in heterozygotes. Third, mice homozygous for *nee* have hearing impairment and middle ear pathology (Figure 7). ABR measurements revealed that *nee* mice have elevated thresholds to broad-band click and 8 kHz, 16 kHz, and 32 kHz pure tone stimuli (Figure 7a). Hearing impairment was neither progressive nor frequency dependent, as elevated ABR thresholds (40–50 dB above normal) were found in all four stimuli at all ages tested (n = 13 *nee* homozygotes and 3 heterozygous control mice; 34–92 days of age). Histological analysis further revealed that hearing impairment in these mice was likely due to middle ear inflammation (otitis media, Figure 7b, c). Serous fluid with diffuse neutrophils was found in the middle ear cavities of all *nee* homozygotes examined, but not in control mice (n = 6 *nee* homozygotes and 3 heterozygous control mice), and the surrounding epithelium was markedly thickened by fibrous connective tissue and embedded neutrophils. No other structural abnormalities were observed. Similar results have previously been observed; mice with craniofacial abnormalities that include middle ear cavity or Eustachian tube dysmorphologies often develop otitis media (Mao, Thedens et al. 2009). Together, these results indicate that *nee*-mediated hearing deficiency is likely a secondary consequence of the craniofacial abnormalities of *nee* homozygotes, which presumably render the middle ear sensitive to infection. Finally, *nee* homozygotes developed a form of lipodystrophy (Figure 8). Initially noted in dissections (Figure 8a, b), and subsequently confirmed with MRI (Figure 8c–h), adult *nee* homozygotes had severely depleted visceral and subcutaneous white adipose tissue (n = 3 mice examined, 6–11 months in age). In contrast, residual interscapular brown adipose tissue was still present. Adipose defects were less striking in young mice. While adipose defects were not observable by MRI in young mice, DEXA analyses showed a subtle reduction in percent body fat in 12-week-old *nee* homozygotes compared to heterozygous littermate

controls (14% vs 19% respectively, $n = 20$ mice per group; $P < 0.001$; Student's *t*-test). With the exception of aBMD, no other sex-specific differences were observed in any phenotypes of *nee* mice. Aside from the above mentioned defects, *nee* homozygotes were otherwise relatively healthy, with many mice living to at least 12 months of age.

The *nee* mutation maps as a recessive factor to Chr 11

In order to identify the molecular basis of the *nee* mutation, an intersubspecific intercross between CAST/EiJ and *nee* mice was performed (Figure 9). Whereas on the B10.A-*H2*^{h4}/(4R)SgDvEg genetic background, the *nee* mutation was fully penetrant and close to the expected 25% of affected progeny were produced in heterozygous matings (60 mutants / 300 total mice born = 20%), heterozygotes from the intercross with CAST/EiJ produced lower than the expected number of mutants in the F2 generation (27 mutants / 224 total mice born = 12%) and of the mice born, 5% of homozygotes died before weaning. Linkage analysis revealed that *nee* segregates as a simple recessive factor. Haplotype analysis based on 45 F2 affected mice mapped the mutation to a region on Chr 11 (Figure 9a). The minimal critical region defining the *nee* interval was delimited proximally by marker *D11Mit19* and distally by marker *D11Mit186*, spanning a 9.7 Mb region.

The *nee* mutation is caused by a 1 bp deletion in *Sh3pxd2b*

According to the Ensembl genome database, the *nee* critical region included a total of 65 protein coding genes encompassed by 718 exons. A sequence-driven approach was utilized to identify the mutation. Based on previously described phenotypes of targeted mutations in mice, several genes in the interval were initially considered reasonable candidates, including *Fgf18* and *Npm1* (Ohbayashi, Shibayama et al. 2002; Grisendi, Bernardi et al. 2005). However, sequencing of all known exons from these

candidates failed to detect any changes. In continuing analysis of the region, a total of 225 different exons divided among multiple genes were analyzed. From these, the *nee* mutation was identified as a 1 bp deletion in the last exon of *Sh3pxd2b* at nucleotide position 1303 of the predicted mRNA (Figure 9b). The 1303delA change was the only change detected and was confirmed by independent amplification and sequencing of two additional affected mice (data not shown).

To stringently confirm the status of the 1303delA alteration as a unique mutation, a restriction enzyme based assay distinguishing this allele was designed. The 1303delA deletion disrupts an *Rsa*I restriction site. Therefore, DNA containing the wild-type allele should be sensitive to *Rsa*I digestion while *nee* DNA should be resistant. Using this assay, 10 phenotypically normal inbred mouse strains were examined for the potential presence of the *nee* allele (Figure 9c). Resistance to *Rsa*I digestion was present only in *nee* DNA and not in DNA from other phenotypically normal strains, confirming that the 1 bp deletion in *Sh3pxd2b* was unique and highly likely to be the mutation of *nee* mice.

The *Sh3pxd2b* gene is predicted to encode a 908 amino acid protein with an N-terminus PX domain and four SH3 domains (Figure 9d). The 1303delA deletion is predicted to cause a frameshift altering 37 amino acids before causing a premature stop codon and protein truncation altering a portion of the third SH3 domain and completely deleting the fourth SH3 domain (Figure 9d). To investigate the potential influence of the1303delA deletion on localization of the SH3PXD2B protein, GFP fusion constructs encoding the wild-type (GFP-SH3PXD2B) and mutant proteins (GFP-SH3PXD2B^{1303delA}) were transfected into HEK 293T cells (Figure 10). As previously observed by others (Hishida, Eguchi et al. 2008), the absence or presence of SH3 domains in SH3PXD2B influenced localization. Whereas wild-type SH3PXD2B was restricted to the cytoplasm (Figure 10a), the mutant protein was present throughout the cell, including prominent localization within the nucleus (Figure 10b). Thus, the

Sh3pxd2b^{nee} mutation is predicted to encode a truncated protein, which as a consequence of the mutation, likely has altered subcellular distribution.

SH3PXD2B is a widely expressed podosomal-adaptor protein

The SH3PXD2B protein, and the closely-related SH3PXD2A, have both been demonstrated in cell culture studies to function as adaptor proteins required for formation of podosomes (Abram, Seals et al. 2003; Seals, Azucena et al. 2005; Buschman, Bromann et al. 2009). The PX domains of both SH3PXD2B and SH3PXD2A bind to the lipids PtdIns(3)P and PtdIns(3,4)P_2 while their SH3 domains bind and influence various matrix metalloproteinases and ADAM family proteinases (Abram, Seals et al. 2003; Buschman, Bromann et al. 2009). Through these interactions, SH3PXD2A and SH3PXD2B are thought to tether and regulate the localization of ECM modifying enzymes to precise cellular compartments such as podosomes. To further test how the *Sh3pxd2b*^{nee} mutation might influence podosomes important to murine postnatal growth and development, we next tested whether SH3PXD2B localizes to podosomes and whether the deleted SH3 domain was capable of mediating a protein-protein interaction with a candidate protein, ADAM15 (Figure 11).

Properties of podosomes have been well described in *Src* transformed fibroblasts (Tarone, Cirillo et al. 1985). To test whether SH3PXD2B localizes to podosomes in these cells, NIH3T3 cells were transfected with a constitutively active form of *Src* (Y529F) and localization of endogenous SH3PXD2B tested with an anti-SH3PXD2B specific antibody (Figure 11a–c). While SH3PXD2B localized to the cytoplasm in untransfected cells (data not shown), a portion of SH3PXD2B localized to podosome clusters and rosettes in *Src* (Y529F) transfected fibroblasts. Consistent with other recent findings (Buschman, Bromann et al. 2009), this result independently confirms that SH3PXD2B localizes to podosomes.

Although direct protein binding partners for SH3PXD2B have not previously been described, several interactions for the closely related SH3PXD2A protein are known. It has previously been demonstrated by *in vitro* binding assays that SH3PXD2A can form protein-protein interactions with ADAM family proteins, including ADAM12, ADAM15, and ADAM19. These interactions are mediated by multiple PxxP motifs present within the cytoplasmic tail of ADAMs and the fifth SH3 domain of SH3PXD2A (Abram, Seals et al. 2003). Because the fifth SH3 domain of SH3PXD2A has homology to the fourth SH3 domain of SH3PXD2B (55% identity), we reasoned that the proteins may have similar binding partners. To test this, a GST pull-down experiment was performed with a candidate of interest, ADAM15 (Figure 11d). A fusion protein containing the fourth SH3 domain of SH3PXD2B was incubated with lysates of 293T cells transfected with a MYC-tagged full-length ADAM15. While negative controls containing GST alone did not interact with ADAM15, the fusion protein containing the fourth SH3 domain of SH3PXD2B did. This result is consistent with a role of SH3PXD2B as an adaptor protein. Furthermore, because the mutant *Sh3pxd2b*^{nee} allele is predicted to encode a protein in which all of this fourth SH3 domain is absent, this result suggests that misregulation of ADAM15 likely contributes to mutant phenotypes of *nee* mice.

In order to further relate functions of SH3PXD2B to the mutant phenotypes of *nee* mice, western blot analysis was utilized to determine the tissue distribution and levels of SH3PXD2B in wild-type mice (Figure 11e). A band of 120 kDa was detected in protein lysates isolated from tissues of adult wild-type mice. Presumably a consequence of post-translational modifications, the apparent molecular weight of SH3PXD2B shown on SDS-PAGE gel was slightly larger than predicted (102 kDa). Because the anti-SH3PXD2B antibody was generated against a portion of the SH3PXD2B protein deleted by the *nee* mutation, it was not possible to test levels or localization of the mutant protein. However, wild-type SH3PXD2B was present in the majority of tissues, including eye,

white adipose tissue, brown adipose tissue, lung, heart, brain, spleen, stomach, liver, and skeletal muscle. No protein was detected in the kidney or bone marrow, indicating that the protein is not ubiquitously expressed. With the exception of lung and skeletal muscle tissue, the relative amount of protein in each tissue resembled previously reported *Sh3pxd2b* mRNA levels in these tissues (Hishida, Eguchi et al. 2008; Buschman, Bromann et al. 2009).

Discussion

Phenotype-driven genetics is a powerful approach for studying genetic pathways important to human health and disease. One advantage of this approach is that it often gives rise to animal models with a diversity of mutant alleles and genetic backgrounds. Here, we have utilized the *nee* mutation, which spontaneously arose on a B10.A-*H2*^{h4}/(4R)SgDvEg genetic background, to link functions of the *Sh3pxd2b* gene with multiple defects of postnatal growth and development. Initially recognized because of runted growth, craniofacial abnormalities, and ocular anterior segment dysgenesis recognizable from an early age, we have also found that adult mice homozygous for the *nee* mutation exhibit infertility, hearing deficiency, reduced areal bone mineral density, and a form of lipodystrophy depleting white adipose tissue. Mapping of the causative mutation led to identification of a protein truncating mutation in *Sh3pxd2b*, a gene about which relatively little is known (Seals, Azucena et al. 2005; Hishida, Eguchi et al. 2008; Buschman, Bromann et al. 2009). Based on previous work (Buschman, Bromann et al. 2009), and our own direct data presented here, *Sh3pxd2b* encodes a widely expressed podosomal-adaptor protein. In nearly all of the tissues affected by the *Sh3pxd2b*^{nee} mutation, podosomes have previously been observed and implicated in functional

contributions. Combined, these data add to the mounting evidence linking roles for podosomes in multiple physiological contexts involving ECM regulation.

Role of podosomes in *nee* affected tissues

Podosomes and ECM remodeling are both known to play significant roles in bone biology (Krane and Inada 2008; Ory, Brazier et al. 2008; Saltel, Chabadel et al. 2008). Podosomes have been particularly well studied in osteoclasts, a specialized cell that digests bone matrix in a process involving formation of podosomes. Growth retardation and craniofacial defects have previously been noted in mice with mutations influencing osteoclast function (Holmbeck, Bianco et al. 1999; Kornak, Kasper et al. 2001; Chen, Yang et al. 2007; Hishida, Eguchi et al. 2008). As would be expected for a podosomal-protein influencing osteoclasts, mutations in *Src* result in growth retardation, craniofacial defects, and osteopetrosis (Soriano, Montgomery et al. 1991). Interestingly, mutations in other genes linked to podosomes, such as genes encoding various metalloproteinases, can lead to decreases in bone mineral density (Holmbeck, Bianco et al. 1999; Egeblad, Shen et al. 2007; Mosig, Dowling et al. 2007). Our observation of decreased areal bone density in *nee* homozygotes suggests that *Sh3pxd2b* is an important member of this later type of genetic pathway influencing skeletal and craniofacial development.

In the eye, podosome-like structures have been observed in trabecular meshwork cells. When cultured on a layer of collagen, these cells exhibit focal degradations of collagen overlapping spots of podosome-like structures (Hishida, Eguchi et al. 2008). The trabecular meshwork is an ECM-rich filter for aqueous humor outflow located in the irideocorneal angle. Trabecular meshwork defects can cause elevated intraocular pressure and likely contribute to human glaucoma (Acott and Kelley 2008). From the constellation of ocular phenotypes we have observed, it is likely that developmental malformation of the irideocorneal angle or inefficient ECM remodeling mediated by a disruption of

podosomes results in elevated intraocular pressure (causing increased depth of the anterior chamber) and damaging the corneal endothelium (causing corneal opacities). Given these observations, it is possible that *nee* homozygotes may also develop glaucoma, a hypothesis we are currently testing directly.

There are also links between podosomes and fertility. In males, the tubulobulbar complex, a type of intercellular junction important in sperm release and spermatocyte translocation, is thought to have properties resembling podosomes (Kim, Huang et al. 2007). Thus, SH3PXD2B may influence male fertility through function of these structures. Another distinct possibility is that SH3PXD2B might contribute to fertility via regulation of ADAMs (Meyer, Valtot et al. 1994; Evans 2001). ADAM15, the protein we have shown may interact with SH3PXD2B through its last SH3 domain, is present in mouse spermatozoa (Pasten-Hidalgo, Hernandez-Rivas et al. 2008) and binds effectively to oocytes (Meyer, Valtot et al. 1994). Thus, the infertility of *nee* mice may also be a consequence of ADAM15 mislocalization. In females, potential links to podosomes are less clear, but it is noteworthy that defects in the female reproductive tract have previously been observed in mice with targeted mutations of other genes associated with podosomes (Holmbeck, Bianco et al. 1999; Shimizu, Maruyama et al. 2005).

Podosomes have not previously been reported in adipose tissue, but may well exist. Aside from our observation that mice homozygous for the *nee* mutation develop a form of lipodystrophy, a role for SH3PXD2B in adipose tissue has recently been independently reported in differentiation of 3T3-L1 preadipocyte cells (Hishida, Eguchi et al. 2008). Based on the finding that *Sh3pxd2b* was expressed early in the differentiation process of 3T3-L1 preadipocytes, Hishida et al. performed RNAi-mediated knockdown experiments and found that *Sh3pxd2b* function is required for preadipocyte differentiation and clonal expansion. Interestingly, adipocyte differentiation is also influenced by multiple proteases, including MMP14 (MT1-MMP), MMP2, and MMP9 (Bourlier, Zakaroff-Girard et al. 2005; Chun, Hotary et al. 2006).

In addition to influencing podosomes, an alternative hypothesis is that SH3PXD2B may regulate metalloproteinases with sheddase activity. For example, MMP14 (MT1-MMP) negatively regulates osteoclastogenesis by causing ectodomain shedding of TNFSF11 (RANKL) (Hikita, Yana et al. 2006). It is therefore plausible that SH3PXD2B might influence areal bone mineral density by regulating membrane localization and sheddase activity of MMP14. Likewise, SH3PXD2B might influence sheddase activities in other tissues as well. Given the previous demonstration of sheddase regulation by SH3PXD2A (Malinin, Wright et al. 2005), a similar function for SH3PXD2B remains possible.

Molecular biology and genetics of *Sh3pxd2b*

At the molecular level, it will be of particular importance to define additional SH3PXD2B interacting proteins. Our current experiments have been guided in two ways, previous identification of proteins interacting with SH3PXD2A/SH3PXD2B and our molecular identification of the *nee* mutation; leading to the suggestion that SH3PXD2B may interact with ADAM15. However, many additional interacting proteins likely remain to be identified. Previous studies have demonstrated interactions of SH3PXD2A with ADAM12, ADAM15, ADAM19 (Abram, Seals et al. 2003), and WASL (Oikawa, Itoh et al. 2008). In addition, MMP14 (MT1-MMP) localization has previously been shown to be influenced by SH3PXD2B (Buschman, Bromann et al. 2009). The possibility of interactions between SH3PXD2B and these candidates, as well as others, remain to be tested.

With a growing list of tissues displaying phenotypes associated with Invadosomes, genes such as *SH3PXD2B* are attractive candidates for contributing to a number of diseases and complex traits. For example, genetic association studies for human obesity have detected suggestive linkage with *SH3PXD2B* at 5q35 (Zhao, Pearson

et al. 2003; Liu, Wang et al. 2008), although some studies have failed to replicate the association (Vogel, Greene et al. 2009). It is also interesting that a quantitative trait locus for growth in mice has previously been mapped near the chromosomal location of *Sh3pxd2b* (Rocha, Eisen et al. 2004).

Concluding remarks

In conclusion, a phenotype-driven search for new mouse models of human disease led to identification of multiple phenotypes caused by the *Sh3pxd2b*^{nee} mutation in mice. *Sh3pxd2b* encodes a widely expressed podosomal-adaptor protein influencing postnatal growth and development of several mesenchymal derived tissues, including craniofacial structures, the ocular irideocorneal angle, and white adipose tissue. To our knowledge, this is the first report of mutant *in vivo* phenotypes associated with either *Sh3pxd2b*, or the closely related *Sh3pxd2a* genes. While most studies of Invadosomes to date have been dominated by studies of osteoclasts, macrophages, and tumor cells, the current findings suggest previously unknown roles for podosomes in several additional tissues. In ongoing work, it will be of particular interest to use mice with the *Sh3pxd2b*^{nee} mutation as a resource to further delineate the genetic pathways regulating function of Invadosomes, to continue mechanistic studies of SH3PXD2B in specific cell-types, and to assess potential contributions of podosomal-adaptor proteins to human health and disease.

Figure 5. Externally visible phenotypes of *nee* mice.

Comparing littermate controls homozygous for wild-type alleles (*left column*) to mutant mice homozygous for the *nee* mutation (*right column*), *nee* mutants exhibit abnormal growth, craniofacial, and ocular phenotypes. **(a, b)** *nee* homozygotes exhibit small body size, as evident in this comparison of 4-month-old females. **(c, d)** Craniofacial abnormalities of *nee* homozygotes characterized by shortened noses and domed skulls. **(e–h)** Two different ophthalmic slit-lamp views of the same eyes from 1-month-old mice. Note that while wild-type mice have a clear cornea and normal anterior chamber depth (e), *nee* homozygotes have a cloudy cornea and enlarged anterior chamber (f, *black double arrow*). Viewed in this orientation, the normal mouse iris and cornea appear very close to one another, leaving little to no discernable depth to the anterior chamber. The irideocorneal angle of wild-type mice is characterized by a sharply defined limbus (g, *arrowhead*), whereas the irideocorneal angle of *nee* homozygotes has severe peripheral anterior synechia (h, *double arrow*).

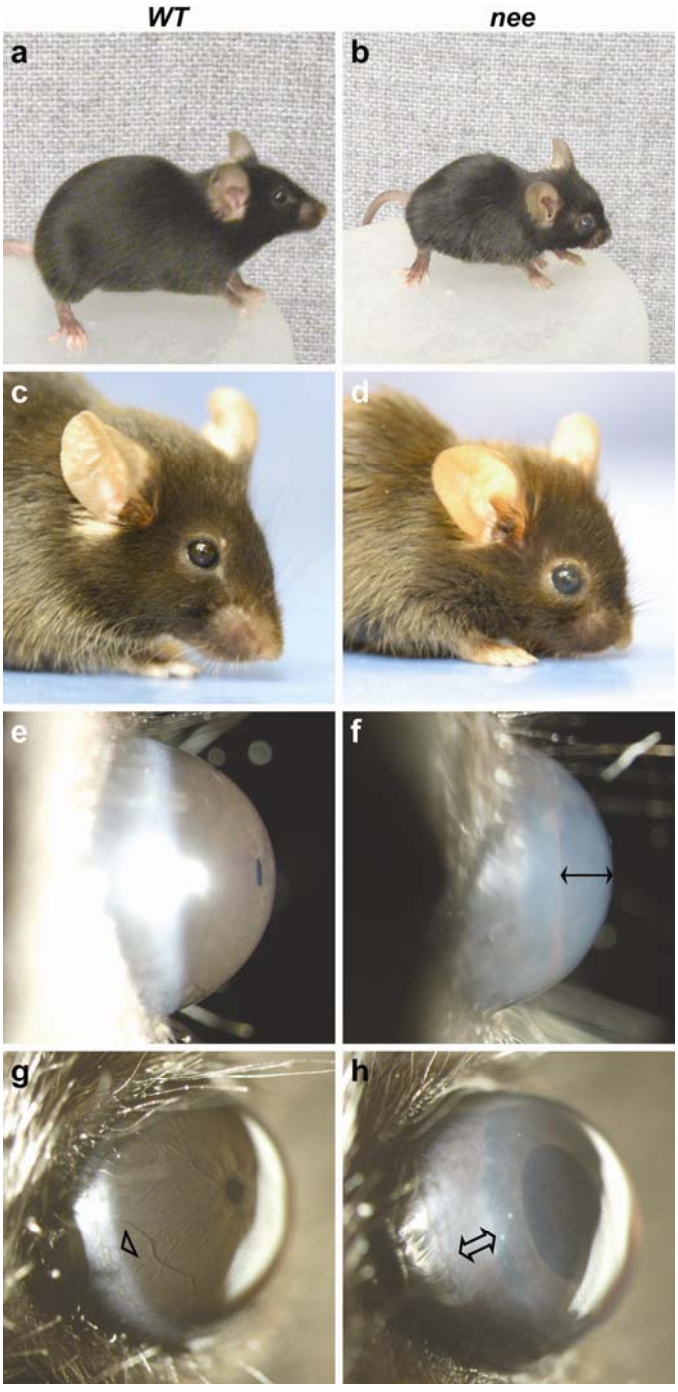
WT
nee
a
b
c
d
e
f
g
h

Figure 6. Skeletal defects of *nee* mice.

X-ray imaging of mutant *nee* mice and wild-type littermate controls indicates the presence of multiple skeletal abnormalities in *nee* homozygotes. **(a)** Adult *nee* homozygotes have a proportionally smaller skeleton in comparison to wild-type littermate controls. **(b, c)** Higher magnification dorsal views of skulls showing a drastically reduced anterior-posterior length and slightly reduced width in *nee* homozygotes. **(d, e)** Higher magnification view showing that hind legs of *nee* homozygotes are reduced in size, but otherwise largely normal in anatomical appearance. Images from the same pair of 12-month-old female mice; littermate control is homozygous for the wild-type allele.

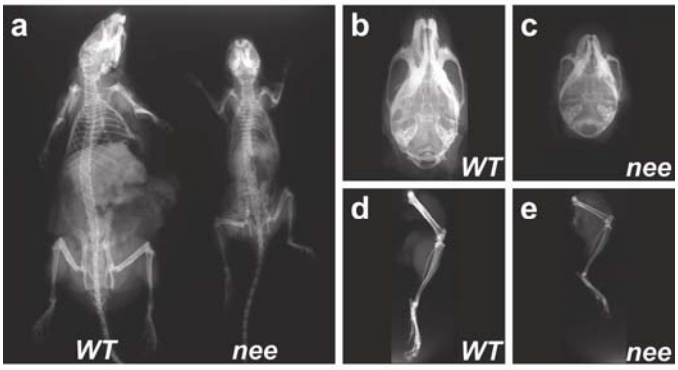
a
WT
nee
b
WT
c
nee
d
WT
e
nee

Figure 7. Hearing impairment and ear pathology associated with the *nee* mutation. Physiologic and histologic analyses demonstrate a hearing deficiency in *nee* homozygotes associated with inflammation of the middle ear (otitis media). **(a)** ABR thresholds in response to different auditory stimuli, comparing 13 mice homozygous for the *nee* mutation to 3 heterozygous controls. Mean ABR thresholds (dB SPL) ± SEM. All mice were tested at 34–92 days of age. **(b)** Histological section of inner and middle ear from a heterozygous control showing normal anatomy and absence of cellular infiltrate in the middle ear (*arrow*). **(c)** Histological section of inner and middle ear from *nee* homozygote showing inflammation indicated by the presence of neutrophils in the middle ear cavity (*arrow*) and thickened surrounding epithelium. All inner ear structures are normal in appearance. The apparent different size of the middle ear cavity between panels b and c is an artifactual consequence of slightly different planes of section. Scale bar = 200 μm.

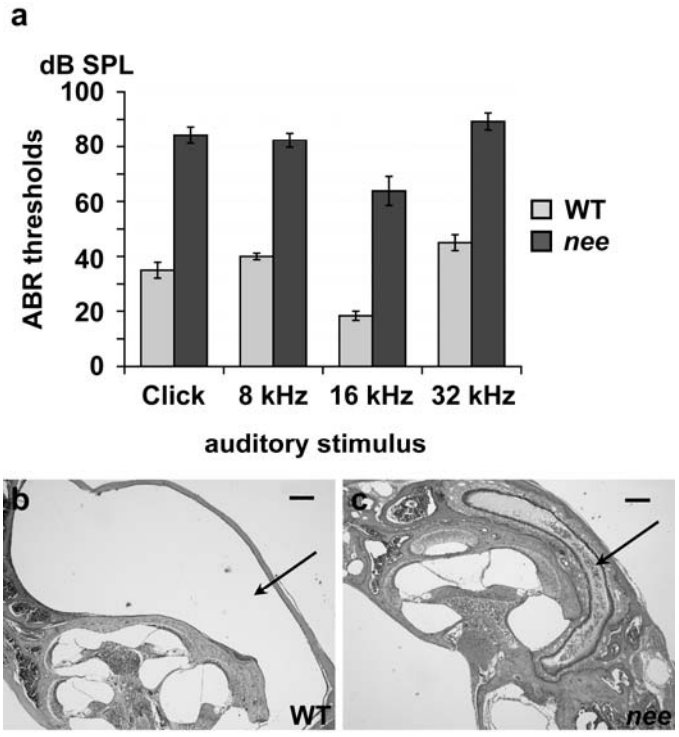
a
dB SPL
100
80
60
40
20
0
ABR thresholds
WT
nee
Click
8 kHz
16 kHz
32 kHz
auditory stimulus
b
WT
c
nee

Figure 8. Adipose defects of *nee* mice.

Dissections and MRI analysis of mutant *nee* mice and wild-type littermate controls show that mice homozygous for the *nee* mutation develop a form of lipodystrophy. **(a)** Ventral and **(b)** dorsal views of wild-type littermate and *nee* homozygote. As observed in perigenital fat (*open arrow*), *nee* homozygotes show a severe depletion of white adipose tissue. In contrast, as observed in interscapular fat (*black arrow*), brown adipose tissue is maintained. **(c–h)** Coronal slices obtained by MRI showing an absence of subcutaneous and visceral adipose tissue in *nee* homozygotes. With this pulse-sequence, fat appears white and muscle and water appear gray or black. Images from the same pair of 8-month-old female mice; littermate control is homozygous for the wild-type allele.

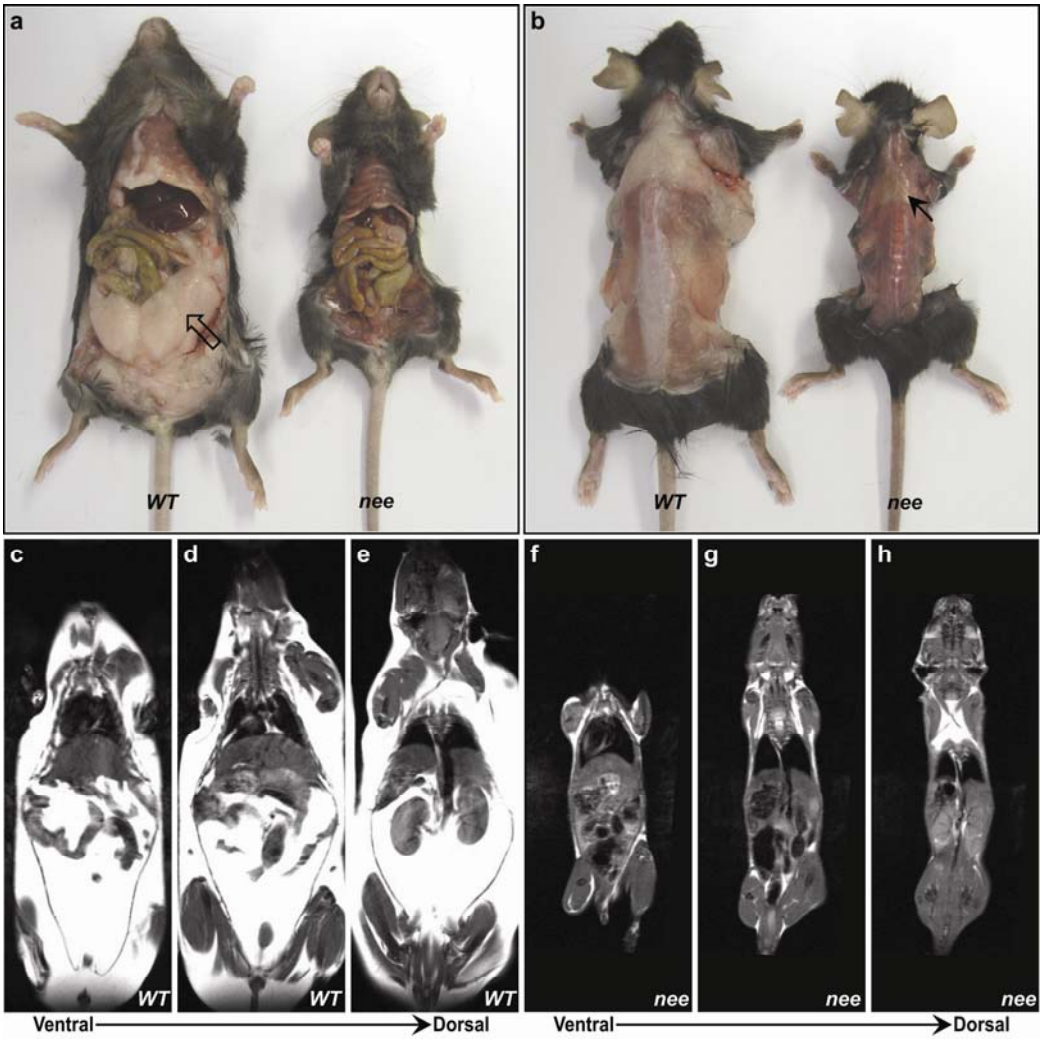
a
WT
nee
b
WT
nee
c
WT
d
WT
e
WT
Ventral
Dorsal
f
nee
g
nee
h
nee
Ventral
Dorsal

Figure 9. Molecular identification of the *nee* mutation.

(a) Genetic mapping of the *nee* mutation. Haplotype analyses of 45 mice from an intersubspecific intercross between *nee* and CAST/EiJ mice (*filled boxes*, *nee* allele; *open boxes*, CAST/EiJ allele). The number of chromosomes with each haplotype is indicated below each column. Linkage to several markers on mouse Chr 11 was observed with no recombination with *D11Mit 215*. **(b)** DNA sequence identifying a 1 bp deletion in *Sh3pxd2b*. **(c)** Restriction enzyme analysis of *nee* spanning amplicons from a wild-type littermate, *nee* heterozygote, *nee* homozygote, and 10 different inbred strains not exhibiting the *nee* phenotype. Only DNA from mice with the *nee* allele failed to be digested, indicating that the 1 bp deletion of *nee* is unique to this strain (WT, parental wild-type strain; Het, *nee* littermate heterozygous for wild-type and *nee* alleles; MT, mutant *nee* homozygote; PL, PL/J; AKR, AKR/J; R3, RIIIS/J; D2, DBA/2J; BALB, BALB/cJ; B6, C57BL/6J; CBA, CBA/J; A, A/J; NZB, NZB/BlNJ; C3H, C3H/HeJ). **(d)** Schematic of *Sh3pxd2b* gene, predicted proteins domains, and location of *nee* mutation. *Top*, the *nee* mutation (1303delA) is predicted to result in a frameshift starting at amino acid 407 altering 37 amino acids before causing a premature stop codon (*boxes*, exons; *red*, coding sequence; *blue*, PX domain; *green*, SH3 domains). *Bottom*, these changes are predicted to alter a portion of the third and entirely delete the fourth SH3 domains (*green text*, third SH3 domain; *underlined text*, frameshift).

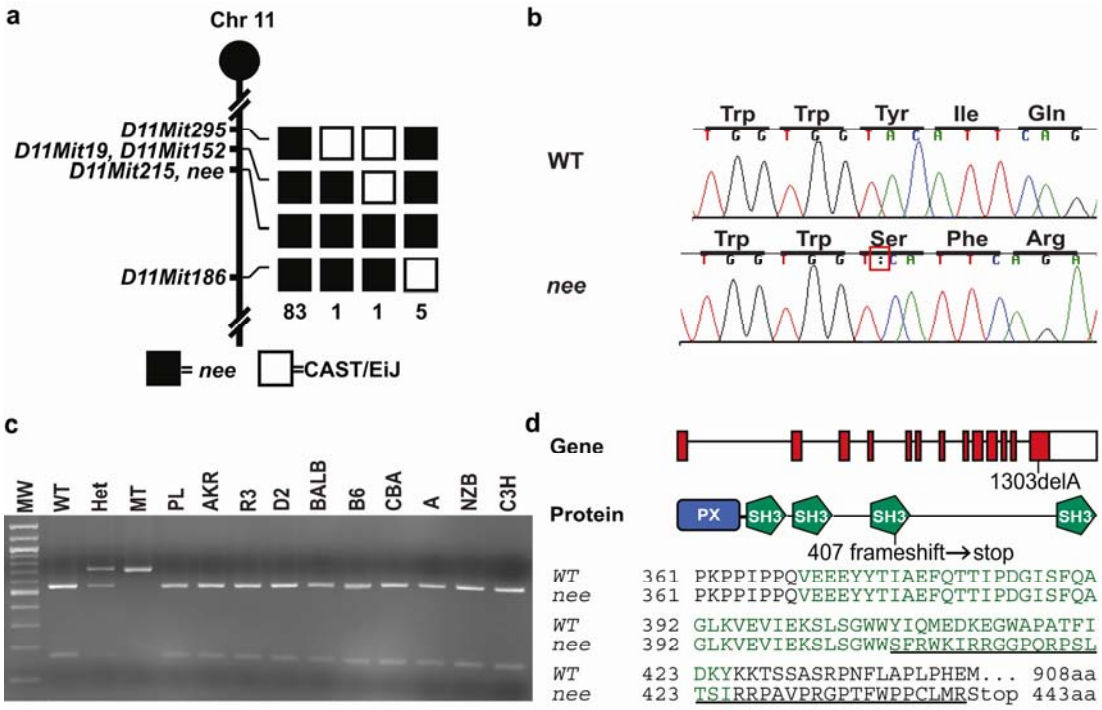
a
Chr 11
D11Mit295
D11Mit19, D11Mit152
D11Mit215, nee
D11Mit186
83 1 1 5
= nee
=CAST/EiJ
b
WT
nee
Trp Trp Tyr Ile Gln
Trp Trp Ser Phe Arg
c
MW WT Het MT PL AKR R3 D2 BALB B6 CBA A NZB C3H
d
Gene
1303delA
Protein
PX SH3 SH3 SH3 SH3
407 frameshift→stop
WT 361 PKPPIPPQVEEEYYTIAEFQTTIPDGISFQA
nee 361 PKPPIPPQVEEEYYTIAEFQTTIPDGISFQA
WT 392 GLKVEVIEKSLSGWWYIQMEDKEGWAPATFI
nee 392 GLKVEVIEKSLSGWWSFRWKIRRGGPQRPSL
WT 423 DKYKKTSSASRPNFLAPLPHEM... 908aa
nee 423 TSIRRPAVPRGPTFWPPCLMRStop 443aa

Figure 10. Altered subcellular distribution of SH3PXD2B^{1303delA}.

HEK 293T cells transfected with GFP-fusion vectors show that the 1303delA deletion alters subcellular localization of SH3PXD2B (*left column*, GFP-SH3PXD2B; *right column*, GFP-SH3PXD2B^{1303delA}). **(a)** GFP fluorescence is present in the cytoplasm but not in the nucleus of cells transfected with GFP-tagged wild-type SH3PXD2B. (**b**) GFP-tagged mutant protein is present throughout the cell, including prominent localization within the nucleus. **(c, d)** Phase-contrast and **(e, f)** merged images of the same fields. Images were collected with a 63X objective; scale bar = 20 μm.

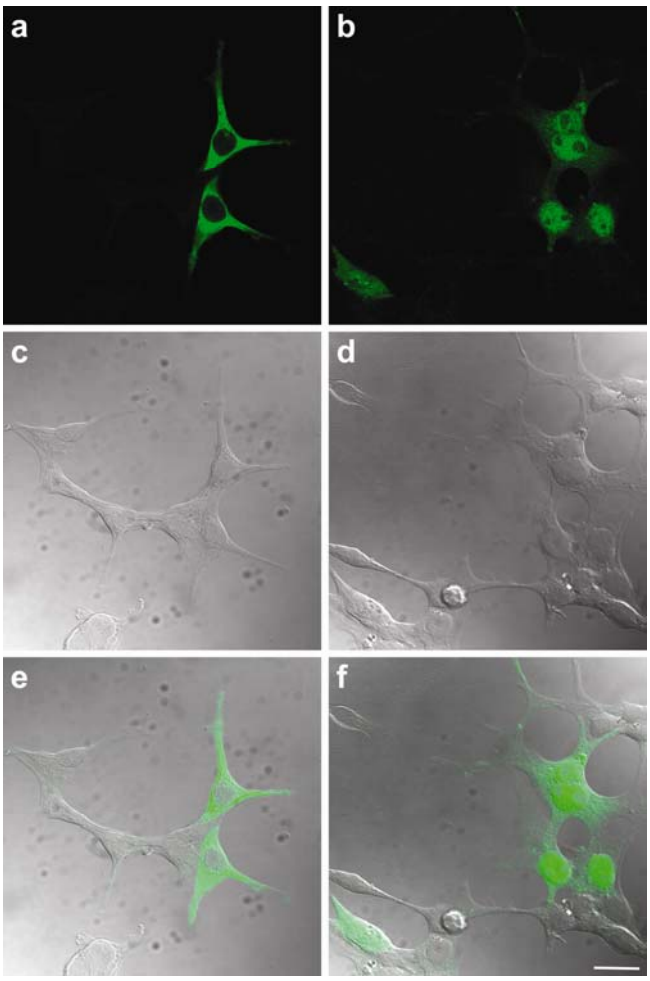
a
b
c
d
e
f

Figure 11. Localization, protein interaction, and tissue distribution of SH3PXD2B. **(a–c)** NIH3T3 cells transiently transfected with constitutively active *Src* (Y529F) contain SH3PXD2B localized to clusters and rosettes of podosomes (*white arrows*, podosomes; *red*, F-actin; *green*, SH3PXD2B; *yellow*, merge). Images were collected with a 63X objective; scale bar = 20 μm **(d)** GST pull-down experiment indicating association between SH3PXD2B and ADAM15. Protein content is evident by the coomassie blue stained SDS-PAGE gel indicating presence of 26 kDa GST and 34 kDa GST-SH3#4. **(e)** Western blot showing that SH3PXD2B has a broad, but not ubiquitous, tissue distribution (WAT, perigenital white adipose tissue; BAT, interscapular brown adipose tissue; sk musc, skeletal muscle; BM, bone marrow).

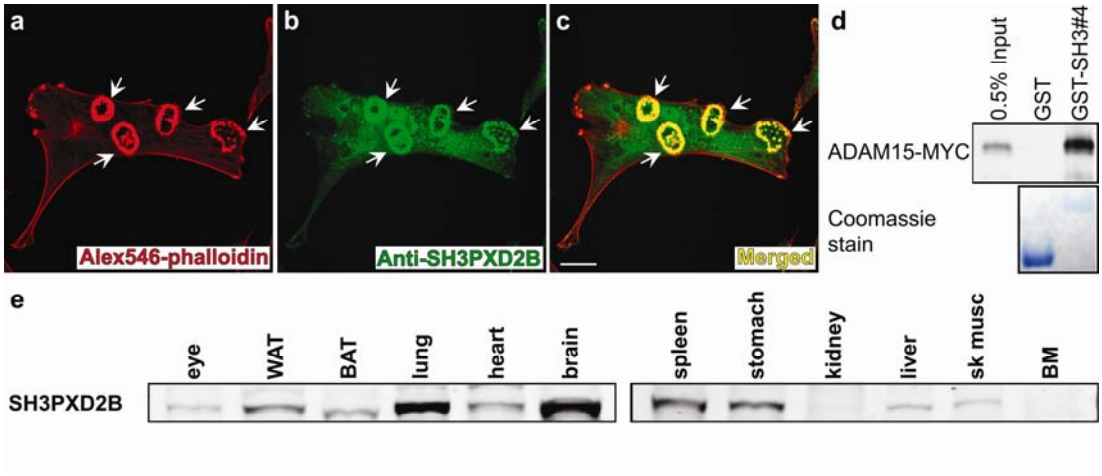
a
b
c
d
Alex546-phalloidin
Anti-SH3PXD2B
Merged
0.5% Input
GST
GST-SH3#4
ADAM15-MYC
Coomassie
stain
e
SH3PXD2B
eye
WAT
BAT
lung
heart
brain
spleen
stomach
kidney
liver
sk musc
BM

CHAPTER 3
NEE MUTANT MICE DEVELOP GLAUCOMA MEDIATED BY SH3PXD2B

Introduction

The glaucomas are a collection of ocular diseases which involve retinal ganglion cell degeneration, optic nerve head excavation and progressive loss of vision (Ritch R 1996; Nickells RW 2002; Allingham RR 2004). Glaucoma is a leading cause of blindness worldwide (Resnikoff, Pascolini et al. 2004). Approximately 70 million people have glaucoma, and the number is estimated to increase in the next decade (Quigley 1996; Quigley and Broman 2006). Glaucoma can be classified into a few categories: open angle glaucoma, closed angle glaucoma, glaucoma associated ocular or systemic developmental defects, and secondary glaucoma caused by other conditions (Allingham RR 2004). Elevated intraocular pressure (IOP) is a causative risk factor for the majority types of glaucoma and is currently the only clinically treatable feature (Kass, Heuer et al. 2002; McKinnon, Goldberg et al. 2008).

Many of the factors precipitating elevations in IOP remain to be identified, as do the molecular pathways that underline additional contributing risk factors. One means of gaining this knowledge is through genetics. While the most common forms of glaucoma often appear sporadic and are presumably genetically complex, a small number of Mendelian acting mutations have been identified (Wiggs 2007; Allingham, Liu et al. 2009). Glaucoma also occurs as part of several broader syndromes in which causative mutations have been identified, including Axenfeld-Rieger syndrome (Tumer and Bach-

Holm 2009), nail-patella syndrome (Dai, Johnson et al. 2009), Weill-Marchesani syndrome (Morales, Al-Sharif et al. 2009) and others.

SH3PXD2B (also previously known as TKS4) is an adaptor protein containing an N-terminal PX domain, four SH3 domains, and multiple PXXP motifs and tyrosine phosphorylation sites (Hishida, Eguchi et al. 2008; Buschman, Bromann et al. 2009). Through their PX and SH3 domains, SH3PXD2B can interact with variety of proteins and phosphoinositides, most of which are key molecules involved in assembly or function of invadosomes. Invadosomes are cell-ECM adhesions with ECM degradation activity (Gatesman, Walker et al. 2004; Mao, Thedens et al. 2009). SH3PXD2B is thus implicated in invadosome related activities such as ECM modulation, cell migration, and invasion. Podosomes have been observed in a variety of tissues, in the eye notably including cells of the trabecular meshwork (Hishida, Eguchi et al. 2008). Thus, these observations suggest that SH3PXD2B is likely important for modulation of an extracellular matrix important to the development or function of the eye.

To study the *in vivo* function of SH3PXD2B, we previously isolated a spontaneous mouse mutant, *nee*, which contains a 1-bp deletion in the last exon of the *Sh3pxd2b* gene, resulting a truncated protein with two disrupted SH3 domains (Mao, Thedens et al. 2009). The *nee* homozygous mutant mice exhibit multiple defects including ocular abnormalities such as corneal opacity, enlarged anterior chamber depth and peripheral iridocorneal adhesion, all likely incidences of elevated IOP and glaucoma. Here, we extend knowledge of SH3PXD2B-mediated phenotypes by directly testing whether mice with *Sh3pxd2b* mutation indeed develop glaucoma and charactering expression of the protein in human eyes. In mice, we find *nee* homozygous mutants

exhibit drastically elevated IOP likely caused by severe iridocorneal adhesion present early in life. Elevated IOP led to a rapid degeneration of the retina and optic nerve, which are hallmarks of glaucoma. By immunofluorescence labeling of human eyes, presence of SH3PXD2B was detected in multiple ocular tissues, including the trabecular meshwork. Taken together, these results confirm the glaucoma relevance of SH3PXD2B and by extension, implicate a new pathway of candidates likely to impact the trabecular meshwork in health and diseases.

Materials and Methods

Animal husbandry

All mice were obtained from The Jackson Laboratory, Bar Harbor, Maine. Mice were subsequently housed and bred at the University of Iowa Research Animal Facility. The spontaneous *nee* mutation arose in strain B10.A-$H2^{h4}$/(4R)SgDvEg at generation F51 (http://mousemutant.jax.org/index.html). Mice were maintained on a 4% fat NIH 31 diet provided *ad libitum* and were housed in cages containing dry bedding (Cellu-dri; Shepherd Specialty Papers, Kalamazoo, MI). The environment was kept at 21°C with a 12-hour light: 12-hour dark cycle. Mice were genotyped by assaying the absence or presence of an *RsaI* restriction enzyme site abolished by the *nee* mutation (Mao, Thedens et al. 2009) and the stock was maintained in heterozygote X heterozygote crosses. All animals were treated in accordance with the Association for Research in Vision and Ophthalmology Statement for the Use of Animals in Ophthalmic and Vision Research. All experimental protocols were approved by the Animal Care and Use Committee of The University of Iowa.

Slit-lamp examination

Anterior chamber phenotypes were assessed with a slit-lamp (SL-D7; Topcon, Tokyo, Japan) and photodocumented with a digital camera (D100; Nikon, Tokyo, Japan). Images were taken with identical camera settings and prepared with identical image software processing. For assessment of anterior chamber phenotypes, a beam of light is shone at an angle across the eye and the anterior chamber is examined for features such as the presence of anterior synechia, cataracts, cornea opacity or neovascularization; dimensions of the anterior chamber; iris color and morphology; and other potential findings. All ocular exams utilized conscious mice.

IOP measurement

IOP was measured using a microneedle cannulation system as previously described (John, Hagaman et al. 1997). Briefly, mice were anesthetized by intraperitoneal injection of a mixture of ketamine (100 mg/kg) and xylazine (9 mg/kg). After anesthetization, mice were placed on a surgical platform under a dissecting microscope. A microneedle was inserted into the anterior chamber by piercing through the central cornea. To avoid damaging to the anterior chamber, the microneedle was advanced with a micromanipulator. The needle tip usually rested approximately 50-100 μm into the chamber. The pressure was recorded for a 1 min period when the eye became stabilized after microneedle insertion.

Histology

Ocular sections were obtained by plastic histology. Mice were euthanatized, enucleated and eyes were immediately fixed with an alcohol based Z-fix which contains

20% isopropyl alcohol and 20% alcoholic concentrated Z-fix (Anatech, Battle Creek, MI) for 24-48 hours at room temperature. Eyes were subsequently rinsed with 0.1M sodium cacodylate, postfixed with 1% osmium tetroxide, rinsed in buffer and dehydrated with graded acetone concentrations. After embedding in Eponate-12 resin, 1 μm sections were cut with an ultramicrotome (Leica EM UC6, Wetzler, Germany), stained with 1% toluidine blue, and imaged (Olympus BX 52, Center Valley, PA). Saggital sections cutting through the optic nerve head were collected for analysis.

Optic nerve cross sections were examined for glaucomatous damage using a paraphenylenediamine (PPD) staining protocol as previously described (Smith RS 2002) with slight modifications. Briefly, mice were euthanatized, enucleated and decapitated, and the majority of the brain was removed from the skull leaving a thin layer of tissue covering the optic nerves. The remaining heads were fixed overnight in half strength Karnovsky's fixative (2.5% glutaraldehyde, 2% paraformaldehyde in 0.1M sodium cacodylate), and the optic nerves were dissected out carefully from the skull and fixed for additional 24 hours. After fixation, the optic nerves were processed following the same procedures for eyes. One micron sections were collected, stained with 1% paraphenylenediamine (PPD) for 40 minutes and imaged with light microscopy. Axon numbers were assessed as previously described (Anderson, Libby et al. 2006) with slight modifications. Briefly, axons from 12 non-overlapping fields were counted at 1000× magnification. These fields were evenly spread throughout the cross-section of the nerve, and the total area of these fields was equal to10% of the total nerve cross-sectional area. The total axon number of each nerve is estimated by the mean axon number of the 12 counted fields multiplied by 10.

Donor eyes

Human donor eyes were obtained from the Iowa Lions Eye Bank (Iowa City, IA) following informed consent from the donors' families. Eyes were processed immediately on receipt. Lenses were removed, and tissues from the anterior and posterior poles were punched using disposable trephines, and punches were fixed with 4% paraformaldehyde in phosphate buffered saline for 2 hr. The removed lenses were fixed separately with a similar approach. For biochemical studies all samples were preserved within 8 h of death, which is within a time frame during which protein composition of ocular tissues is well preserved (Ethen, Reilly et al. 2006). In some cases, ophthalmic records were available, and retinal diagnoses were recorded.

Immunohistochemistry

Tissues were cryopreserved with sucrose gradient and embedded in Optimal Cutting Temperature embedding medium (Tissue-Tek O.C.T. Compound; Sakura Finetek, Torrance, CA), cut at 10μm thickness and transferred to glass slides. The lens was cut at 20 μm thickness to maintain tissue integrity. Sections were air dried for 30 min at room temperature, rehydrated in PBS for 5 min, and blocked with 10% goat serum, 3% bovine serum albumin (BSA) in PBS for 1 h at room temperature. Sections were then incubated with rabbit anti-human SH3PXD2B polyclonal antibody (Millipore, Temecula, CA) diluted at 1:50 in 1% goat serum, 1% BSA in PBS overnight at 4 ^{o}C. After a few washes with 0.1% Tween-20 in PBS, sections were incubated with Alexa488-conjugated goat anti-rabbit antibody (Invitrogen, Carlsbad, CA) diluted at 1:200 in 1% goat serum, 1% BSA in PBS for 1 h at room temperature. Following washes, sections were mounted (ProLong Gold; Invitrogen, Carlsbad, CA) and imaged with a confocal microscope (Zeiss LCM 510; Carl Zeiss MicroImaging, Inc., Thornwood, NY).

Western blot analysis

Normal human trabecular meshwork cells (HTM-5) were lysed in lysis buffer (50mM Tris-HCl pH 7.4, 150mM NaCl, 1mM EDTA, 0.1% Triton X-100, 0.1% SDS) supplemented with 1 mM PMSF and a mix of additional protease inhibitors (Halt Proteinase Inhibitor Cocktail; Thermo Scientific, Rockford, IL). Total cell lysates were centrifuged at 14,000 rpm for 20 min at 4°C. Protein concentration in the resulting supernatant was determined using the BCA protein assay reagent (Sigma-Aldrich, St Louis, MO). Fifty micrograms of lysates were electrophoresed on 7.5% SDS-PAGE gels and transferred to PVDF membranes (Millipore, Bedford, MA). The membrane was blocked at room temperature in 5% dry milk in TBST (Tris-buffered saline with 0.1% Tween-20) for 2 h, followed by incubation with a rabbit anti-human SH3PXD2B polyclonal antibody (Millipore, Temecula, CA) diluted at 1:100 in TBS overnight at 4^{o}C. The membrane was rinsed twice, washed 4 times for 5 minutes each at room temperature in TBS-T with gentle shaking. The membrane was then incubated in 1:4000 dilution of horseradish peroxidase conjugated goat anti-rabbit IgG (Invitrogen, Carlsbad, CA) for 30 minutes at room temperature, followed by 4 times of washes for 5 minutes each. Immunoreactivity was detected by enhanced chemiluminescence methodology (GE Healthcare, Piscataway, NJ).

Results

Early onset iridocorneal adhesion of *nee* mice

Previously, we showed that adult *nee* homozygous mutants exhibit anterior synechia, corneal opacities, and enlarged anterior chambers (Mao, Thedens et al. 2009). To examine whether these ocular defects were due to developmental abnormalities, we examined young mice with a slit lamp. The youngest mice we were able to examine were

17 days old, because mouse eyelids are not open until this age. Unlike humans, of which the eye is fully developed at birth, the majority of mouse ocular tissues are still in development after birth. At P17, the majority of the eye, except for the trabecular meshwork, is formed (Smith, Zabaleta et al. 2001). We found that eyes of *nee* wild-type homozygous mice at P17 are developed normally and exhibited open iridocorneal angle (Figure 12a, $n = 10$), whereas a wide attachment of the iris and cornea was present in the entire circumference of the eye (Figure12f, $n = 14$). At this age, no signs of cornea cloudiness and deep anterior chamber were observed (Figure 12b, c, d and e). Occasionally, a few eyes had misshapen or open pupils, which were likely a consequence of the severe iris cornea adhesions that prevent normal iris muscle function. The adhesion of the iris and cornea persisted throughout life (Figure 12l and r). Corneal damage was first observed at around 1 month of age. By 3 months of age, the entire cornea was completely cloudy (Figure 12g, wild-type homozygotes, $n = 14$; Figure 12j, *nee* homozygotes, $n = 16$), and by 10 month, neovascularization was seen in the majority of eyes (Figure 12m, wild-type homozygotes, $n = 6$; Figure 12p, *nee* homozygotes, $n = 6$). Enlarged anterior chambers were evident at 3 months of age (Figure 12k). Combined, these observations suggest that early developmental defects cause malformed angle, resulting in iridocorneal adhesion. Later, as aqueous humor begins to be secreted, the iridocorneal adhesions block aqueous humor out flow, and lead to elevated intraocular pressure (causing increased depth of the anterior chamber) and damaging the corneal endothelium (causing corneal opacities).

Elevation of intraocular pressure of *nee* mutants

In order to test whether the iridocorneal adhesion of *nee* mice causes elevated IOP, IOP was measured in cohorts of age matched wild-type and *nee* homozygotes (Figure 13a). At 3-4 months of age, control mice homozygous for wild-type alleles

exhibited an IOP of 16.0 ± 2.6 mmHg (mean ± SD; $n = 15$), a value within the range of normal pressures observed in nonglaucomatous inbred mice (Smith, Zabaleta et al. 2001). In comparison, *nee* homozygous mutants had significantly elevated IOP of 30.8 ± 12.5 mmHg (mean ± SD; $n = 15$; $P < 0.0006$, Student's two tailed *t*-test). In examining the onset of elevated IOP, mice with significantly elevated IOP were observed as early as 1 month of age and late as 12 months of age (Figure 13b). These data indicate that *nee* mice likely have a congenital elevation of IOP which can remain elevated for substantial periods of time.

Retinal ganglion cell loss, optic nerve head excavation and axon damage of *nee* mice

Since elevated IOP usually associates with retinal ganglion cell degeneration, retinas of *nee* homozygotes were examined by histology (Figure 14). At P17, *nee* homozygous mutants were morphologically normal compared to age matched wild-type homozygotes (Figure 14a and b). The retinal ganglion cell layer was continuous and contains 1-2 cell layers thick. A robust nerve fiber layer was present and other retinal layers were also intact. By 3 months of age, loss of retinal ganglion cells was clearly observable in all of the retinas examined (Figure 14d, e and f). However, there was a variation of the severities of retinal damage between retinas. In some eyes, only the retinal ganglion cell layer appeared to be affected (Figure 14d). In other eyes, a serve depletion of all layers was observed and the thickness of the retina was significantly reduced (Figure 14e and f). Retinal thinning has been previously observed in other glaucomatous mouse strains. In some DBA/2J mice, the bipolar cell layer reduces to 3-4 cells thick (John, Smith et al. 1998), and in strain AKXD-28/Ty which exhibits a similar IOP to DBA/2J but more severe optic nerve damage and rapid disease progression, trans-retinal thinning is also present (Anderson, Smith et al. 2001).

In addition to the loss of retinal ganglion cell bodies, severe optic nerve head excavation also occurred in *nee* mutants at an early age (Figure 15). In both *nee* homozygous wild-type and mutant mice, thick nerve fiber layers containing axons projecting to the optic nerve head were evident at 17 days of age (Figure 15a and b). In contrast, by 3 months of age, advanced optic nerve head atrophy extending to a level beyond the choroid was clearly identifiable in every *nee* homozygotes mutant (Figure 15c and d). To further confirm the damage to axons of the retinal ganglion cells, cross sections of optic nerves were cut and stained with PPD to visualize myelinated axons. As expected, *nee* homozygous mutants exhibited optic nerve atrophy (Figure 16). At 17 days of age, axons within the optic nerves of both wild-type and *nee* homozygotes appeared healthy, containing tightly packed myelin sheath surrounding individual axons (Fig 16a and b). Interestingly, the total number of myelinated axons from the P17 wild-type homozygotes and *nee* homozygotes was slightly different. While the wild-type homozygous mice had an average of 25860 ± 3656 axons (mean ± SD; $n = 13$), *nee* homozygous mutants showed an average of 20988 ± 2183 (mean ± SD; $n = 10$; $P < 0.0008$, Student's two tailed *t*-test). Thus, *nee* appears to cause a subtle, but significant, developmental defect in axon number, which is not surprising giving the *nee* mice are also smaller than wild-type homozygotes. With age, axons within nerves of the *nee* homozygous mutants underwent degeneration. While wild-type homozygotes still contained numerous healthy myelinated axons by 3 months of age (Figure 16c), the majority of axons within optic nerves of *nee* homozygous mutants were degenerated. At this age, the remnants of optic nerves were composed of areas of degenerating axons (spots of darkly stained structures) and gliosis (Figure 16d). Taken together, these results suggest that *nee* homozygous mutants develop an early onset form of glaucoma associated with iridocorneal adhesion and elevated IOP.

In addition to glaucoma, histological examination also revealed cataracts in adult *nee* homozygous mutants (Figure 17). Normal lenses contain three parts: lens capsule,

lens fibers and the lens epithelium. Lens capsule is a layer of basement membrane surrounding the lens. Lens fibers are long, thin, tightly packed cells arranged in concentric layers which form the bulk of lens. Lens epithelium is a monolayer of cells underneath the anterior lens capsule. No lens epithelial cells are present underneath the posterior capsule. At the lens equatorial region, these epithelium cells give rise to lens fibers. To maintain lens transparency, the majority of lens fibers at the center of the lens have no organelles or nuclei. Insulting factors that cause abnormal arrangement or degeneration of lens fibers can induce opacity of the lens and cause cataracts. Light microscopic examination of *nee* mutants at 17 days of age showed a lens indistinguishable from wild-type homozygotes (Figure 17 a-d, $n = 11$ per genotype). By 3 months, many mutant eyes (9 out of 19 eyes examined) developed cataracts, characterized by atypically enlarged lens fibers and the presence of cell nuclei at the posterior region (Figure 17h).

Expression of *Sh3pxd2b* in the eye

Previously we have showed that the SH3PXD2B protein is present in the mouse eye by western blot (Mao, Thedens et al. 2009). In order to understand the pathogenesis of glaucoma in *nee* homozygous mutant mice, we examined protein expression patterns in the eye by immunofluorescence. We first attempted to utilize our previously characterized anti-mouse antibody to cryosections obtained from both wild-type homozygotes and *nee* homozygotes. The antibody was generated against a portion of SH3PXD2B (amino acid # 440-751) which is predicted to be absent in *nee* homozygous mutants due to the 1-bp deletion. Therefore, we expected to observe the labeling only in wild-type homozygotes. However, we detected similar levels of labeling in both *nee* homozygous wild-type and mutants, suggesting signal was from background labeling of nonspecific epitopes. We next utilized two commercial rabbit polyclonal antibodies

generated against a portion of either mouse or human SH3PXD2B proteins. Unfortunately, neither of the antibodies could recognize mouse SH3PXD2B by western blot (data not shown). However, the antibody against human SH3PXD2B recognized a specific band from lysates of a human transformed meshwork cell line (HTM-5) (Figure 18a). Therefore, we obtained ocular cryosections from healthy human donors, and performed immunofluorescence labeling. Presence of SH3PXD2B was demonstrated in multiple tissues in the eye, including the cornea epithelium and cornea stroma, ciliary body muscle, retina, trabecular meshwork, lens epithelium cells and lens fibers and the ciliary body smooth muscles (Figure 18b-k). The result is consistent with a few microarray studies of ocular cell lines and tissues from mice and human which also suggest a broad ocular expression (Lively, Jiang et al.; Zhao, Pearson et al. 2003; Steele, Inman et al. 2006; Zhou, Li et al. 2006; Fuchshofer, Stephan et al. 2009; Luna, Li et al. 2009; Shi, Cui et al. 2009). Thus, these data suggest SH3PXD2B is widely expressed in adult human eyes.

Discussion

We provide evidence here that mutation in the *Sh3pxd2b* gene in *nee* mice resulted in elevated IOP and glaucoma. In the past, we have noticed that adult *nee* homozygous mutants exhibit anterior synechia, corneal cloudiness and enlarged anterior chambers (Mao, Thedens et al. 2009). By examining mice at a younger age, we noticed a severe anterior synechia as the only abnormality present in the eye, suggesting that anterior synechia is the primary defect occurred in *nee* mice. Peripheral anterior synechia in these mice likely blocked aqueous humor outflow through both the trabecular meshwork and uveoscleral pathways, leading to the drastic elevation of IOP. Elevated IOP in turn contributed to cloudy corneas, retinal degeneration and optic nerve cupping.

Combined, our data suggests that *nee* mice represent a model of early onset form of closed angle glaucoma.

Mechanisms of *Sh3pxd2b*-mediated defects

The mammalian eye is derived from three main tissue cell types: surface ectoderm, neuronal ectoderm and periocular mesenchyme. The surface ectoderm gives rise to the corneal epithelium and lens, and the neuronal ectoderm contributes to the retina, iris epithelium and ciliary body epithelium (Sowden 2007). In mice, at around E10.5, a rudimentary eye called optic vesicle is formed which contains primordial cornea, lens and retina. After the initial formation of the optic vesicle, periocular mesenchymal cells of the neural crest or mesodermal origin migrate in between the edge of future cornea and retina. These progenitor cells will give rise to a variety of cell lineages in the eye, including the corneal stroma, corneal endothelium, ciliary stroma and smooth muscles, iris stroma, and trabecular meshwork (Gould, Smith et al. 2004). The tissues listed are in sequential order. Abnormal cell-cell adhesion, cell migration and differentiation can result in a spectrum of anterior segment dysgenesis disorders such as the Axenfeld-Rieger anomaly, Peter's anomaly and others, which typically involve a combination of iridal and corneal defects and have a high incidence of developing glaucoma (Alward 2000).

In both humans and mice, mutation in genes such as *Foxc1*, *Foxc2*, *Pitx2* can lead to abnormal attachment of the iris and cornea along with several other signs of anterior segment dysgenesis (Gage, Suh et al. 1999; Hong, Lass et al. 1999; Smith, Zabaleta et al. 2000; Libby, Smith et al. 2003). Although these genes are known as transcriptional factors, the majority of their downstream factors are unclear. Some of their target genes are known to affect ECM stability (Hjalt, Amendt et al. 2001). Thus, misregulation of the ECM was thought to be one consequence of these mutations that affects normal

development (Gould, Smith et al. 2004). Because of the role of SH3PXD2B in podosomes and ECM remodeling, it is tempting to speculate whether SH3PXD2B and these transcriptional factors participate in an overlapping molecular pathway. However, to our knowledge, it is not currently known whether *Sh3pxd2b* is a transcriptional target of FOXC1 (Tamimi, Lines et al. 2004; Berry, Skarie et al. 2008) and other two transcriptional factors. Future studies on the transcriptional regulation of the *Sh3pxd2b* gene and its spatial and temporal expression patterns during eye development are needed to expand its molecular pathway. In addition, since the only known function of SH3PXD2B is in invadosome assembly, our data suggest that defective invadosome assembly may contribute to abnormal ocular development. Therefore, it is tempting to speculate proteins that interact with SH3PXD2B or participate in invadosome assembly may contribute to anterior segment dysgenesis as well.

Mouse models of glaucoma

Mouse models are useful tools to study the basic biology of glaucoma and test the efficacy of potential medical treatments. There are both induced and spontaneous mouse models of glaucoma, which all have their own advantages and disadvantages. Mice can be induced to have ocular hypertension by blocking the aqueous humor outflow with a variety of experimental approaches such as those occluding the episcleral veins with laser, cautery or hyaluronic acid (Pang and Clark 2007). These approaches, however, usually require a certain level of technical proficiency. In addition, generally the glaucoma in induced models is relatively modest with mild IOP elevation and limited retinal ganglion cell and axon loss (McKinnon, Schlamp et al. 2009). The spontaneous models such as the widely used DBA/2J mice are relatively easy to manipulate, and the disease is relatively more severe. However, the onset of glaucoma in the majority of the currently available models is usually late. Sometimes over a year of aging of the strain is

needed before disease develops (John, Smith et al. 1998; Anderson, Smith et al. 2001; Danias, Lee et al. 2003; Mabuchi, Lindsey et al. 2004), which makes them less cost effective. The *nee* homozygous mutant mice have several unique features that make them a better model of glaucoma studies. The mice develop a spontaneous elevation of IOP at around 1 month, and complete axon loss at around 3 month, thus reduce the requirement of ocular manipulation as in induced models. The high frequency, rapid progression and the severity of the disease may make them a better model than other spontaneous models since using *nee* could reduce the cost of strain maintenance.

In summary, we have demonstrated *nee* homozygous mutants develop a spontaneous glaucoma phenotype mediated by SH3PXD2B. The *nee* mice will not only serve as a valuable spontaneous mouse model, but will also expand our understanding of ocular development and the pathogenesis of glaucoma in humans.

Figure 12. Clinical defects of *nee* mice at different age.

Slit-lamp examination of eyes from wild-type homozygotes and *nee* homozygotes at ages of 17 days (**a-f**), 3 months (**g-l**) and 10 months (**m-r**) show that mice homozygous for the *nee* mutation have developed iridocorneal adhesion at P17, which leads to cloudy corneas and enlarged anterior chamber. Three different views of the same eyes are shown in each group. Wild-type mice at all ages have a clear cornea (**a**, **g** and **m**). At P17, corneas of *nee* mutants also appear normal (**d**), whereas cloudy cornea and corneal neovascularization occur later (**j** and **p**, respectively). Complete corneal opacity blocks the view of the anterior chamber and the limbus in **l** and **r**. Wild-type homozygotes at all ages (**b**, **h** and **n**) and *nee* mutants at P17 (**e**) also have normal anterior chamber depth. In this view, the iris and cornea appear close to each other in normal eyes. In contrast, enlarged anterior chambers can be observed in *nee* mutants at 3 months of age (**k**, *double arrow*). The irideocorneal angle of wild-type mice is characterized by a sharply defined limbus (**c**, **i** and **o**, *arrowhead*), whereas the irideocorneal angle of *nee* homozygotes has severe peripheral anterior synechia (**f** and **l**, *double arrow*). Note the *nee* mutant eyes at P17 appear smaller than wild-type littermates because their eyelids are not fully open.

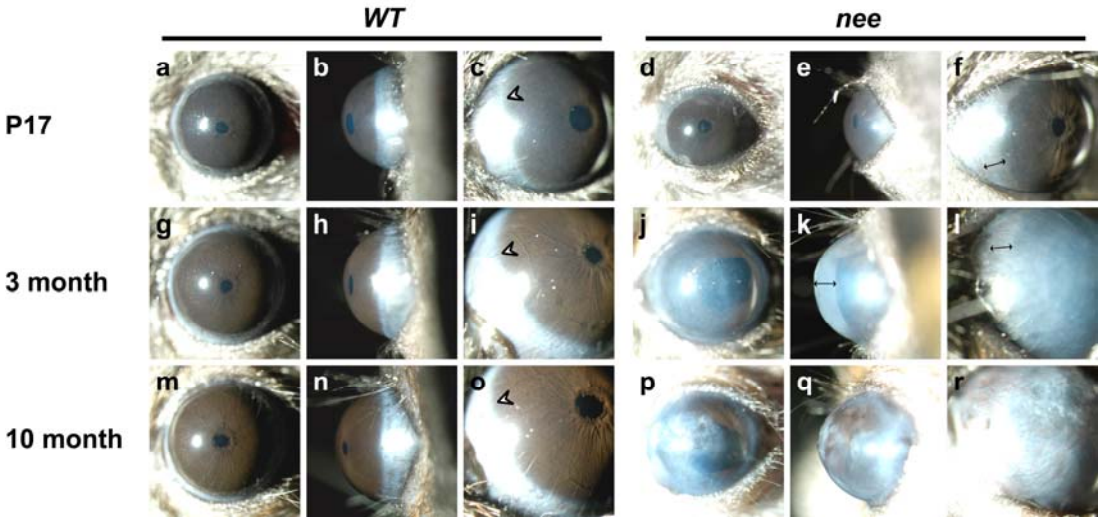
WT
nee
P17
3 month
10 month
a
b
c
d
e
f
g
h
i
j
k
l
m
n
o
p
q
r

Figure 13. Elevated intraocular pressure of *nee* mutants.

(**a**) IOP measurements of wild-type homozygotes and *nee* homozygotes at 3-4 months of age. IOP measurements are shown as the mean ± SD. The asterisk indicates a p-value of less than 0.05 (**b**) IOP measurements of individual *nee* homozygous mutants at various ages. The line indicates two and a half standard deviation above the mean IOP of wild-type homozygotes at 3-4 months of age.

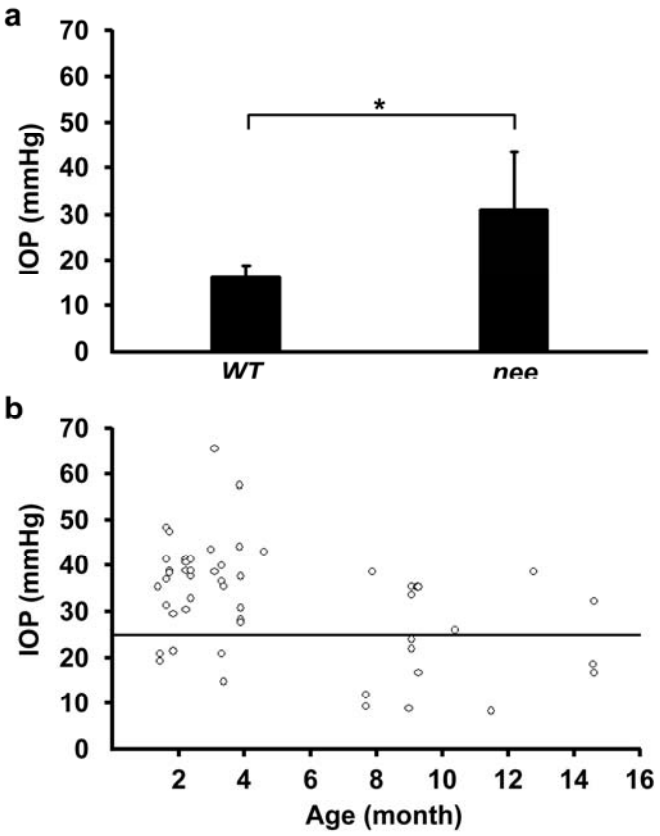
a
70
60
50
40
30
20
10
0
IOP (mmHg)
*
WT
nee
b
70
60
50
40
30
20
10
0
IOP (mmHg)
2
4
6
8
10
12
14
16
Age (month)

Figure 14. Retinal degeneration in *nee* mutants.

Histological examination of eyes from age matched wild-type homozygotes and *nee* homozygotes were performed, and posterior retinas were imaged. (**a, b**) Cross sections of eyes at 17 days of age. The retina is well developed and all laminae are present and intact in both wild-type and *nee* homozygotes. A thick nerve fiber layer (*black arrow*) and healthy ganglion cell layer (*empty arrow head*) was evident. Wild-type homozygotes, n = 11; *nee* homozygotes, n = 12 (**c, d**) Cross sections of eyes at 3 months of age. While wild-type retina was healthy, *nee* mutants lacked the retinal ganglion cell layer (*empty arrow head*). Wild-type homozygotes, n = 12; *nee* homozygotes, n =19 (**e, f**) Cross sections of two *nee* mutant eyes at 3 months of age, showing the presence of trans-retinal thinning. Scale bar = 200 μm.

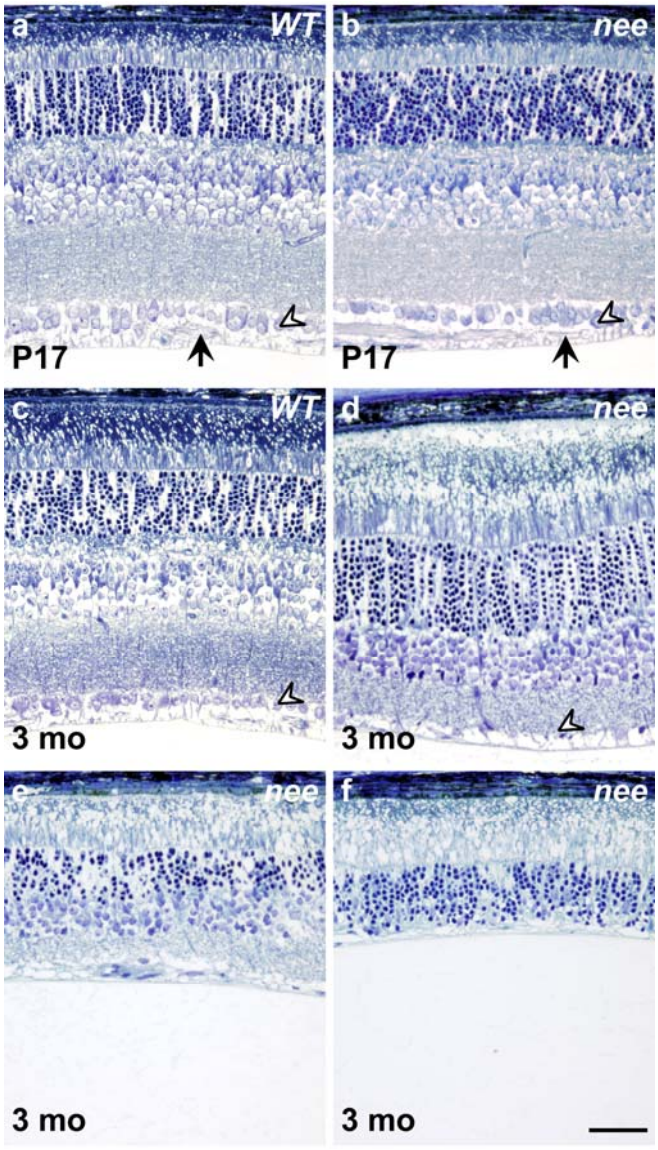
a
WT
P17
b
nee
P17
c
WT
3 mo
d
nee
3 mo
e
nee
3 mo
f
nee
3 mo

Figure 15. Optic nerve head excavation of *nee* mice.

(**a, b**) Optic nerve head of wild-type homozygotes and *nee* homozygotes at P17 are normal, as characterized by a thick nerve fiber layer (*black arrow*) entering the optic nerve region. Wild-type homozygotes, $n = 11$; *nee* homozygotes, $n = 12$. (**c, d**). In contrast, at 3 month of age, *nee* mutant mice exhibit a serve excavation (*empty arrowhead*) that extends to a level below the choroid. Wild-type homozygotes, $n = 11$; *nee* homozygotes, $n = 12$. Scale bar = 150 μm.

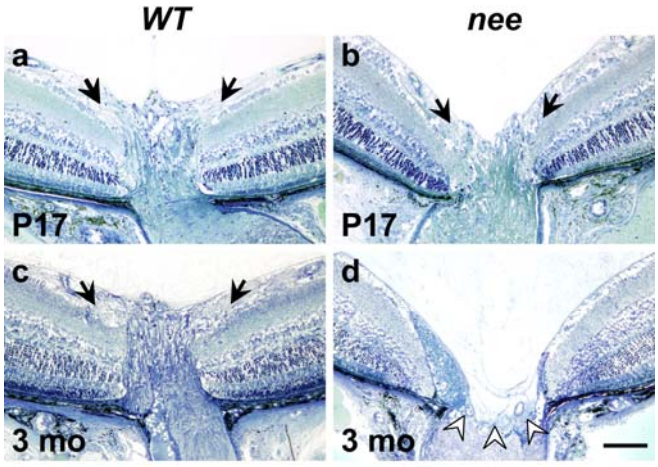
WT
nee
a
b
P17
P17
c
d
3 mo
3 mo

Figure 16. Axon degeneration of optic nerves from *nee* mutants.

Cross sections of optic nerves from wild-type homozygotes and *nee* homozygotes were stained with PPD, which stains the myelin sheath of healthy optic nerves and the axoplasm of damaged axons. (**a, b**) Optic nerves of mice at P17 days of age. Both wild-type homozygotes and *nee* homozygotes had healthy optic nerves, as characterized by numerous ring-like shaped structures, which are healthy axons with integrate myelin sheath. Axons from *nee* mutants appeared sparser than wild-type, however, no signs of damaged axons were identified. Note myelination of axons from the optic nerves at this stage is not fully completed, so axons are sparser in comparison to adult optic nerves. Wild-type homozygotes, $n = 13$; *nee* homozygotes, $n = 10$. (**c, d**) Optic nerves of mice at 3 months of age. Optic nerves from *nee* mutants exhibit severe degeneration, as characterized by spots of darkly stained structures and areas of gliosis in the optic nerves. No healthy axons were discernible. Wild-type homozygotes, $n = 12$; *nee* homozygotes, $n = 19$. Scale bar = 20 μm.

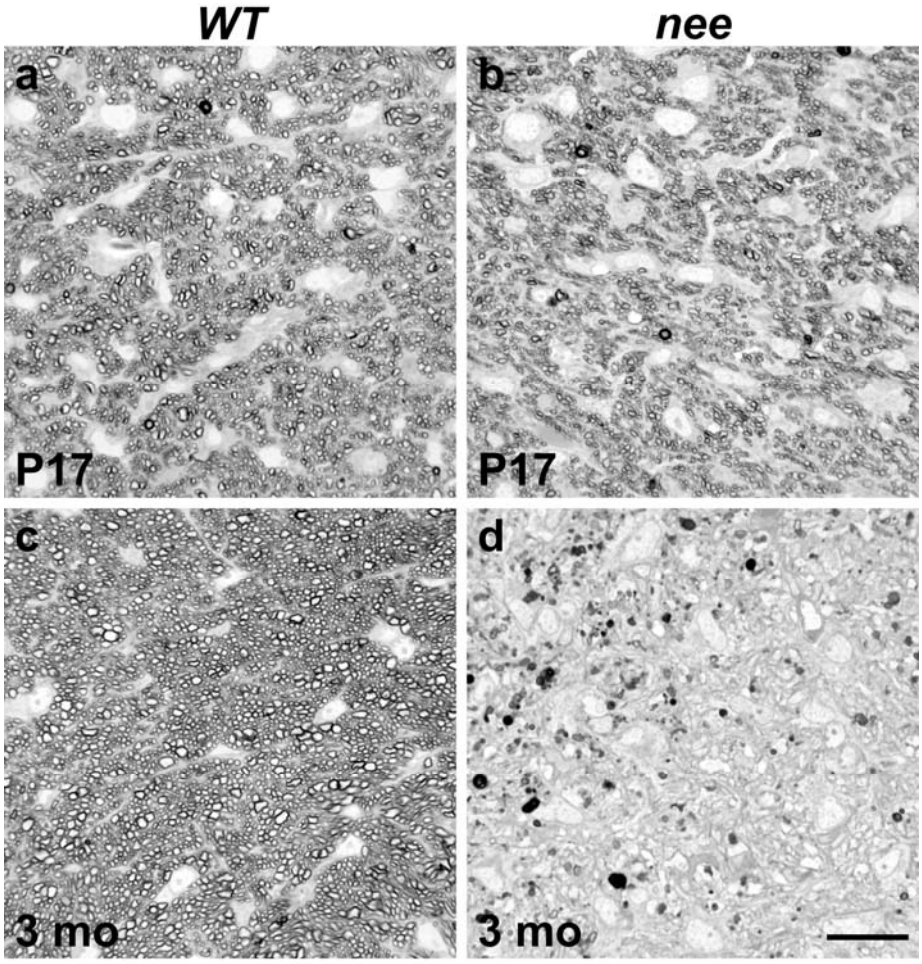
WT
nee
a
b
P17
P17
c
d
3 mo
3 mo

Figure 17. Cataract in *nee* mutants.

Plastic sections of *nee* lenses show the mutant mice develop cataract starting at 3 month of age. (**a-d**) Wild-type and *ne*e homozygotes at 17 days of age. Scale bar = 200 μm **(e-f)** Wild-type and *ne*e homozygotes at 17 days of age. Scale bar = 20 μm. Images are arranged with wild-type homozygotes on the left and *nee* mutants on the right. **a, c, e** and **g** were taken under 4X magnification, while **b**, **d**, **f** and **h** were images from the posterior lens (the boxed area in a, c, e and g, respectively) taken under 40X magnification. While *nee* mutant lens appeared normal at 17 days of age, the posterior lens fibers from 3 month old *nee* mutants were abnormally enlarged (*arrowhead*), and curved away from the polar axis. Moreover, posterior migration of cells, which should only be present beneath the anterior lens capsule and at the lens equatorial region, was also seen, as indicated by the nuclei (*arrow*).

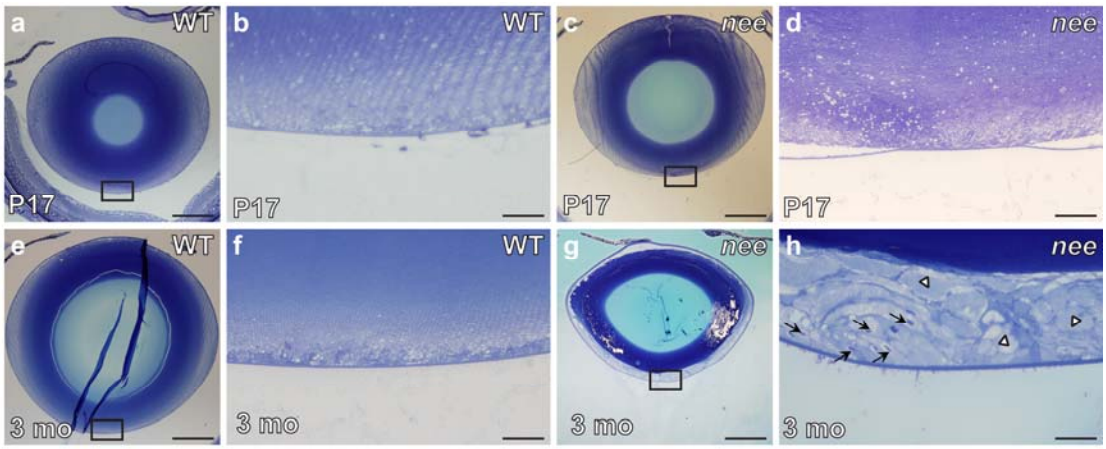
a
WT
P17
b
WT
P17
c
nee
P17
d
nee
P17
e
WT
3 mo
f
WT
3 mo
g
nee
3 mo
h
nee
3 mo

Figure 18. Ocular expression of SH3PXD2B.

(**a**) Western blot showing that a rabbit polyclonal antibody against human SH3PXD2B can specifically recognizes a band at the expected size for SH3PXD2B. Lysates were made from cultured human trabecular meshwork cells. (**b-k**) Immunofluorescent labeling of ocular sections from human tissue using the anti-human SH3PXD2B antibody. Expression of SH3PXD2B was detected in cornea epithelium and cornea stroma (**b**), in all layers of the retina (**c**), in trabecular meshwork (**d**), lens epithelium and lens fibers (**e**) and ciliary body smooth muscles (**f**). Negative controls were adjacent sections stained with no primary antibody (**g-k**). All images were taken with a confocal microscope at 40X. Scale bar = 50 μm.

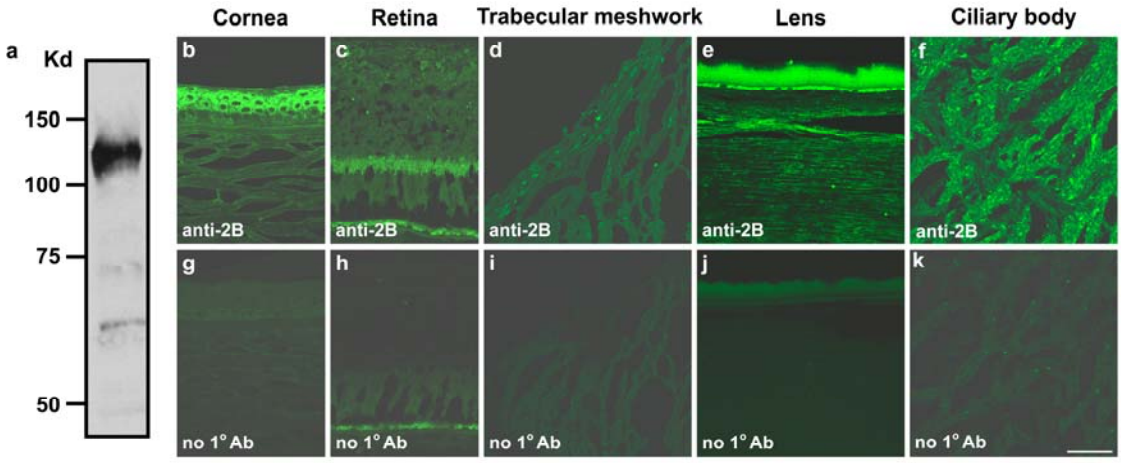
a
Kd
150
100
75
50
Cornea
Retina
Trabecular meshwork
Lens
Ciliary body
b
c
d
e
f
anti-2B
anti-2B
anti-2B
anti-2B
anti-2B
g
h
i
j
k
no 1° Ab
no 1° Ab
no 1° Ab
no 1° Ab
no 1° Ab

CHAPTER 4
HUMAN RELEVANCE OF SH3PXD2B

Introduction

Mice have a similar genome and physiology to humans, and studies that begin with mice can often lead to the identification of disease causing mutations in humans. As mentioned in previous chapters, the spontaneously arising mouse mutant *nee*, which has a mutation in gene *Sh3pxd2b*, develops several defects including runted growth and craniofacial abnormalities, hearing loss, and lipodystrophy. In addition, these mice develop a form of early onset closed angle glaucoma. Based on this, we investigated whether mutations in *SH3PXD2B* could cause defects in humans. By collaborating with other labs, we tested if mutations in *SH3PXD2B* might be present in three groups of patients briefly described here.

Methods

Cohort of patients with glaucoma

All patients (congenital glaucoma, $n = 15$; Rieger's anomaly, $n = 22$; developmental glaucoma, $n = 29$; primary open angle glaucoma, $n = 119$) and control subjects ($n > 150$) were from the same outpatient ophthalmology clinic population at the University of Iowa. Subjects underwent complete eye examinations which included anterior segment examination, gonioscopy, IOP measurement by Goldmann applanation tonometry, pachymetry, refraction and a mydriatic optic disc assessment. Genomic DNA was isolated from peripheral blood samples.

Comparative genomic hybridization

CGH has been performed using 385K and 2.1 M microarrays produced by Nimblegen following the manufacturer's recommendations. The microarrays were scanned using the GenePix 4000B Scanner, analyzed using the NimbleScan software and displayed by the SignalMap software from Nimblegen.

Results

SH3PXD2B and glaucoma

This work was done in collaboration with Dr. John Fingert in the Department of Ophthalmology and Visual Sciences at the University of Iowa. The human ortholog of *Sh3pxd2b* is on chromosome 5q35.1, a loci not previously linked to glaucoma (Wiggs 2007). The gene contains 13 exons with a total of 7793 base pairs. Each exon was amplified from genomic DNA by PCR and DNA sequencing analysis was performed on the entire coding region and the splicing junctions of *SH3PXD2B*. In patients with developmental forms of glaucoma (congenital glaucoma, Rieger's anomaly and other rare forms of developmental glaucoma), 3 different homozygous point mutations were identified (Table 3). In addition, a homozygous TC to CT change was identified in an intronic region. No severe mutations such as deletions, insertions or nonsense mutations were found. Because it is possible that severe mutations cause early onset glaucoma while mild mutations cause a late onset disease, we also tested whether there are mutations in POAG patients. Similarly, 5 different homozygous and heterozygous point mutations in the coding region and 1 in the intron were identified. The point mutations were not known SNPs and they were not present in more than 300 chromosomes from the

control groups (Table 3). The point mutations in the coding region are all missense mutations expect for one synonymous mutation. Several of them are highly conserved among different species, suggesting a possibility of disease causing mutations.

SH3PXD2B and a patient with a microdeletion on Chr 5q35.1

This work was done in collaboration with Dr. Peter Nagy in the Department of Pathology and Dr. Arlene Drake in the Department of Ophthalmology and Visual Sciences at the University of Iowa. Dr. Peter Nagy has been working on identification of copy number variations (CNVs) using Comparative Genomic Hybridization (CGH) to detect alterations in the copy number of genomic segments. These can be deletions or duplications either inherited from one's parents or arising *de novo* during gametogenesis. Given the recent realization of CNVs as a common type of disease causing mutation, we collaborated to ask whether CNVs influencing *SH3PXD2B* might contribute to human diseases.

Our identification of a patient with a CNV influencing *SH3PXD2B* began with Dr. Nagy's independent study of a patient with autism-like features. The patient's mother also had learning disabilities and had to be placed in special education as a child. The patient's father has had a history of seizures and an upper right extremity congenital malformation. Based upon this information it was suspected that the patient's symptoms may be due to a potentially inherited chromosomal abnormality. Nimblegen CGH microarrays were used to determine the cause of the autistic spectrum disorder. The patient's DNA was compared with DNA of either parent using CGH. A 1.2Mb *de novo* deletion was found on chromosome 5q35.1 that was not present in either parent (Figure 19). Subsequently the deletion was confirmed using a reference DNA combined from six normal female individuals using a 2.1 Million feature Nimblegen microarray. Based on this experiment, the deletion extends from coordinates 171,074,475 to 172,303,453 on

chromosome 5 and includes *SH3PXD2B* along with 5 other genes (Table 4). Detailed ophtalmological examination revealed that the patient have unilateral congenital cataract (Figure 20) at 10 years old which falls in the spectrum of anterior segment dysgenesis. This result suggests that deleting *SH3PXD2B* might cause all these defects in humans.

SH3PXD2B and SHORT syndrome

This work was done in collaboration with Dr. Ordan Lehmann in the Department of Ophthalmology and Medical Genetics at the University of Alberta in Canada. Because *nee* mutant mice develop congenital glaucoma as part of what appears to be a broader syndrome, we began a search in the literature for syndromes involving glaucoma, reduced body size, and lipodystrophy. SHORT syndrome (OMIM# 269880) is a rare disease in which affected patients typically have short statures, hyperextensibility of joints and or inguinal hernia, ocular depression, Rieger's anomaly, teething delay, lipodystrophy and facial abnormalities. Some patients have congenital glaucoma with elevated IOP, deafness, delayed bone age, developmental delay, and insulin resistance. The inheritance pattern is not clear, as both autosomal dominant and autosomal recessive inheritance have been reported. To date, the only known genetic defects is a (1;4)(q31.2;q25) translocation reported in one pedigree, which is near the *PITX2* gene (Karadeniz, Kocak-Midillioglu et al. 2004). To test whether *SH3PXD2B* mutations might contribute to SHORT syndrome, we are performing DNA sequencing analysis in a pedigree with one affected parent and two affected children. Although this experiment is not yet complete, 1 single nucleotide substitution, G2398A, which causes a V743M missense substitution in a linker region between the third and fourth domains of SH3PXD2B, was identified in the affected parent. Analysis of the affected children is underway. If the same substitution segregates within the family, future experiments will be needed to determine the influence of the missense variation.

Discussion

As most genes have a functional conservation between mouse and human, the defects in *nee* homozygous mutant mice led us to examine whether *SH3PXD2B* mutations could cause diseases in humans. Analysis of developmental and primary open angle glaucoma patients identified a few single nucleotide substitutions, most of which are missense substitutions affecting conserved amino acids. Although these results suggest that *SH3PXD2B* might not be a common cause of glaucoma, however, we can not rule out their possibility as being disease causing mutations. The developmental forms of glaucoma are rare diseases (Francois 1980; Meyer-Marcotty, Weisschuh et al. 2008), and large patient sets are not available. Thus, although the occurrence of each point mutation identified in the developmental forms of glaucoma patients is rare, this can be explained by the limited sample size included in the analysis. To move forward, assays determining the functional influence of these point mutations are needed to test them as disease causing mutations. Alternatively, it is still possible that the mutation might be in the unanalyzed promoter region or intronic sequences which might influence gene expression.

Studies with the patient with a microdeletion at Chr 5q35.1 suggest that *SH3PXD2B* may contribute to congenital cataract. The deletion disrupts 6 genes including *SH3PXD2B*. None of the deleted genes have known role in any ocular diseases (Laumet, Petitprez et al.; Suzuki, Chiba et al. 2000; Liu, An et al. 2003; Breuza, Halbeisen et al. 2004; Das, Chu et al. 2006; Koolen, Herbergs et al. 2006; Liu, Wang et

al. 2008; Belkina, Liu et al. 2009). However, since *nee* homozygous mutant mice develop cataract (see Chapter 3), it suggests that *SH3PXD2B* is likely to be the causative gene for congenital cataract in this patient. There are few reports previously described with deletions encompassing 5q35.1 (Baekvad-Hansen, Tumer et al. 2006; Rauch and Dorr 2007). However, it is interesting that there is no mention of congenital cataracts in the other patients. This might be due to lack of in depth ophtalmologic examination of those patients, although we cannot exclude at this point that the overlap of the phenotype between mice and this human subject is purely coincidental. Clearly more patients with congenital cataracts should be tested for microdeletions affecting the *SH3PXD2B* gene.

Recently, a group reported mutations in the *SH3PXD2B* gene cause Frank-Ter Haar syndrome (Iqbal, Cejudo-Martin et al. 2010). Frank-Ter Haar syndrome (OMIM # 249420) is an autosomal ressive disease characterized by skeletal dysplasia, cardiac abnormalities, facial dysplasia, hypertelorism and congenital glaucoma. Other defects such as growth retardation are also reported. In one patient, loss of subcutaneous fat was reported as well. In 13 families examined, 7 families contained mutations in *SH3PXD2B*. Five mutations, including one microdeletion, one 1 bp insertion, one 1 bp deletion, one splicing acceptor site mutation and one missense mutation, were identified in 10 out of 17 patients. Although we have not identified any severe mutations in SHORT syndrome patients, it is interesting that SHORT syndrome patients have overlapping clinical signs with Frank-Ter Haar syndrome including the craniofacial and ocular abonormalities, and perphaps lipodystrophy. It is therefore tempting to speculate that SHORT syndrome and Frank-Ter Haar syndrome may represent different points of a phenotypic spectrum linked by a comon molecular etiology.

Figure 19. Comparative Genomic Hybridization analysis of a patient with autism-like features.

A 1.2Mb microdeletion at Chr 5q35.1 was identified. The genes involved in the1.2Mb microdeletion are indicated with red arrows.

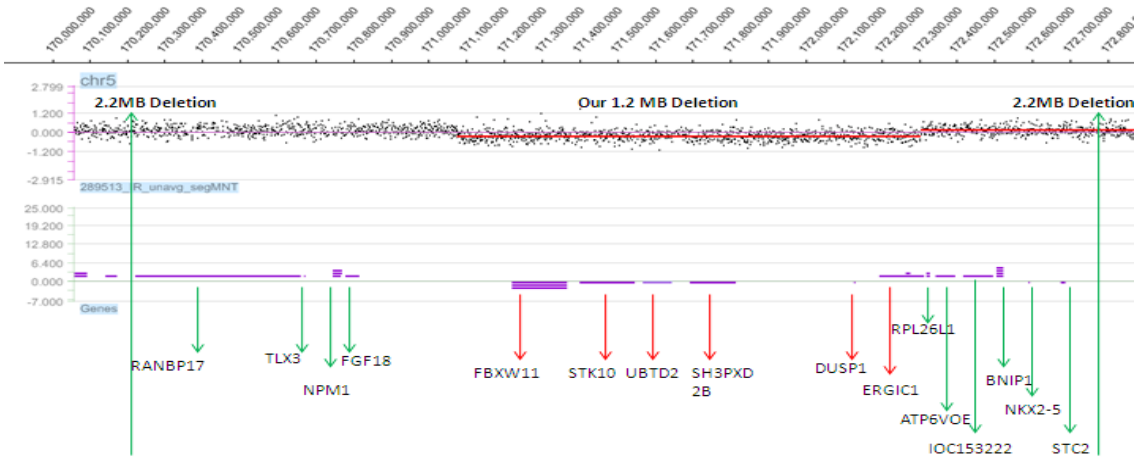
chr5
2.2MB Deletion
Our 1.2 MB Deletion
2.2MB Deletion
RANBP17
TLX3
NPM1
FGF18
FBXW11
STK10
UBTD2
SH3PXD 2B
DUSP1
ERGIC1
RPL26L1
ATP6VOE
IOC153222
BNIP1
NKX2-5
STC2

Figure 20. Cataract in the patient with a microdeletion on Chr 5q35.1

The eye of the patient is dilated and slit lamp examination was performed. The opaque spot in the center of the lens indicates the presence of cataract.

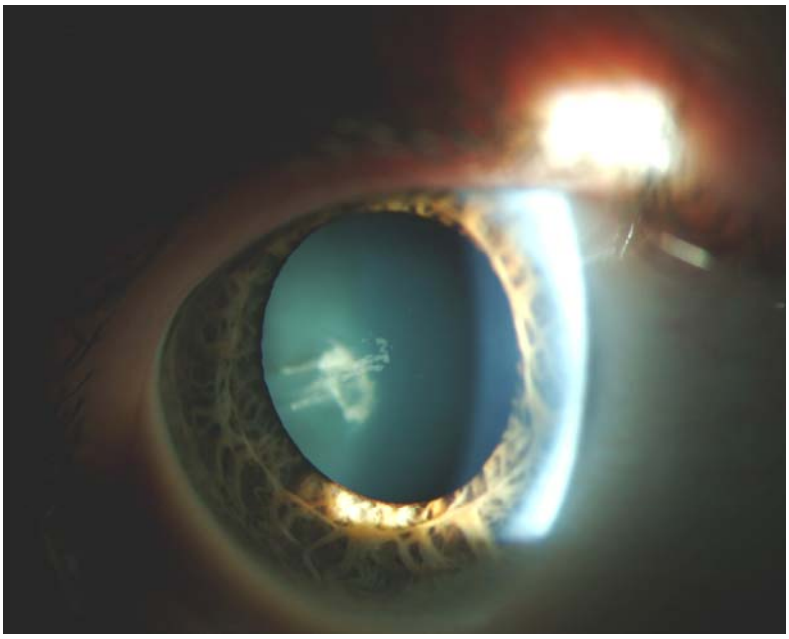

Table 3. Mutations identified in human glaucoma patients

Exon	Mutations	Congenital *n* = 15	Rieger's *n* = 22	Other Developmental *n* = 29	POAG *n* = 119	Normals
Ex. 4	IVS3-28 a>g Hom	0	0	0	1	0/162
Ex. 8	Ala195Ala GCC>GCG Het	0	0	0	1	0/151
Ex. 9	Gly245Arg GGG>AGG Het	0	0	0	1	0/160
Ex. 10	Ala309Val GCG>GTG Hom	0	1	0	0	0/155
Ex. 12	Arg356Gln CGA>CAA Hom	0	0	0	1	0/165
Ex. 12	IVS11-8 C>T; IVS11-9 T>C Hom	1	0	1	0	0/165
Ex. 12	Glu396Lys GAG>AAG Hom	0	0	1	0	0/165
Ex. 13	Ala431Thr GCG>ACG Hom	0	0	1	0	0/169
Ex. 13	Gly481Arg GGG>AGG Hom	0	0	0	1	0/294
Ex. 13	ILE832VAL ATT>GTT Hom	0	0	0	1	0/171

Table 4. Genes disrupted in the 1.2 Mbp deletion on Chr 5q35.1

Gene	Protein	Function
FBXW11	F-Box and WD40 Domain Protein 11	This protein takes part in the ubquitin protein ligase complex, SCF essential for cell cycle regulation (Suzuki H, et al. 2000)
STK10	Serine/threonine Protein Kinase 10	This gene encodes a a major ERM (ezrin-radixin-moesin) protein kinase in resting lymphocytes and regulates cytoskeletal rearrangement (Belkina NV, et al. 2009)
UBTD2	Dendritic Cell-Derived Ubiquitin-like Protein	Not much is known about this gene. It may participate in TRAIL-induced apoptosis or retinod acid receptor alpha signaling processes (Liu S, et al. 2003)
SH3PXD2B	SH3 and PX domains 2B	This gene encodes for a podosomal-adaptor protein that is essential to postnatal growth and development, especially with regards to physiologic contexts pertaining to the extracellular matrix (Mao M, et al. 2009)
DUSP1	Dual Specificity Phosohatase 1	This gene is important to cell cycle regulation. DUSP1 plays a vital part in the human cellular response to environmental stress. It may also play a role in the negative regulation of cellular proliferation (Liu YX, et al. 2008)
ERGIC1	ER-Golgi Intermediate Compartment 32 kDa Protein	This is a cycling membrane protein which functions in the transport between the endoplasmic reticulum (ER), the intermediate compartment (ERGIC), and the Golgi (Breuza, L et al. 2004)

CHAPTER 5
CONCLUSIONS AND FUTURE DIRECTIONS

Glaucoma is a group of diseases with complex etiology. Genetics is one approach to dissect the complex molecular mechanisms underlying glaucoma. Over recent years, genetic studies in humans have made important achievements as many genes and loci have been identified. These genes or loci, however, only account for a small fraction of glaucoma cases, and the majority of the causative mutations remain to be defined. Genetic studies in humans face many challenges, because most glaucoma cases are late onset, have a heterogeneous or multifactorial genetic basis, and are susceptible to environmental factors. Studies using mouse models can serve as a complimentary approach to human genetic studies, because mice can have a controlled genetic background and environment, reducing the complexity of genetic analysis. Due to the lack of understanding of the biological processes of glaucoma, forward mouse genetics can be particularly valuable, because it allows a "hypothesis-free" type of analysis which can lead to studies of genes which otherwise will not be considered. The goal of this dissertation study was to apply such a forward mouse genetics approach to expand the glaucoma genetic pathway by utilizing a spontaneous mutant mice strain with features resembling glaucoma. By this approach, we were able to identify a class of proteins which previously have never been suggested as candidates important to glaucoma.

nee mutant strain is a new mouse model of glaucoma

Mice can develop glaucoma spontaneously; however these models are rare. In fact, almost all current glaucoma studies with spontaneous models of glaucoma utilize a sole model, DBA/2J mice. Here, I have presented a new mouse model of glaucoma

occurring in *nee* mutant mice. This strain was a spontaneous mutant strain which arose on an inbred background. The mutant mice were initially noticed because of their small body size, abnormal craniofacial morphology and ocular abnormalities including bulging eyes, and cloudy corneas. With detailed clinical and histological examinations, I have shown that *nee* mutants recapitulate features of glaucoma, including elevated IOP, retinal ganglion cell loss and optic nerve head excavation. Therefore, *nee* mutant strain is a model of glaucoma.

One unique feature for the *nee* glaucoma model is the early onset and rapid progression of the disease. Almost all other currently available spontaneous models are late onset. In this regard, *nee* mice will be beneficial for glaucoma studies such as those testing the effectiveness of glaucoma treatments, because the *nee* model could obviously save time, cost and effort by eliminating the need for extensive aging. In addition, the *nee* mouse model can be used for studies such as those testing new hypothesis involved in IOP regulation and optic nerve degeneration by breeding to other genetically manipulated strains. Since the majority of the genetically manipulated strains are maintained on the B6 background, B6 congenic strains containing the *nee* allele have been generated. Currently the exact phenotype of the B6 congenic strain has yet been fully established. However, if the B6 congenic strain develops glaucoma similar to *nee*, these mice might be a better model than DBA/2J, since genetic studies using DBA/2J need extensive backcrossing to remove the background effect.

SH3PXD2B is a candidate contributing to glaucoma

The SH3PXD2B protein, along with its homolog SH3PXD2A, has not been previously implicated in glaucoma. These adaptor proteins are a type of molecule that has just started to gain some attention. To date, the majority of studies in the literature focus

on the role that these molecules play in the assembly of invadosomes. Therefore, the main function of SH3PXD2B is thought to involve ECM remodeling, cell migration and invasion. While useful, all of the knowledge about SH3PXD2B was gained from experiments done at the molecular and cellular level. The function of SH3PXD2B at the physiological level has not previously been reported.

My work with *nee* mutants has allowed the identification of SH3PXD2B as a contributor for glaucoma. As described in Chapter 2, by mapping analysis of *nee* mutants, we identified a 1-bp deletion in the last exon of the *Sh3pxd2b* gene, which cause a premature stop codon and a protein truncation disrupting the last two SH3 domains. Based on our molecular studies of SH3PXD2B, it is likely that the 1-bp deletion disrupts important protein-protein interactions of SH3PXD2B, and cause a mislocalization of the protein to a different subcellular compartment.

Studies with mice can help suggest candidates for analysis mutations in humans. As described in Chapter 4, we have begun searching for mutations in *SH3PXD2B* in human glaucoma patients. Thus far we have identified a few missense variations in patients with glaucoma. Since these variations do not cause an obvious defect to the message RNA or the protein, at this point, we are not able to tell whether they are disease causing mutations. To answer this question, assays testing the potential influence on the function of SH3PXD2B are needed.

Because the main known function of SH3PXD2B is in invadosome assembly, an assay testing the influence of these variant alleles on invadosomes can be used. For example, it should be possible to isolate cells from patients containing variants and test whether they are capable of forming invadosomes. Previously, I have tried to isolate primary skin fibroblasts from wild-type and *nee* mutant mice and induce them to form podosomes by transfecting with a constitutively active *Src* (Y529F) construct. By performing this experiment, I was trying to ask whether the *nee* allele will disrupt podosome formation. Unfortunately, due to some technical issues such as low

transfection efficiency, the assay was not sensitive enough to tell the difference between wild-type and *nee* mutant cells. However, because human skin fibroblasts are thought to be relatively easier to be transfected than mouse fibroblasts, it may be possible to perform the similar assay in human cells. Alternatively, primary macrophages could be isolated from peripheral blood. Although culturing primary macrophages might be more difficult and time consuming than culturing fibroblasts, macrophages can form podosomes spontaneously (Linder, Nelson et al. 1999), thus alleviating the problem of transfection. Once the assay is established, parameters such as the number of cells with podosomes, the dynamics of podosomes, and their ability to degrade ECM could be tested. One problem with these kinds of experiments might be due to the availability of human tissues. Thus, instead of performing experiments in primary cells, it should be possible to introduce the mutant alleles into cells without *SH3PXD2B* (e.g. a stable knockdown cell line) and test if these missense variations will rescue the podosome formation phenotype.

Alternatively, biochemical assays might provide some insights to the effects of potential mutant alleles. For example, protein integrity and subcellular localization of SH3PXD2B, and its ability to form interaction with known binding partners could be examined. However, these assays can only test for certain, but not all mutations. Increasing understanding of the molecular properties of SH3PXD2B in the future may help design more assays.

Mechanisms of glaucoma mediated by SH3PXD2B

As described in Chapter 3, our data showing an early onset of iridocorneal adhesion suggests glaucoma in *nee* mutants is likely due to developmental defects of the iridocorneal angle which blocks the aqueous humor outflow pathway. To further support the conclusion, the spatial and temporal expression pattern of SH3PXD2B during eye

development needs to be analyzed. In addition, because almost all other known mutations in humans involved in anterior segment dysgenesis are transcriptional factors, knowing the expression pattern of SH3PXD2B might provide some clues to possible links between them.

One technical limitation for our current study is the lack of a good antibody which can be used on ocular sections. With increasing attention on SH3PXD2B, a better antibody might be available in the future. Alternatively, in situ hybridization analysis could provide some insights on the expression pattern at the messenger level. I have generated probes for performing in situ hybridization and initiated experiments but no results are yet available. Because the major defects were observed at the iridocorneal angle, we expect that expression of SH3PXD2B protein would include the periocular mesenchyme that ultimately develops into the cornea stroma and endothelium, iris stroma, and trabecular meshwork.

Although my work only suggests the role of SH3PXD2B in eye development, it does not exclude the possibility of its function in adult eyes. Given that expression of SH3PXD2B can be detected in the trabecular meshwork of adult eyes, and that invadosome-like structures are present in the trabecular meshwork cells, I hypothesize that SH3PXD2B may also have a tissue specific function at the trabecular meshwork, that is to participate in IOP regulation via invadosomes. Understanding the function of SH3PXD2B in IOP regulation is important, since it can help elucidate the mechanism of the most common form of glaucoma, primary open angle glaucoma.

To test this hypothesis, it should be possible to overexpress *Sh3pxd2b* in the trabecular meshwork using an adenovirus based gene delivery method (Budenz, Bennett et al. 1995). If SH3PXD2B does influence outflow resistance, overexpression of *Sh3pxd2b* in the trabecular meshwork will promote ECM remodeling and decrease outflow resistance. Therefore, a decrease of IOP is expected. I have purified adenoviruses

containing a cytomegalovirus-promoted wild-type *Sh3pxd2b* gene fused with GFP. These viruses can be injected into the anterior chamber in the future.

Expanding the molecular pathway of SH3PXD2B

SH3PXD2B is an adaptor protein which by itself may not exert any function. Molecular analysis in my study supports the interaction of SH3PXD2B with one group of molecules, the ADAMs. However, it is likely that other interactions are also present. The hypothesis of SH3PXD2B function in glaucoma is currently based on its role in invadosomes. Knowing other interacting proteins can help generate novel hypotheses.

To expand the SH3PXD2B molecular pathway, biochemical approaches to identify its binding partners can be utilized. For instance, proteins that form complex with SH3PXD2B can be mapped by affinity purification followed by mass spectrometry. It should be possible to create a TAP (tandem affinity purification) tagged SH3PXD2B, express the protein in cell lines of interest (e.g. trabecular meshwork cells), purify the protein complex and perform a mass spectrometry to identify novel interactions. The TAP tag based protein-protein interaction assay was initially developed in yeast, and it has been successfully applied to mammalian cells (Angrand, Segura et al. 2006; Poser, Sarov et al. 2008; Fernandez, Collins et al. 2009). The goal for this kind of approach is to identify interactions under close-to-physiological conditions. Strategies have been developed to ensure expression of the bait protein at endogenous levels, such as using a BAC transgene which are usually large enough to contain the regulatory elements, using a promoter with expression range close to endogenous levels, or generating a knock-in animal with the TAP tagged protein. It has been shown that some molecules can interact with multiple SH3 domains in SH3PXD2A (Oikawa, Itoh et al. 2008), consequently missing one SH3 domain may cause subtle effect. Therefore, it might be more important

to examine missing interactions in *nee* mutants by comparing binding partners of wild-type and *nee* versions of TAP tagged proteins.

Alternatively, genetic approaches can be utilized. For instance, mouse strains with phenotypes similar to *nee* might provide some insights. The strain *cartoon*, which contains a missense mutation (P466S) in the *MMP14* gene, exhibit growth defects, craniofacial abnormalities and large-appearing eyes which is an indication of high IOP (Mutagenetix 2008). Although closer examination of the ocular phenotypes have not been performed, given that MMP14 is enriched in podosomes, and that in cells deficient of SH3PX2B MMP14 no longer localizes to podosomes (Buschman, Bromann et al. 2009), it is possible that *cartoon* mice have a similar ocular phenotypes. If this is the case, genetic epistasis experiments can be utilized to test whether SH3PXD2B and MMP14 genetically interact with each other. Another genetic approach is to generate congenic strains by crossing *nee* to a different background and test whether there is a phenotypic modification effect. Currently, B6 congenic strain has been generated. With the limited number of mice I have examined, I have not observed a significant modification of the ocular phenotype. Further analysis is needed to draw a conclusion.

Contribution of SH3PXD2B to other diseases

My work on *nee* mutant mice suggests that SH3PXD2B might be involved in other diseases. As obesity is often associated with chronic diseases such as heart disease, stroke, some types of cancer, high blood pressure, high cholesterol and the number of people with obesity is growing, it thus might be interesting to study obesity. As described in Chapter 1, a whole genome linkage scan for QTLs contributing to obesity identified suggestive linkage to the *SH3PXD2B* locus. In addition, *Sh3pxd2b* has been implicated in adipogenesis, as knocking down *Sh3pxd2b* by RNAi impedes fat cell differentiation. Our

result showed that *nee* homozygous mutants with disrupted SH3PXD2B protein lack fat. Based on these lines of evidence, I hypothesize that there might be a dosage dependent effect of *sh3pxd2b* on fat cell differentiation, and that obesity can be caused by increased levels of SH3PXD2B. Assays such as generating a transgenic strain overexpressing wild-type *Sh3pxd2b* can be used to test this hypothesis. Alternatively, lipodystrophy could simply be a secondary consequence of factors other than differentiation defects. As *nee* mice are blind, deaf, small and have craniofacial dysmorphism, it is possible that they have disturbed feeding behavior. Therefore, food uptake should be measured to exclude this possibility. In addition, to further support the role of SH3PXD2B in fat differentiation, primary preadipocytes or embryonic fibroblasts isolated from *nee* mice can be tested on whether they can be induced to differentiate into mature adipocytes (Kim, Huang et al. 2007; Wojtanik, Edgemon et al. 2009).

Phenotype autonomy

In considering the current state of all that is currently known about the *nee* mouse, one question that arises pertains to whether some of the observed phenotypes are simple secondary consequences of each other or are truly autonomous. Perhaps most importantly, could the glaucoma of *nee* mice be a secondary consequence of craniofacial abnormalities? Although I have not done experiments to address this, the literature does contain some hints relevant to this question.

Glaucoma and craniofacial abnormalities can occur together, though they most frequently do not. As mentioned in previous chapters, there are several rare diseases (such as Axenfeld-Rieger syndrome, SHORT syndrome, and Frank-Ter Haar syndrome, etc) in which patients have systemic malformations including both craniofacial dysmorphism, ocular malformation and accompanying glaucoma. It is generally thought

that developmental arrest of the neural crest cells, which give rise to bones, cartilage of the skull, and the majority of the eye, lead to craniofacial and ocular defects (Gould and John 2002; Tumer and Bach-Holm 2009). High IOP and glaucoma, as a consequence, is thought to occur due to blockage of the aqueous humor outflow pathway caused by malformation of the anterior segment. However, it is still possible that glaucoma develops due to malformation of the skull. For instance, a malformed or small orbit could lead to impingement on the optic nerve and cause optic neuropathy. To test this possibility, it might be important to measure the size of optic foramen. More importantly, to address the autonomy of *nee* phenotypes directly, it will be crucial to determine tissue specific functions of SH3PXD2B. Therefore, eye and bone specific knockouts could be generated and tested whether the craniofacial and ocular phenotypes develop independently (availability and specificity of such promoters could be a critical limiting issue, however). Alternatively, tissue specific rescue experiments (e.g. adenovirus based gene delivery of wildtype *Sh3pxd2b* to *nee* eyes) can also been performed to address all phenotypic autonomy.

Overall model of SH3PXD2B function

In summary, I have definitively showed that *nee* mutants result from a mutation in gene *Sh3pxd2b*. I have also identified multiple phenotypes, including early onset glaucoma caused by the *nee* mutation. For ongoing experiments by the Anderson Lab, which are likely to focus on the ocular phenotypes, I suggest the following overall model, which might be used as a starting ground for working hypothesis.

SH3PXD2B appears to be an adaptor protein tethering membrane bound metalloproteinases to specific membrane domains. As I discussed in previous chapters, it seems very feasible that SH3PXD2B regulates metalloproteinases required for neural

crest migration in developmental establishment of the irideocorneal angle. It also seems likely that SH3PXD2B also have a function in adult tissues such as the trabecular meshwork. For both of these tissues, the key remaining issue is to identify SH3PXD2B binding partners that participate in the same pathway. However, it is worth remembering as with myocilin, the mechanism driving disease could be distinct from the function of the wild-type protein (Resch and Fautsch 2009). In particular, the finding that mutant SH3PXD2B localizes to the nucleus is worth follow-up investigation, as this suggests a possible role of SH3PXD2B in the nucleus. It would also be interesting to identify transcription factors regulating SH3PXD2B expression. Based on the phenotypes observed, it is tempting to speculate that SH3PXD2B is a downstream target of FOXC1 or PITX2 (in fact, based on nuclear mislocalization, it is possible that SH3PXD2B could be a nuclear binding partner for FOXC1 or PITX2). Thus, my overall model would place FOXC1 or PITX2 upstream of SH3PXD2B, acting to promote specific subcellular localization of metalloproteinases such as MMP14, which functions in neural crest derived ocular tissues.

REFERENCES

Abram, C. L., D. F. Seals, et al. (2003). "The adaptor protein fish associates with members of the ADAMs family and localizes to podosomes of Src-transformed cells." J Biol Chem **278**(19): 16844-51.

Acott, T. S. and M. J. Kelley (2008). "Extracellular matrix in the trabecular meshwork." Exp Eye Res **86**(4): 543-61.

Aga, M., J. M. Bradley, et al. (2008). "Specialized podosome- or invadopodia-like structures (PILS) for focal trabecular meshwork extracellular matrix turnover." Invest Ophthalmol Vis Sci **49**(12): 5353-65.

Agarwal, R., S. K. Gupta, et al. (2009). "Current concepts in the pathophysiology of glaucoma." Indian J Ophthalmol **57**(4): 257-66.

Aihara, M., J. D. Lindsey, et al. (2003). "Aqueous humor dynamics in mice." Invest Ophthalmol Vis Sci **44**(12): 5168-73.

Albiges-Rizo, C., O. Destaing, et al. (2009). "Actin machinery and mechanosensitivity in invadopodia, podosomes and focal adhesions." J Cell Sci **122**(Pt 17): 3037-49.

Allingham RR, D. K., Freedman S, Moroi SE, Shafranov G, Shields MB (2004). Shields' Textbook of Glaucoma., Philadelphia: Lippincott Williams and Wilkins;.

Allingham, R. R., Y. Liu, et al. (2009). "The genetics of primary open-angle glaucoma: a review." Exp Eye Res **88**(4): 837-44.

Allingham, R. R., J. L. Wiggs, et al. (2005). "Early adult-onset POAG linked to 15q11-13 using ordered subset analysis." Invest Ophthalmol Vis Sci **46**(6): 2002-5.

Alvarado, J., C. Murphy, et al. (1984). "Trabecular meshwork cellularity in primary open-angle glaucoma and nonglaucomatous normals." Ophthalmology **91**(6): 564-79.

Alward, W. L. (2000). "Axenfeld-Rieger syndrome in the age of molecular genetics." Am J Ophthalmol **130**(1): 107-15.

Anderson, M. G., R. T. Libby, et al. (2006). "Genetic context determines susceptibility to intraocular pressure elevation in a mouse pigmentary glaucoma." BMC Biol **4**: 20.

Anderson, M. G., R. S. Smith, et al. (2002). "Mutations in genes encoding melanosomal proteins cause pigmentary glaucoma in DBA/2J mice." Nat Genet **30**(1): 81-5.

Anderson, M. G., R. S. Smith, et al. (2001). "Genetic modification of glaucoma associated phenotypes between AKXD-28/Ty and DBA/2J mice." BMC Genet **2**: 1.

Angrand, P. O., I. Segura, et al. (2006). "Transgenic mouse proteomics identifies new 14-3-3-associated proteins involved in cytoskeletal rearrangements and cell signaling." Mol Cell Proteomics **5**(12): 2211-27.

Baekvad-Hansen, M., Z. Tumer, et al. (2006). "Delineation of a 2.2 Mb microdeletion at 5q35 associated with microcephaly and congenital heart disease." Am J Med Genet A **140**(5): 427-33.

Barany, E. H. (1962). "The mode of action of pilocarpine on outflow resistance in the eye of a primate (Cercopithecus ethiops)." Invest Ophthalmol **1**: 712-27.

Basbaum, C. B. and Z. Werb (1996). "Focalized proteolysis: spatial and temporal regulation of extracellular matrix degradation at the cell surface." Curr Opin Cell Biol **8**(5): 731-8.

Belkina, N. V., Y. Liu, et al. (2009). "LOK is a major ERM kinase in resting lymphocytes and regulates cytoskeletal rearrangement through ERM phosphorylation." Proc Natl Acad Sci U S A **106**(12): 4707-12.

Berry, F. B., J. M. Skarie, et al. (2008). "FOXC1 is required for cell viability and resistance to oxidative stress in the eye through the transcriptional regulation of FOXO1A." Hum Mol Genet **17**(4): 490-505.

Bertram, L., D. Blacker, et al. (2000). "Evidence for genetic linkage of Alzheimer's disease to chromosome 10q." Science **290**(5500): 2302-3.

Blouw, B., D. F. Seals, et al. (2008). "A role for the podosome/invadopodia scaffold protein Tks5 in tumor growth in vivo." Eur J Cell Biol **87**(8-9): 555-67.

Borras, T. (2003). "Gene expression in the trabecular meshwork and the influence of intraocular pressure." Prog Retin Eye Res **22**(4): 435-63.

Bourlier, V., A. Zakaroff-Girard, et al. (2005). "Protease inhibitor treatments reveal specific involvement of matrix metalloproteinase-9 in human adipocyte differentiation." J Pharmacol Exp Ther **312**(3): 1272-9.

Bradley, J. M., J. Vranka, et al. (1998). "Effect of matrix metalloproteinases activity on outflow in perfused human organ culture." Invest Ophthalmol Vis Sci **39**(13): 2649-58.

Breuza, L., R. Halbeisen, et al. (2004). "Proteomics of endoplasmic reticulum-Golgi intermediate compartment (ERGIC) membranes from brefeldin A-treated HepG2 cells identifies ERGIC-32, a new cycling protein that interacts with human Erv46." J Biol Chem **279**(45): 47242-53.

Budenz, D. L., J. Bennett, et al. (1995). "In vivo gene transfer into murine corneal endothelial and trabecular meshwork cells." Invest Ophthalmol Vis Sci **36**(11): 2211-5.

Buffone, G. J. and G. J. Darlington (1985). "Isolation of DNA from biological specimens without extraction with phenol." Clin Chem **31**(1): 164-5.

Buschman, M. D., P. A. Bromann, et al. (2009). "The novel adaptor protein Tks4 (SH3PXD2B) is required for functional podosome formation." Mol Biol Cell **20**(5): 1302-11.

Caldieri, G. and R. Buccione (2010). "Aiming for invadopodia: organizing polarized delivery at sites of invasion." Trends Cell Biol **20**(2): 64-70.

Carman, C. V. (2009). "Mechanisms for transcellular diapedesis: probing and pathfinding by 'invadosome-like protrusions'." J Cell Sci **122**(Pt 17): 3025-35.

Carman, C. V., P. T. Sage, et al. (2007). "Transcellular diapedesis is initiated by invasive podosomes." Immunity **26**(6): 784-97.

Chabadel, A., I. Banon-Rodriguez, et al. (2007). "CD44 and beta3 integrin organize two functionally distinct actin-based domains in osteoclasts." Mol Biol Cell **18**(12): 4899-910.

Challa, P. (2004). "Glaucoma genetics: advancing new understandings of glaucoma pathogenesis." Int Ophthalmol Clin **44**(2): 167-85.

Challa, P. (2008). "Glaucoma genetics." Int Ophthalmol Clin **48**(4): 73-94.

Chang, B., N. L. Hawes, et al. (2005). "Mouse models of ocular diseases." Vis Neurosci **22**(5): 587-93.

Chang, B., R. S. Smith, et al. (1999). "Interacting loci cause severe iris atrophy and glaucoma in DBA/2J mice." Nat Genet **21**(4): 405-9.

Chen, W., S. Yang, et al. (2007). "Novel pycnodysostosis mouse model uncovers cathepsin K function as a potential regulator of osteoclast apoptosis and senescence." Hum Mol Genet **16**(4): 410-23.

Chen, W. T. (1996). "Proteases associated with invadopodia, and their role in degradation of extracellular matrix." Enzyme Protein **49**(1-3): 59-71.

Chun, T. H., K. B. Hotary, et al. (2006). "A pericellular collagenase directs the 3-dimensional development of white adipose tissue." Cell **125**(3): 577-91.

Clark, A. F. (1998). "New discoveries on the roles of matrix metalloproteinases in ocular cell biology and pathology." Invest Ophthalmol Vis Sci **39**(13): 2514-6.

Clark, A. F., S. T. Miggans, et al. (1995). "Cytoskeletal changes in cultured human glaucoma trabecular meshwork cells." J Glaucoma **4**(3): 183-8.

Clark, A. F. and T. Yorio (2003). "Ophthalmic drug discovery." Nat Rev Drug Discov **2**(6): 448-59.

Coroneo, M. T., C. Korbmacher, et al. (1991). "Electrical and morphological evidence for heterogeneous populations of cultured bovine trabecular meshwork cells." Exp Eye Res **52**(4): 375-88.

Crimaldi, L., S. A. Courtneidge, et al. (2009). "Tks5 recruits AFAP-110, p190RhoGAP, and cortactin for podosome formation." Exp Cell Res **315**(15): 2581-92.

Dai, J. X., R. L. Johnson, et al. (2009). "Manifold functions of the Nail-Patella Syndrome gene Lmx1b in vertebrate development." Dev Growth Differ **51**(3): 241-50.

Danesh-Meyer, H. V. and L. A. Levin (2009). "Neuroprotection: extrapolating from neurologic diseases to the eye." Am J Ophthalmol **148**(2): 186-191 e2.

Danias, J., K. C. Lee, et al. (2003). "Quantitative analysis of retinal ganglion cell (RGC) loss in aging DBA/2NNia glaucomatous mice: comparison with RGC loss in aging C57/BL6 mice." Invest Ophthalmol Vis Sci **44**(12): 5151-62.

Das, S. K., W. S. Chu, et al. (2006). "Polymorphisms in the glucokinase-associated, dual-specificity phosphatase 12 (DUSP12) gene under chromosome 1q21 linkage peak are associated with type 2 diabetes." Diabetes **55**(9): 2631-9.

Destaing, O., F. Saltel, et al. (2005). "A novel Rho-mDia2-HDAC6 pathway controls podosome patterning through microtubule acetylation in osteoclasts." J Cell Sci **118**(Pt 13): 2901-11.

Destaing, O., A. Sanjay, et al. (2008). "The tyrosine kinase activity of c-Src regulates actin dynamics and organization of podosomes in osteoclasts." Mol Biol Cell **19**(1): 394-404.

Diaz, B., G. Shani, et al. (2009). "Tks5-dependent, nox-mediated generation of reactive oxygen species is necessary for invadopodia formation." Sci Signal **2**(88): ra53.

Edwards, A. O., R. Ritter, 3rd, et al. (2005). "Complement factor H polymorphism and age-related macular degeneration." Science **308**(5720): 421-4.

Egeblad, M., H. C. Shen, et al. (2007). "Type I collagen is a genetic modifier of matrix metalloproteinase 2 in murine skeletal development." Dev Dyn **236**(6): 1683-93.

Ethen, C. M., C. Reilly, et al. (2006). "The proteome of central and peripheral retina with progression of age-related macular degeneration." Invest Ophthalmol Vis Sci **47**(6): 2280-90.

Evans, J. P. (2001). "Fertilin beta and other ADAMs as integrin ligands: insights into cell adhesion and fertilization." Bioessays **23**(7): 628-39.

Fernandez, E., M. O. Collins, et al. (2009). "Targeted tandem affinity purification of PSD-95 recovers core postsynaptic complexes and schizophrenia susceptibility proteins." Mol Syst Biol **5**: 269.

Flammer, J. and M. Mozaffarieh (2007). "What is the present pathogenetic concept of glaucomatous optic neuropathy?" Surv Ophthalmol **52 Suppl 2**: S162-73.

Flammer, J., S. Orgul, et al. (2002). "The impact of ocular blood flow in glaucoma." Prog Retin Eye Res **21**(4): 359-93.

Foster, P. J., R. Buhrmann, et al. (2002). "The definition and classification of glaucoma in prevalence surveys." Br J Ophthalmol **86**(2): 238-42.

Francois, J. (1980). "Congenital glaucoma and its inheritance." Ophthalmologica **181**(2): 61-73.

Friedman, D. S., R. C. Wolfs, et al. (2004). "Prevalence of open-angle glaucoma among adults in the United States." Arch Ophthalmol **122**(4): 532-8.

Fuchshofer, R., D. A. Stephan, et al. (2009). "Gene expression profiling of TGFbeta2- and/or BMP7-treated trabecular meshwork cells: Identification of Smad7 as a critical inhibitor of TGF-beta2 signaling." Exp Eye Res **88**(6): 1020-32.

Gabelt, B. T. and P. L. Kaufman (2005). "Changes in aqueous humor dynamics with age and glaucoma." Prog Retin Eye Res **24**(5): 612-37.

Gage, P. J., H. Suh, et al. (1999). "Dosage requirement of Pitx2 for development of multiple organs." Development **126**(20): 4643-51.

Gatesman, A., V. G. Walker, et al. (2004). "Protein kinase Calpha activates c-Src and induces podosome formation via AFAP-110." Mol Cell Biol **24**(17): 7578-97.

Gianni, D., B. Diaz, et al. (2009). "Novel p47(phox)-related organizers regulate localized NADPH oxidase 1 (Nox1) activity." Sci Signal **2**(88): ra54.

Gimona, M. and R. Buccione (2006). "Adhesions that mediate invasion." Int J Biochem Cell Biol **38**(11): 1875-92.

Gong, H., J. Ruberti, et al. (2002). "A new view of the human trabecular meshwork using quick-freeze, deep-etch electron microscopy." Exp Eye Res **75**(3): 347-58.

Gottfredsdottir, M. S., T. Sverrisson, et al. (1999). "Chronic open-angle glaucoma and associated ophthalmic findings in monozygotic twins and their spouses in Iceland." J Glaucoma **8**(2): 134-9.

Gould, D. B. and S. W. John (2002). "Anterior segment dysgenesis and the developmental glaucomas are complex traits." Hum Mol Genet **11**(10): 1185-93.

Gould, D. B., R. S. Smith, et al. (2004). "Anterior segment development relevant to glaucoma." Int J Dev Biol **48**(8-9): 1015-29.

Graff, C., S. F. Urbak, et al. (1995). "Confirmation of linkage to 1q21-31 in a Danish autosomal dominant juvenile-onset glaucoma family and evidence of genetic heterogeneity." Hum Genet **96**(3): 285-9.

Grant, W. M. (1963). "Experimental aqueous perfusion in enucleated human eyes." Arch Ophthalmol **69**: 783-801.

Green, M. (1952). "A rapid method for clearing and staining specimans for the demonstration of bone." The Ohio Journal of Science **52**: 31-33.

Grisendi, S., R. Bernardi, et al. (2005). "Role of nucleophosmin in embryonic development and tumorigenesis." Nature **437**(7055): 147-53.

Harold, D., L. Jehu, et al. (2007). "Interaction between the ADAM12 and SH3MD1 genes may confer susceptibility to late-onset Alzheimer's disease." Am J Med Genet B Neuropsychiatr Genet **144B**(4): 448-52.

Hewitt, A. W., S. Sharma, et al. (2008). "Ancestral LOXL1 variants are associated with pseudoexfoliation in Caucasian Australians but with markedly lower penetrance than in Nordic people." Hum Mol Genet **17**(5): 710-6.

Hikita, A., I. Yana, et al. (2006). "Negative regulation of osteoclastogenesis by ectodomain shedding of receptor activator of NF-kappaB ligand." J Biol Chem **281**(48): 36846-55.

Hishida, T., T. Eguchi, et al. (2008). "A novel gene, fad49, plays a crucial role in the immediate early stage of adipocyte differentiation via involvement in mitotic clonal expansion." Febs J **275**(22): 5576-88.

Hishida, T., M. Nishizuka, et al. (2009). "The role of C/EBPdelta in the early stages of adipogenesis." Biochimie **91**(5): 654-7.

Hjalt, T. A., B. A. Amendt, et al. (2001). "PITX2 regulates procollagen lysyl hydroxylase (PLOD) gene expression: implications for the pathology of Rieger syndrome." J Cell Biol **152**(3): 545-52.

Holmbeck, K., P. Bianco, et al. (1999). "MT1-MMP-deficient mice develop dwarfism, osteopenia, arthritis, and connective tissue disease due to inadequate collagen turnover." Cell **99**(1): 81-92.

Hong, H. K., J. H. Lass, et al. (1999). "Pleiotropic skeletal and ocular phenotypes of the mouse mutation congenital hydrocephalus (ch/Mf1) arise from a winged helix/forkhead transcriptionfactor gene." Hum Mol Genet **8**(4): 625-37.

Hurst, I. R., J. Zuo, et al. (2004). "Actin-related protein 2/3 complex is required for actin ring formation." J Bone Miner Res **19**(3): 499-506.

Iqbal, Z., P. Cejudo-Martin, et al. (2010). "Disruption of the Podosome Adaptor Protein TKS4 (SH3PXD2B) Causes the Skeletal Dysplasia, Eye, and Cardiac Abnormalities of Frank-Ter Haar Syndrome." Am J Hum Genet **86**(2): 254-61.

Jacobs, K. B., M. Yeager, et al. (2009). "A new statistic and its power to infer membership in a genome-wide association study using genotype frequencies." Nat Genet **41**(11): 1253-7.

John, S. W., M. G. Anderson, et al. (1999). "Mouse genetics: a tool to help unlock the mechanisms of glaucoma." J Glaucoma **8**(6): 400-12.

John, S. W., J. R. Hagaman, et al. (1997). "Intraocular pressure in inbred mouse strains." Invest Ophthalmol Vis Sci **38**(1): 249-53.

John, S. W., R. S. Smith, et al. (1998). "Essential iris atrophy, pigment dispersion, and glaucoma in DBA/2J mice." Invest Ophthalmol Vis Sci **39**(6): 951-62.

Johnson, M. (2006). "'What controls aqueous humour outflow resistance?'" Exp Eye Res **82**(4): 545-57.

Kaneko, T., L. Li, et al. (2008). "The SH3 domain--a family of versatile peptide- and protein-recognition module." Front Biosci **13**: 4938-52.

Karadeniz, N. N., I. Kocak-Midillioglu, et al. (2004). "Is SHORT syndrome another phenotypic variation of PITX2?" Am J Med Genet A **130A**(4): 406-9.

Kass, M. A., D. K. Heuer, et al. (2002). "The Ocular Hypertension Treatment Study: a randomized trial determines that topical ocular hypotensive medication delays or prevents the onset of primary open-angle glaucoma." Arch Ophthalmol **120**(6): 701-13; discussion 829-30.

Kim, S., L. W. Huang, et al. (2007). "A mouse model of conditional lipodystrophy." Proc Natl Acad Sci U S A **104**(42): 16627-32.

Klein, R. J., C. Zeiss, et al. (2005). "Complement factor H polymorphism in age-related macular degeneration." Science **308**(5720): 385-9.

Koolen, D. A., J. Herbergs, et al. (2006). "Holoprosencephaly and preaxial polydactyly associated with a 1.24 Mb duplication encompassing FBXW11 at 5q35.1." J Hum Genet **51**(8): 721-6.

Kornak, U., D. Kasper, et al. (2001). "Loss of the ClC-7 chloride channel leads to osteopetrosis in mice and man." Cell **104**(2): 205-15.

Krane, S. M. and M. Inada (2008). "Matrix metalloproteinases and bone." Bone **43**(1): 7-18.

La Rosa, F. A. and D. A. Lee (2000). "Collagen degradation in glaucoma: will it gain a therapeutic value?" Curr Opin Ophthalmol **11**(2): 90-3.

Laumet, G., V. Petitprez, et al. "A study of the association between the ADAM12 and SH3PXD2A (SH3MD1) genes and Alzheimer's disease." Neurosci Lett **468**(1): 1-2.

Leske, M. C., A. Heijl, et al. (1999). "Early Manifest Glaucoma Trial: design and baseline data." Ophthalmology **106**(11): 2144-53.

Libby, R. T., R. S. Smith, et al. (2003). "Modification of ocular defects in mouse developmental glaucoma models by tyrosinase." Science **299**(5612): 1578-81.

Linder, S. (2009). "Invadosomes at a glance." J Cell Sci **122**(Pt 17): 3009-13.

Linder, S., D. Nelson, et al. (1999). "Wiskott-Aldrich syndrome protein regulates podosomes in primary human macrophages." Proc Natl Acad Sci U S A **96**(17): 9648-53.

Liu, S., H. An, et al. (2003). "Cloning and identification of a novel human ubiquitin-like protein, DC-UbP, from dendritic cells." Biochem Biophys Res Commun **300**(3): 800-5.

Liu, Y. X., J. Wang, et al. (2008). "DUSP1 is controlled by p53 during the cellular response to oxidative stress." Mol Cancer Res **6**(4): 624-33.

Lively, G. D., B. Jiang, et al. "Genetic dependence of central corneal thickness among inbred strains of mice." Invest Ophthalmol Vis Sci **51**(1): 160-71.

Lock, P., C. L. Abram, et al. (1998). "A new method for isolating tyrosine kinase substrates used to identify fish, an SH3 and PX domain-containing protein, and Src substrate." Embo J **17**(15): 4346-57.

Luna, C., G. Li, et al. (2009). "Alterations in gene expression induced by cyclic mechanical stress in trabecular meshwork cells." Mol Vis **15**: 534-44.

Lutjen-Drecoll, E., T. Shimizu, et al. (1986). "Quantitative analysis of 'plaque material' in the inner- and outer wall of Schlemm's canal in normal- and glaucomatous eyes." Exp Eye Res **42**(5): 443-55.

Luxenburg, C., D. Geblinger, et al. (2007). "The architecture of the adhesive apparatus of cultured osteoclasts: from podosome formation to sealing zone assembly." PLoS One **2**(1): e179.

Mabuchi, F., J. D. Lindsey, et al. (2004). "Optic nerve damage in mice with a targeted type I collagen mutation." Invest Ophthalmol Vis Sci **45**(6): 1841-5.

Malinin, N. L., S. Wright, et al. (2005). "Amyloid-beta neurotoxicity is mediated by FISH adapter protein and ADAM12 metalloprotease activity." Proc Natl Acad Sci U S A **102**(8): 3058-63.

Mao, M., D. R. Thedens, et al. (2009). "The podosomal-adaptor protein SH3PXD2B is essential for normal postnatal development." Mamm Genome **20**(8): 462-75.

McKinnon, S. J., L. D. Goldberg, et al. (2008). "Current management of glaucoma and the need for complete therapy." Am J Manag Care **14**(1 Suppl): S20-7.

McKinnon, S. J., C. L. Schlamp, et al. (2009). "Mouse models of retinal ganglion cell death and glaucoma." Exp Eye Res **88**(4): 816-24.

Meyer-Marcotty, P., N. Weisschuh, et al. (2008). "Morphology of the sella turcica in Axenfeld-Rieger syndrome with PITX2 mutation." J Oral Pathol Med **37**(8): 504-10.

Meyer, A., F. Valtot, et al. (1994). "[Linkage between juvenile glaucoma and chromosome 1q in 2 French families]." C R Acad Sci III **317**(6): 565-70.

Morales, J., L. Al-Sharif, et al. (2009). "Homozygous mutations in ADAMTS10 and ADAMTS17 cause lenticular myopia, ectopia lentis, glaucoma, spherophakia, and short stature." Am J Hum Genet **85**(5): 558-68.

Morrison, J. C., E. C. Johnson, et al. (2005). "Understanding mechanisms of pressure-induced optic nerve damage." Prog Retin Eye Res **24**(2): 217-40.

Mosig, R. A., O. Dowling, et al. (2007). "Loss of MMP-2 disrupts skeletal and craniofacial development and results in decreased bone mineralization, joint erosion and defects in osteoblast and osteoclast growth." Hum Mol Genet **16**(9): 1113-23.

Moulding, D. A., M. P. Blundell, et al. (2007). "Unregulated actin polymerization by WASp causes defects of mitosis and cytokinesis in X-linked neutropenia." J Exp Med **204**(9): 2213-24.

Mutagenetix, D. X. B. B. (2008). Cartoon is an allele of Mmp14 associated with craniofacial anomolies, retarded growth and reduced viability.

Nickells RW, J. H., Zack DJ (2002). In Emery & Rimoins Principles and Practices of Medical Genetics.

Nilsson, S. F. (1997). "The uveoscleral outflow routes." Eye (Lond) **11 (Pt 2)**: 149-54.

Ohbayashi, N., M. Shibayama, et al. (2002). "FGF18 is required for normal cell proliferation and differentiation during osteogenesis and chondrogenesis." Genes Dev **16**(7): 870-9.

Oikawa, T., T. Itoh, et al. (2008). "Sequential signals toward podosome formation in NIH-src cells." J Cell Biol **182**(1): 157-69.

Oikawa, T. and T. Takenawa (2009). "PtdIns(3,4)P2 instigates focal adhesions to generate podosomes." Cell Adh Migr **3**(2): 195-7.

Olivier, A., L. Jeanson-Leh, et al. (2006). "A partial down-regulation of WASP is sufficient to inhibit podosome formation in dendritic cells." Mol Ther **13**(4): 729-37.

Onel, S. F. and R. Renkawitz-Pohl (2009). "FuRMAS: triggering myoblast fusion in Drosophila." Dev Dyn **238**(6): 1513-25.

Ory, S., H. Brazier, et al. (2008). "Rho GTPases in osteoclasts: orchestrators of podosome arrangement." Eur J Cell Biol **87**(8-9): 469-77.

Osborne, N. N. (2009). "Recent clinical findings with memantine should not mean that the idea of neuroprotection in glaucoma is abandoned." Acta Ophthalmol **87**(4): 450-4.

Overby, D. R., W. D. Stamer, et al. (2009). "The changing paradigm of outflow resistance generation: towards synergistic models of the JCT and inner wall endothelium." Exp Eye Res **88**(4): 656-70.

Page-McCaw, A., A. J. Ewald, et al. (2007). "Matrix metalloproteinases and the regulation of tissue remodelling." Nat Rev Mol Cell Biol **8**(3): 221-33.

Paigen, K. (1995). "A miracle enough: the power of mice." Nat Med **1**(3): 215-20.

Pang, I. H. and A. F. Clark (2007). "Rodent models for glaucoma retinopathy and optic neuropathy." J Glaucoma **16**(5): 483-505.

Parshley, D. E., J. M. Bradley, et al. (1996). "Laser trabeculoplasty induces stromelysin expression by trabecular juxtacanalicular cells." Invest Ophthalmol Vis Sci **37**(5): 795-804.

Parshley, D. E., J. M. Bradley, et al. (1995). "Early changes in matrix metalloproteinases and inhibitors after in vitro laser treatment to the trabecular meshwork." Curr Eye Res **14**(7): 537-44.

Pasten-Hidalgo, K., R. Hernandez-Rivas, et al. (2008). "Presence, processing, and localization of mouse ADAM15 during sperm maturation and the role of its disintegrin domain during sperm-egg binding." Reproduction **136**(1): 41-51.

Poincloux, R., F. Lizarraga, et al. (2009). "Matrix invasion by tumour cells: a focus on MT1-MMP trafficking to invadopodia." J Cell Sci **122**(Pt 17): 3015-24.

Poser, I., M. Sarov, et al. (2008). "BAC TransgeneOmics: a high-throughput method for exploration of protein function in mammals." Nat Methods **5**(5): 409-15.

Proszynski, T. J., J. Gingras, et al. (2009). "Podosomes are present in a postsynaptic apparatus and participate in its maturation." Proc Natl Acad Sci U S A **106**(43): 18373-8.

Quigley, H. A. (1996). "Number of people with glaucoma worldwide." Br J Ophthalmol **80**(5): 389-93.

Quigley, H. A. and A. T. Broman (2006). "The number of people with glaucoma worldwide in 2010 and 2020." Br J Ophthalmol **90**(3): 262-7.

Ra, H. J. and W. C. Parks (2007). "Control of matrix metalloproteinase catalytic activity." Matrix Biol **26**(8): 587-96.

Rauch, A. and H. G. Dorr (2007). "Chromosome 5q subtelomeric deletion syndrome." Am J Med Genet C Semin Med Genet **145C**(4): 372-6.

Resch, Z. T. and M. P. Fautsch (2009). "Glaucoma-associated myocilin: a better understanding but much more to learn." Exp Eye Res **88**(4): 704-12.

Resnikoff, S., D. Pascolini, et al. (2004). "Global data on visual impairment in the year 2002." Bull World Health Organ **82**(11): 844-51.

Richards, J. E., P. R. Lichter, et al. (1994). "Mapping of a gene for autosomal dominant juvenile-onset open-angle glaucoma to chromosome Iq." Am J Hum Genet **54**(1): 62-70.

Richtsmeier, J. T., L. L. Baxter, et al. (2000). "Parallels of craniofacial maldevelopment in Down syndrome and Ts65Dn mice." Dev Dyn **217**(2): 137-45.

Ritch, R. and U. Schlotzer-Schrehardt (2001). "Exfoliation syndrome." Surv Ophthalmol **45**(4): 265-315.

Ritch R, S. M., Krupin T (1996). The Glaucomas, St Louis Mosby.

Rocha, J. L., E. J. Eisen, et al. (2004). "A large-sample QTL study in mice: I. Growth." Mamm Genome **15**(2): 83-99.

Rohen, J. W. and R. Witmer (1972). "Electrn microscopic studies on the trabecular meshwork in glaucoma simplex." Albrecht Von Graefes Arch Klin Exp Ophthalmol **183**(4): 251-66.

Ronkko, S., P. Rekonen, et al. (2007). "Matrix metalloproteinases and their inhibitors in the chamber angle of normal eyes and patients with primary open-angle glaucoma and exfoliation glaucoma." Graefes Arch Clin Exp Ophthalmol **245**(5): 697-704.

Saltel, F., A. Chabadel, et al. (2008). "Actin cytoskeletal organisation in osteoclasts: a model to decipher transmigration and matrix degradation." Eur J Cell Biol **87**(8-9): 459-68.

Sarfarazi, M. (1997). "Recent advances in molecular genetics of glaucomas." Hum Mol Genet **6**(10): 1667-77.

Sato, T. K., M. Overduin, et al. (2001). "Location, location, location: membrane targeting directed by PX domains." Science **294**(5548): 1881-5.

Seals, D. F., E. F. Azucena, Jr., et al. (2005). "The adaptor protein Tks5/Fish is required for podosome formation and function, and for the protease-driven invasion of cancer cells." Cancer Cell **7**(2): 155-65.

Sheffield, V. C., E. M. Stone, et al. (1993). "Genetic linkage of familial open angle glaucoma to chromosome 1q21-q31." Nat Genet **4**(1): 47-50.

Shi, X., B. Cui, et al. (2009). "Removal of Hsf4 leads to cataract development in mice through down-regulation of gamma S-crystallin and Bfsp expression." BMC Mol Biol **10**: 10.

Shimizu, A., T. Maruyama, et al. (2005). "Impairment of decidualization in SRC-deficient mice." Biol Reprod **73**(6): 1219-27.

Smith RS, Z. A., John SW, Bechtold LS, Ikeda S, Relyea MJ, Sundberg JP, Kao WW-Y, Liu C-Y (2002). General and Special Histopathology. In Systemic Evaluation of the Mouse Eye. Boca Raton, CRC Press.

Smith, R. S., A. Zabaleta, et al. (2000). "Haploinsufficiency of the transcription factors FOXC1 and FOXC2 results in aberrant ocular development." Hum Mol Genet **9**(7): 1021-32.

Smith, R. S., A. Zabaleta, et al. (2001). "The mouse anterior chamber angle and trabecular meshwork develop without cell death." BMC Dev Biol **1**: 3.

Soriano, P., C. Montgomery, et al. (1991). "Targeted disruption of the c-src proto-oncogene leads to osteopetrosis in mice." Cell **64**(4): 693-702.

Sowden, J. C. (2007). "Molecular and developmental mechanisms of anterior segment dysgenesis." Eye (Lond) **21**(10): 1310-8.

Sowka, J. (2004). "Pseudoexfoliation syndrome and pseudoexfoliative glaucoma." Optometry **75**(4): 245-50.

Spinardi, L. and P. C. Marchisio (2006). "Podosomes as smart regulators of cellular adhesion." Eur J Cell Biol **85**(3-4): 191-4.

Steele, M. R., D. M. Inman, et al. (2006). "Microarray analysis of retinal gene expression in the DBA/2J model of glaucoma." Invest Ophthalmol Vis Sci **47**(3): 977-85.

Stone, E. M., J. H. Fingert, et al. (1997). "Identification of a gene that causes primary open angle glaucoma." Science **275**(5300): 668-70.

Stylli, S. S., T. T. Stacey, et al. (2009). "Nck adaptor proteins link Tks5 to invadopodia actin regulation and ECM degradation." J Cell Sci **122**(Pt 15): 2727-40.

Sunden, S. L., W. L. Alward, et al. (1996). "Fine mapping of the autosomal dominant juvenile open angle glaucoma (GLC1A) region and evaluation of candidate genes." Genome Res **6**(9): 862-9.

Suzuki, H., T. Chiba, et al. (2000). "Homodimer of two F-box proteins betaTrCP1 or betaTrCP2 binds to IkappaBalpha for signal-dependent ubiquitination." J Biol Chem **275**(4): 2877-84.

Symons, M. (2008). "Cell biology: watching the first steps of podosome formation." Curr Biol **18**(19): R925-7.

Tamimi, Y., M. Lines, et al. (2004). "Identification of target genes regulated by FOXC1 using nickel agarose-based chromatin enrichment." Invest Ophthalmol Vis Sci **45**(11): 3904-13.

Tamm, E. R. (2009). "The trabecular meshwork outflow pathways: structural and functional aspects." Exp Eye Res **88**(4): 648-55.

Tan, J. C., D. M. Peters, et al. (2006). "Recent developments in understanding the pathophysiology of elevated intraocular pressure." Curr Opin Ophthalmol **17**(2): 168-74.

Tarone, G., D. Cirillo, et al. (1985). "Rous sarcoma virus-transformed fibroblasts adhere primarily at discrete protrusions of the ventral membrane called podosomes." Exp Cell Res **159**(1): 141-57.

Teti, A., S. Colucci, et al. (1992). "Protein kinase C affects microfilaments, bone resorption, and [Ca2+]o sensing in cultured osteoclasts." Am J Physiol **263**(1 Pt 1): C130-9.

Thomas, R., G. C. Sekhar, et al. (2004). "Glaucoma management in developing countries: medical, laser, and surgical options for glaucoma management in countries with limited resources." Curr Opin Ophthalmol **15**(2): 127-31.

Thompson, O., I. Kleino, et al. (2008). "Dystroglycan, Tks5 and Src mediated assembly of podosomes in myoblasts." PLoS One **3**(11): e3638.

Thorleifsson, G., K. P. Magnusson, et al. (2007). "Common sequence variants in the LOXL1 gene confer susceptibility to exfoliation glaucoma." Science **317**(5843): 1397-400.

Tumer, Z. and D. Bach-Holm (2009). "Axenfeld-Rieger syndrome and spectrum of PITX2 and FOXC1 mutations." Eur J Hum Genet **17**(12): 1527-39.

Van Buskirk, E. M. and G. A. Cioffi (1992). "Glaucomatous optic neuropathy." Am J Ophthalmol **113**(4): 447-52.

Vogel, C. I., B. Greene, et al. (2009). "Non-replication of an association of CTNNBL1 polymorphisms and obesity in a population of Central European ancestry." BMC Med Genet **10**: 14.

Vogel, C. I., B. Greene, et al. (2009). "Non-replication of an association of CTNNBL1 polymorphisms and obesity in a population of Central European ancestry." BMC Med Genet **10**(1): 14.

Vrabec, J. P. and L. A. Levin (2007). "The neurobiology of cell death in glaucoma." Eye (Lond) **21 Suppl 1**: S11-4.

Wax, M. B. and G. Tezel (2002). "Neurobiology of glaucomatous optic neuropathy: diverse cellular events in neurodegeneration and neuroprotection." Mol Neurobiol **26**(1): 45-55.

Weaver, A. M. (2006). "Invadopodia: specialized cell structures for cancer invasion." Clin Exp Metastasis **23**(2): 97-105.

Weaver, A. M. (2008). "Cortactin in tumor invasiveness." Cancer Lett **265**(2): 157-66.

Weaver, A. M. (2009). "Regulation of cancer invasion by reactive oxygen species and Tks family scaffold proteins." Sci Signal **2**(88): pe56.

Weinreb, R. N. (2000). "Uveoscleral outflow: the other outflow pathway." J Glaucoma **9**(5): 343-5.

Wientjes, F. B. and A. W. Segal (2003). "PX domain takes shape." Curr Opin Hematol **10**(1): 2-7.

Wiggs, J. L. (2007). "Genetic etiologies of glaucoma." Arch Ophthalmol **125**(1): 30-7.

Wiggs, J. L., J. L. Haines, et al. (1994). "Genetic linkage of autosomal dominant juvenile glaucoma to 1q21-q31 in three affected pedigrees." Genomics **21**(2): 299-303.

Wilson MR, M. J. (1996). Epidemiology of chronic open-angle glaucoma. St. Louis, Mosby.

Wojtanik, K. M., K. Edgemon, et al. (2009). "The role of LMNA in adipose: a novel mouse model of lipodystrophy based on the Dunnigan-type familial partial lipodystrophy mutation." J Lipid Res **50**(6): 1068-79.

Yamaguchi, H., M. Lorenz, et al. (2005). "Molecular mechanisms of invadopodium formation: the role of the N-WASP-Arp2/3 complex pathway and cofilin." J Cell Biol **168**(3): 441-52.

Yip, J. L. and P. J. Foster (2006). "Ethnic differences in primary angle-closure glaucoma." Curr Opin Ophthalmol **17**(2): 175-80.

Zhao, X., K. E. Pearson, et al. (2003). "Effects of prostaglandin analogues on human ciliary muscle and trabecular meshwork cells." Invest Ophthalmol Vis Sci **44**(5): 1945-52.

Zhou, M., X. M. Li, et al. (2006). "Transcriptional profiling of enriched populations of stem cells versus transient amplifying cells. A comparison of limbal and corneal epithelial basal cells." J Biol Chem **281**(28): 19600-9.

Zhou, Z., R. Althin, et al. (2004). "Persistency and treatment failure in newly diagnosed open angle glaucoma patients in the United Kingdom." Br J Ophthalmol **88**(11): 1391-4.